KDU 5/6(05)

KOSOVA ACADEMY OF SCIENCES AND ARTS
SECTION OF NATURAL SCIENCES

RESEARCH 24 KËRKIME

PRISHTINË
2019

KDU 5/6(05)

AKADEMIA E SHKENCAVE DHE E ARTEVE E KOSOVËS
KOSOVA ACADEMY OF SCIENCES AND ARTS

SEKSIONI I SHKENCAVE TË NATYRËS
SECTION OF NATURAL SCIENCES

RESEARCH
24
KËRKIME

Published/publikohet: Once a year/një herë në vit

PRISHTINË
2019

Editorial Office/Zyra Editoriale
Kosova Academy of Sciences and Arts
Akademia e Shkencave dhe e Arteve e Kosovës
Rr. "Agim Ramadani", Nr. 305, 10000, Prishtinë, Republika e Kosovës
Tel. +383 38 249 303; E-mail: research@ashak.org

Publisher/Publikuesi
Kosova Academy of Sciences and Arts
Akademia e Shkencave dhe e Arteve e Kosovës
Rr. "Agim Ramadani", Nr. 305, 10000 Prishtinë, Republika e Kosovës
Tel. +383 38 249 303; E-mail: research@ashak.org

KDU 5/6(05)

AKADEMIA E SHKENCAVE DHE E ARTEVE E KOSOVËS
KOSOVA ACADEMY OF SCIENCES AND ARTS

SEKSIONI I SHKENCAVE TË NATYRËS
SECTION OF NATURAL SCIENCES

RESEARCH
24
KËRKIME

Published/publikohet: Once a year/një herë në vit

PRISHTINË
2019

PËRMBAJTJA

KDU 541.2

DEVELOPMENT OF REVERSE OSMOSIS MEMBRANE MATERIALS AND FUTURE ADVANCEMENT: A REVIEW

Salih T. Gashi*

Abstract

In the last few decades on many occasions, commercial conventional separation processes in the industry were based on membrane separation processes; due to: low-cost fabrication, energetic availability, non-polluting, defect-free and perfectly save industrial production processes. Reverse Osmosis (RO) is currently the most important desalination process and it is experiencing significant growth due to the technological development and improved performance in selectivity and permeability of the membrane. This review includes the definition and the classification of RO membranes, highlights the early development of organic membrane materials (polymeric membrane materials), their chemistry, the surface modification of thin-film composite RO membranes, and desalination performance of commercially available membranes. Further more, novel: nanostructured RO inorganic membrane materials (zeolites), composite (inorganic-organic hybrid materials), and carbon – nanotube-based materials for making new RO membranes are presented. The key future prospects of membranes are also addressed.

* Academy of Science and Arts of Kosova, Rr. Agim Ramadani nr.305, 10000 Prishtina, Republic of Kosova, E-mail: salihgashi@ashak.org

Keywords: RO membranes, Synthesis, Surface modification, Membrane materials, Novel membranes, Organic and Inorganic materials, Nanostructures, Hybrid, carbon-nano tube.

Introduction

With the growth of population and fast industrial development in the past few decades the fresh water demand was rapidly increased. This development led to a reduction in freshwater availability due to pollution and the effects of climate change. There are more than 2.5 billion people (about 40 % of the world population) that do not have access to sanitation systems. From the global water reserves, only 2.5% is fresh water and the rest is saline. Thus, water purification for human use, agriculture industry and ecosystem management, is emerging as a leading global priority and is crucial for the world social and economic growth. One solution to achieve water supply and energy sustainability treatment is to develop viable technologies to gradually replace non-renewable fossil fuel. These include energy conversion from renewable and/or natural resources (e.g. biomass, wind, solar, water membrane energy) into usable energy (e.g. electricity) and energy storage [1, 2]. Therefore, the most pressing challenges today include the recovery of clean drinking water from sea water, by far the most abundant global water resource, and the treatment and recycle of wastewater. Desalination and water reclamation are of paramount importance in water security, where desalination happens to be one of the main life supporters in many arid regions. From membrane technologies, RO plays an important role in water desalination (rejecting monovalent and multivalent ions, viruses, bacteria and suspended solids) and membrane sustainability.

Desalination by RO, wastewater treatment by membrane reactors (MBR) are already applied at industry scale. On the other hand, they

need to be improved in terms of cost and affordability energy consumption and expertise. Therefore, to achieve these objectives the advances in membrane materials are needed. They include development in membrane materials and module design, process design, feed pre-treatment, reduction in energy consumption etc. further advances are needed. The enhanced mechanical, biological and chemical strength of RO membranes, as well as increased permeability (through minimizing fouling and concentration polarization) have reduced the membrane cost per unit volume of water produced more than 10 times over 40 years and decrease the energy consumption to less than 2.0 $kWhm^{-3}$[2].

Over the past few decades, the development of different membranes materials has been oriented in search of suitable RO materials chemical composition) and membrane formation mechanisms in order to enhance membrane performance. Despite this, the reviews of RO membrane materials have been rare and were focused on already existing membrane materials. In addition to ongoing research into conventional polymeric RO membrane materials, nanotechnology has opened the way to incorporate nanomaterials into the RO process. The chronological description of this process provides the reader with a quick overview of RO membranes that operate by different mechanisms and their impact on the desalination, which enables to look forward to the novel nanostructured materials that will shape future trends in membrane material research. This review gives more insight of about the RO membrane materials development to date, visualize their performance advancement for creation of RO membranes and key future prospects.

Membrane definition

A precise and complete definition of a membrane that covers all its aspects is rather elusive, even when discussion is limited to synthetic structures as in this outline. In the most general sense, a synthetic membrane is an interphase that separates two phases and restricts the

transport of various chemical species in rather specific manner. In the other words a membrane is a thin physical interface that moderates certain species to pass through depending on their physical and/or chemical properties. The term "membrane" therefore includes a great variety of materials and structures, and a membrane can often be better described in terms of what it does rather than what it is. Some materials, though not meant to be membranes, show typical membrane properties, and in fact are membranes, e.g. protective coatings, or packaging materials. All materials operating as membranes have one characteristic property in common: they restrict the passage of various chemical species in very specific manner [3,4].

A membrane can be homogeneous or heterogeneous, symmetric or asymmetric in structure: it may be solid or liquid and may be either neutral, or may carry positive or negative charges, or both. Its thickness may vary between less than 100*nm* to more than a centimeter. The electrical resistance may vary from thousands of mega ohms to a fraction of an ohm. Mass transport through membrane may be caused by diffusion of individual molecules or by convection induced by gradients: electrical potential, concentration, pressure or temperature. Common methods to fabricate polymeric membranes include phase inversion, interfacial polymerization, stretching, track-etching, and electrospinning.

Membrane classification

In general, there are two classes of membranes (often defined as a cross-section): isotropic and anisotropic membranes as shown in Figure1. Isotropic membranes have chemically homogenous composition whereas anisotropic membranes are heterogeneous both chemically and structurally [5]. These membranes are chemically uniform in composition and physical nature across the cross-section of membranes.

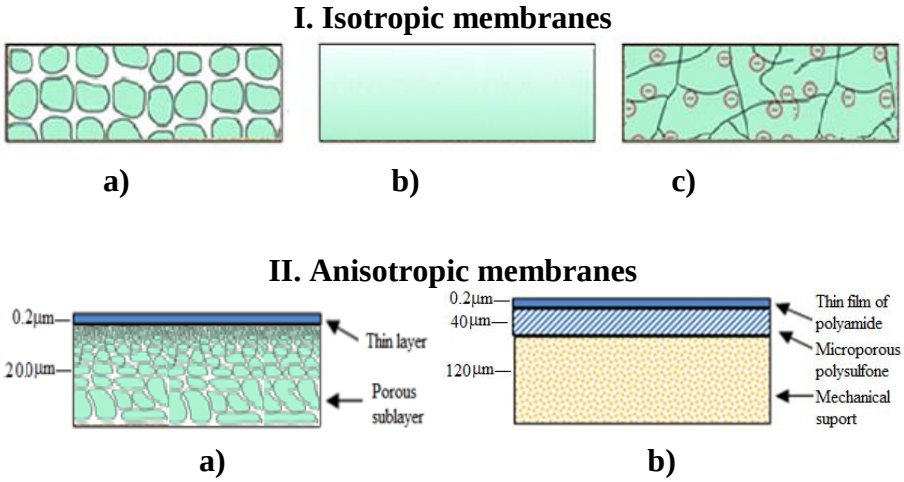

Fig. 1. Schematic illustration of various membrane classes: Isotropic: Ia) microporous, Ib) nonporous dense, and Ic) electrically charged and anisotropic: IIa) integrally anisotropic and IIb) thin-film composite membranes (Adopted from ref 5)

Isotropic (symmetrical) membranes

Isotropic membranes can be divided into various subcategories: microporous membranes, nonporous dense films and electrically charged membranes, as in Figure 1. (Ia, b, and c). Microporous membranes are often prepared from rigid polymeric materials with large voids that create interconnected pores Figure 1 (Ia). Isotropic membranes can also be dense films which either are lack of pores or contain pores that are so small as to render the membrane effectively non porous. These films are prepared by casting followed by solvent evaporation or melt extrusion Figure 1 (Ib). In the case of nonporous dense films, transport is due to diffusion driven by an applied force such as pressure, concentration or electric gradients. Therefore, the separation of solutes is governed by their relative transport rates. Electrically charged membranes can be either nonporous dense films or microporous structures consisting of positively or negatively charged ions

on the membrane walls (known as anion-exchange or cation-exchange membranes) Figure 1 (Ic). Separation of solutes is primary achieved by analyte ion concentration and charge exclusion (i.e. solute with the same charge as the ions on the membrane walls is rejected by Coulombic repulsion).

The most common microporous membranes are phase inversion membranes. These are produced by casting film from a solution of polymer and solvent and immersing the cast film in a nonsolvent for the polymer. SEM images of these membranes are shown in Figure 2a. Microporous membranes generally separate solutes based on the size of particulate and the size of their pore diameter typically ranges from 0.1 μm in comparison with conventional filters larger than 1-10 μm, so their pore diameter is typically larger than 5 μm [5].

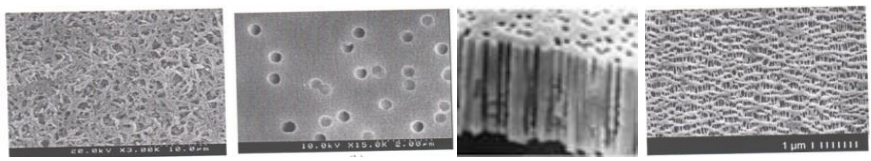

a) b) c)

Fig. 2. SEM images of isotropic microporous membranes: a) phase inversion membranes b) top surface and cross-section of the track-etched membrane and c) expanded film membranes. [Adopted from ref 5]

Another type of microporous membrane is the track-etched membrane Figure 2b. This type of membrane is prepared by irradiation a polymer film with charged particles (heavy ions to form tracks through the film) that attack the polymer chains, leaving behind sensitized track of damaged molecules, thereby forming pores. Pores are uniform cylinders, many of which are perpendicular to the membrane surface.

Expanded film membranes are oriented crystalline polymers with voids created by an extrusion and stretching process fig 2c. First, the material is extruded near its melting temperature using a rapid draw–

down rate. Then, the extruded material is cooled, annealed, and stretched up to 300% of its original length. This stretching process creates slit-like pores ranging in size from 20 - 250 nm. These films are prepared by solution casting followed by solvent evaporation or melt extrusion.

Anisotropic (asymmetric) Membranes

There are two main types of anisotropic membranes: phase separation membranes (Loeb-Sourirajan) and composite membranes such as thin film, coated films, and self-assembled structures. Loeb-Sourirajan membranes are homogeneous in chemical composition similar to isotropic microporous membranes, but pore sizes and porosity vary across the membrane thickness. The anisotropic membranes are of two types: integral asymmetric and thin-film composite membranes. Anisotropic (asymmetric) membranes are non-uniform over membrane cross-section, and they typically consist of a number of layers which vary in structure and/or chemical composition. These membranes contain different layers, structures and permeabilities. A typical anisotropic membrane has relatively dense and extremely thin surface layer (i.e. the "skin", also called permeselectivity layer) supported on an open, much thicker porous substructure, Figure 1 (IIa). The separation properties and permeation rates are determined exclusively by the surface layer; and substructure functions as mechanical support, with virtually no separation function. The resistance to mass transfer is determined largely or completely by the thin surface layer. The membrane can be made thick enough to withstand the compressive forces used in separation. The thin films always are on the high-pressure side of the membrane that is the feed side, since in this way maximum use of the support layer is made to preserve the thin film. These membranes had the advantage of higher fluxes and almost all commercial processes use such membranes [3-5].

Composite membranes

A composite is a material made from two or more materials with different physical or chemical properties which remain separate and distinct on a macroscopic level within the finished structure. Composite membranes such as thin-film membranes are chemically and structurally heterogeneous. A thin surface layer is supported by a much thicker porous structure (functioning that serves as a mechanical support) and these structures are traditionally made of different polymeric materials. These classes of membranes prepared by methods such as interfacial polymerization, solution coating, and plasma polymerization have been established for various filtration processes. The separation of solutes and permeation rates of the membrane are exclusively determined by the thin surface layer, which results in a high flux [6]. The images of these membranes are presented in Figure 1 (II b). These are more widely described later in this review.

Liquid Membranes

Liquid membranes have become increasingly significant in the context of facilitated transport, which utilizes "carriers" to selectively transport components such as metal ions at a relatively high rate across the membrane interface. Liquid membranes are used today in two different configurations. In the first, the liquid membrane is composed as a thin film stabilized by a surfactant in an emulsion – type mixture and the second configuration are generally referred to as supported liquid membranes. Here, the separation medium is a microporous polymer structure the pores of which are filled with a liquid membrane phase. In this configuration the microporous structure provides the mechanical strength while the liquid-filled pores function as the selective separation barrier. Liquid membranes are formed by making an emulsion of two immiscible phases. The continuous phase of the emulsion forms the liquid membranes and the disperse droplets in the emulsion form the so-

called "inner phase". The emulsion can be either oil-in-water or water-in-oil. The liquid membrane phase normally contains surfactants and additives, which are used to control the stability, the permeability and selectivity of the membrane. The emulsion then is dispersed in a third phase (the continuous outer phase), which is normally miscible with an inner phase, Figure 3a. The supported (immobilized) liquid membranes are obtained by impregnating a microporous polymer support with a liquid containing a carrier molecule, Figure 3b. Liquid membranes are used on a pilot-plant scale for selective removal of heavy-metal ions and organic solvents from industrial waste streams. They have also been used for the separation of oxygen and nitrogen [7].

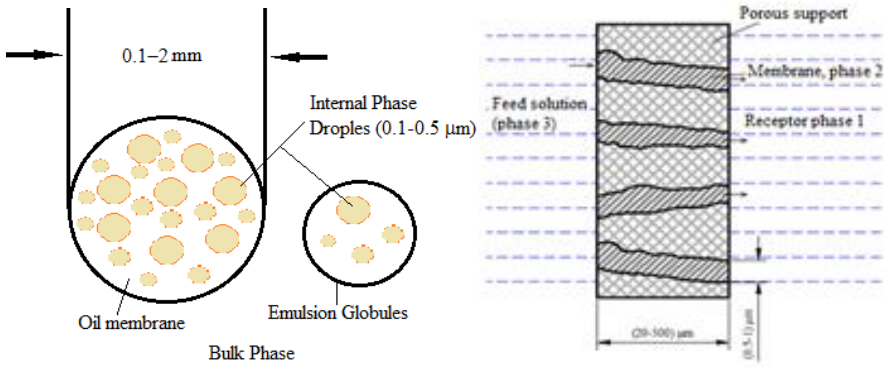

a) b)

Fig. 3. Schematic representation of liquid membranes: a) emulsion membranes, b) supported membranes. (Adopted from ref 5)

Membrane materials

A number of membrane materials and membrane preparation techniques have been used to make RO membranes. It is very difficult to provide a set of concrete criteria for the selection of polymer materials suitable for the hyper filtration process, but there exists a strong link between polymer structure and its physical RO properties. The following factors should be considered in order to design effective membranes: choice of membrane

materials, high water flux, highest possible solute rejection (> 90)%), high resistance to chemical and biological attack, strong mechanical structure to cast into thin films and be resistant under pressure, capability to be fabricated with high surface to volume ratio, wide operating range for temperature and pressure**,** module configuration, mechanical/chemical/thermal/temporal stability, system design including processability at large scale, and operating conditions for cost-effectiveness. The performance of a membrane is mainly governed by the structure of its pores and the physical/chemical properties of the material. The intensive effort has been invested both in exploring new membrane materials/processes and in modifying traditionally used materials. Membrane materials according to structures and properties can be organic or inorganic or mixed (hybrid) organic –inorganic.

Organic membranes (Polymeric materials)

Chemistry development chronic of asymmetric membranes started from the late 1950s, when Reid and Breton have been reported about thin symmetrical cellulose acetate (CA) membrane. They demonstrated that desalination capabilities of CA film, could retain salt effectively, achieving 98% rejection, but flux was very low < 10 $mLm^{-2}\ h^{-1}$ [8]. They concluded that CA showed requisite the same semi permeability properties for practical application, but the improvement in flux and durability were required for commercial viability. The first viable (RO) membrane as an integrally skinned asymmetric cellulose acetate semi-permeable membrane of high performance has been made by Loeb and Sourirajan at UCLA in 1959 and patented in 1960, The resulting membrane was made with a dense 200 *nm* thin layer over a thick supported microporous thick layer. This membrane promoted the reverse osmosis membrane commercial viability due to the significantly improved flux, which was 10 times that of other known membrane materials at the time. The Loeb Sourirajan CA membranes had the flux 0.35 $m^3m^{-2}day^{-1}$ and the rejection 99% at ~100 $x10^5$

Pa for 4000 *ppm* NaCl solution. Since then, CA has been applied in a wide range of filtration processes from RO to MF driven by CA's relatively low cost (cellulose is the most abundant natural biomaterial on earth, ~700 billion tons per year) and its hydrophilic properties [9, 10]. The cellulose acetate (CA) was developed due to high stability in a wide range of temperature and pH as well as having higher resistance to chemical and biological attack when compared with initial cellulose diacetate (CDA) material [11]. However, CTA of (44.2%) acetate has an extremely high water-to salt permeability ratio reflecting it very high selectivity. Unfortunately, the water permeability is lost so these membranes have low water fluxes even at low operating pressure (30 x 10^{5} Pa). The combination (a blend of CDA and CTA), have higher permeability and selectivity than CA membranes, as well as they have greater resistance to the effects of compaction [12]. The specific molecular composition of CA and CTA membranes is outlined, in the next subject in the Figure. 5. There are presented only structures of CA and CTA, but not other cellulosic esters: cellulose acetate butyrate (EAB-381), ethyl cellulose etc. [3] although the CA was the best RO material until 1969. However, these membrane materials were sensitive to hydrolysis in acidic and alkaline conditions, biological attack and limitation in a wide range of application [13]. Although CA is replaced by interfacial composite membranes, they still remain important for specific applications because they are easy to make, mechanically tough and resistant to degradation by chlorine and other oxidants. The further efforts were oriented in materials with higher chemical stability. The current generation of reverse osmosis (RO) membrane materials is based on a composite material patented by FilmTec Corporation in 1970 (now part of Dow Chemical Company).

In the decade after the announcement of Loeb-Sourirajan membrane, has been developed the first non-cellulosic asymmetric aromatic polyamide (PA) hollow fiber membrane commercialized by Du Pont under trade number Permasep B-9 and B-10 membranes. These membranes exhibited higher water flux at slightly lower operating pressure than cellulose acetate membranes. They were used primary for sea water and brackish

water. Though it has relatively low flux and salt rejection; the durability, stability and versality were greater than CA and aromatic polyhydrazides. These membranes have flux $0.67 m^3 m^{-2}$ day^{-1} and 99.5% rejection of 3500 ppm NaCl solution at 100x 10^5Pa 100 *bar*. CA and linear aromatic polyamide membranes were the industrial standard until 1972 when Cadotte prepared the first interfacial composite polyamide membranes. The polyamide predisposition to being attacked by disinfectants, such as ozone and chlorine, was noted after prolonged application of B-9 Permasep membranes. Subsequently, chlorine resistant asymmetric membranes based on polypiperazine-amides were developed as a response (Figure 5 and Table 1). [14-17]. These membranes have comparable permeselectivity to the asymmetric CA membranes. Lower quantities of amidic hydrogen in the membrane likewise improved its overall resistance to chlorine attack [18]. However, this membrane was not commercialized due to its relatively low salt rejection (< 90%) [19]. In this case the presence of the sulphonic and phenyl groups in sulfonated polysulfone were expected to enhance permeability, mechanical, chemical and biological stability, nevertheless the salt rejection was far lower than the acceptable level required for industrial and commercial application. Sulfonated polysulfone membranes have been developed due to their stability in oxidizing environments [20]. Both aliphatic and aromatic polysulfones have been synthesized, but only the latter is of sufficiently high molecular weight family of polymers. Three types of materials are commercially available under the trade names Udel (polysulphone grades (1700 and 3500), Radel (polyphenylsulphone, grade 5000), and Victrex (polyethersulfone, grades 200P and 600P): the first two types are supplied by union carbide, and the third kind is supplied by ICI. The fourth type of aromatic polysulfone, called Astrel 360 (polyarylsulfone) has been manufactured, but it is not available commercially [3]. Nevertheless, strong Donnan effects were still observed, thus suggesting that the shielding effect of divalent cations may drastically lower the monovalent ion rejection. Similarly, carboxylated polysulfone which gives a promising flux also suffers from

uncompetitive salt rejection [21, 22]. While polybenzimidazoline (PBIL) membranes developed by Teijin show excellent permeselectivity even in harsh operating condition, they are susceptible to pressure compaction and chlorine attack [23, 24]. On the other hand, polyoxadiazole is found to have superior mechanical and temperature stability but its salt rejection and permeability are not commercially attractive for RO application [24]. Less important asymmetric membranes polypiperazine-amide was chlorine resistant but showed too low salt rejection, polypiperazine imidazoline show excellent flux but susceptible to chlorine attack. Polyoxadiazole neither salt rejection nor flux are attractive, while carboxylated polysulfone salt rejection was too low.

Thin Film Composite (TFC) Membrane

Only a few soluble polymers can form asymmetric structures in one-step casting, and even less are commercially attractive in terms of the right combination of permeability and salt rejection. In addition, under pressure, the CA asymmetric membrane experienced densification in the middle transition layer. This leads to two-step casting methods that enabled individual optimization of the materials used for the micro-porous support film and for the barrier layer. Thus, a wide variety of polymers were tested for the barrier layer and support layer separately. and the latter for improved mechanical support. These anisotropic type membrane morphologies are now referred as composite membranes [25]. The first TFC membrane was casted by float-casting a CA ultrathin film on the water surface and then followed by the process of laminating an annealing the film onto a pre-formed CA microporous support [26]. A number of empirical studies have suggested that polysulphone was a suitable material for the support layer because of its reasonable flux value, overall resistance to compaction, and its critical stability in acidic environment settings. For further development of the TFC membrane were used interfacial polymerization and acid polycondensation [27- 30].

The current RO membrane market is dominated by TFC thin film composite polyamide membranes. TFC membranes are commonly classified as nanofiltration (NF) and reverse osmosis (RO) membranes. Both types are typically made out of a thin polyamide layer (<200 nm) deposited on top of a polysulfone or polyethersulfone porous layer (about 50 microns) on top of a non-woven fabric support sheet [31, 32]. The three-layer configuration gives the desired properties of high rejection of undesired materials (like salts), high filtration rate, and good mechanical strength. The polyamide top layer is responsible for the high rejection and is chosen primarily for its permeability to water and relative impermeability to various dissolved impurities including salt ions and other small, unfilterable molecules [33].

The polysulphone microporous interlayer is added between the barrier layer and support layer to enable the formation of an ultra-thin barrier layer. Membrane pore size is usually less than 0.6 nm that permits to achieve salt rejection consistently higher than 99%. The selective barrier layer is most often made of aromatic polyamide (e.g. via interfacial polymerization of 1, 3 phenylenediamine also known as 1, 3-benzen diamine and triacid chloride of benzene (trimesoyl chloride) [33]. The chemistry of this membrane based on such reaction is presented in Figure 4.

This membrane was used in modified form by all major RO membrane producers. The solution – coated composite membrane is formed by solution coating a thin (0.5-2.0μm) selective layer on a suitable microporous layer. Because the selective layer of the composite membrane is often very thin and delicate a sealing layer also formed from a highly permeable material, is frequently used to protect such membranes. A dip-coating methodology based on acid polycondensation of low-molecular-weight hydroxyl-containing compounds was proposed to overcome scaling up problems in float casting technology [15, 56]. The first patented product based on this concept was named NS - 200, a product of reaction of polyoxyethylene, sulfuric acid and

furfuryl alcohol showing excellent salt rejection but suffered from irreversible swelling and hydrolysis of the sulphate linkage [35].

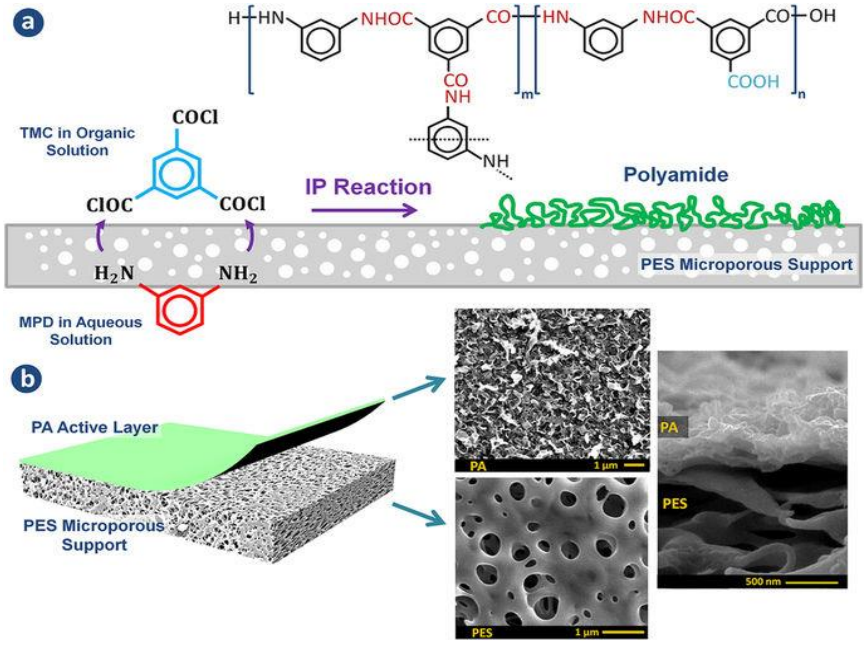

Fig. 4. (a) Schematic representation of the interfacial polymerization reaction between MPD and TMC at the surface of the microporous PES support and the chemical formula of PA layer. The m and n in polymer structure represent the crosslinked and the linear parts, respectively (m + n = 1), (b) Structure of the synthesized TFC membranes with the top and cross-sectional morphologies [34].

Another TFC RO membrane prepared by acid polycondensation using 1,3,5-tris (hydroxyethyl) isocyannuric as a comonomer acid rather than polyoxyethylene was the PEC-1000. This membrane has highest salt and organic solutes rejection respectively 99.9 % and > 95 % from relatively concentrated feed solutions of any membrane developed with adequate flux (492 $Lm^{-2}day^{-1}$) but it was susceptible to chlorine attack as NS 200 membrane [36].

The barrier layer can be created by plasma polymerization, during which the monomer vapor is induced by the energy of the gas plasma, and atomic polymerization is brought to the cool surface, frequently in the form of polysulfone support surface. A range of polymers have been tested and good permselectivity can be obtained from vinylene carbonate/acrylonitirile, vinyl acetate / acrylonitrile, allylamine, acetylene/water/nitrogen, acetylene/water/carbon monoxide combinations [37, 38].

The plasma polymerization and a membrane formed by acetylene, water and nitrogen performed particularly well in sea water desalination test, with 99 % salt rejection for a flux of 1.5 m^3 m^{-2} day^{-1} at 100 *bar* operation but plasma polymerized RO membranes mostly have low chlorine resistance due to their nitrogen-enriched chemical structure, and only one RO membrane has been commercialized by this technique.

Interfacial Polymerization

Interfacial (thin film) composite membrane contains a thin dense film of highly cross-linked polymer formed on the surface of thicker microporous support. The dense polymer layer is extremely thin < 0.1 *mm* so membrane permeability is high. Because it is highly cross-linked, its selectivity is also high. These membranes are widely used in reverse osmosis and nanofiltration.

The chemistry and properties of key TFC RO membranes developed over the past 25 years are summarized in Table 1 and 2 and Figure 5.

Table 1. Some characteristics of TFC RO membranes

Name	Flux m^3/m^2day	Rejection/ %	Working pressure/ *bar* (MPa)	Testing standard solution % NaCl
Sulfonated polysulfone, Hi-Fi, Flux CP [41]	0.06	99	69	3.5
Polyamide via polyethylene-imine NS-100 [33]	0.7	99	100	3.5
Polyamide via Polyepiamine PA-300 or RC-100[42]	1.0	99.4	69	3.5
Polyvinylamine WFX-X006[43]	2	98.7	40	Conductivity = 5000 μS/cm
Polypyrrolidine – [44]	0.8	99.7	40	0.5
Polypiperazine-amide NS-300[45]	3.3	68	100	3.5
Crosslinked Fully Aromatic Polyamide FT-30 [46]	1	99	15	0.2
Crosslinked Fully Aromatic Polyamide UCC series- [47]	0.8	98.5	15	0.5
Crosslinked Aralkyl Polyamide A -15[48]	0.26	98	55	3.2
Crosslinked Fully Aromatic Polyamide X -20 [49]	1	99.3	15	0.2

Table 2. Some of the state-of-the-art SWRO membrane modules in the application

Membrane module brand name	Material & module	Feed	Permeate flux (m^3/day)	Salt rejection (%)	Specific energy consumption (kW/m^3)
DOW FILMTEC ™8 inch SW30HRLE	TFC cross-linked fully aromatic polyamide spiral wound	32g/LNaCl solu., 55 bar, 25°C, pH8 and 8% recovery	28.0	99.60-99.75	3.40 (2.32) Perth SWRO Plant, Australia
Hydranautics 8-inch SWC4+	TFC cross-linked fully aromatic polyamide spiral wound	32g/LNaCl solu., 55 bar, 25°C, pH7 and 10 % recovery	24	99.70-99.80	4.17 (2.88) at Llobregat SWRO Plant, Spain,
Toray 8-inch TM820C	TFC cross-linked fully aromatic polyamide spiral wound	32g/LNaCl solu., 55 bar, 25°C, pH8 and 8%recovery,	19.7-24.6	99.50-99.75	at Tuas SWRO Plant, Singapore
Toyobo 16-inch HB 10255	Asymmetric cellulosetri-acetate hollow fiber	35g/LNaCl solu., 54bar, 25°C, and 30% recovery	60.0-67	99.4 99.0	At Fukuoka SWRO Plant, Japan

The data in Table 2 can't be compared because of different solution feed concentrations. The number in brackets is the energy for the RO unit.

The continuous improvement of membrane material performance has led to development of several membrane module configuration, with significant cost reduction.

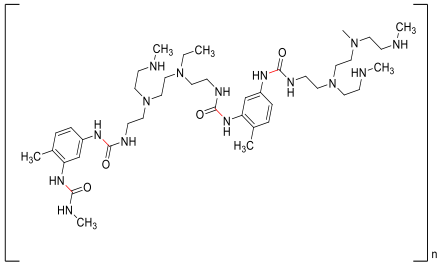

PAP: Trade name NS-100

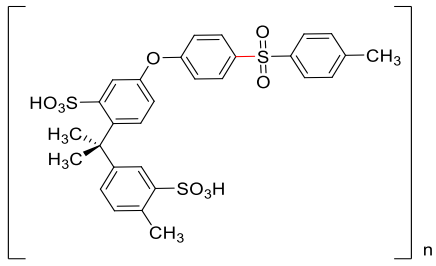

PSU: Trade name Hi-Flux CP PEP

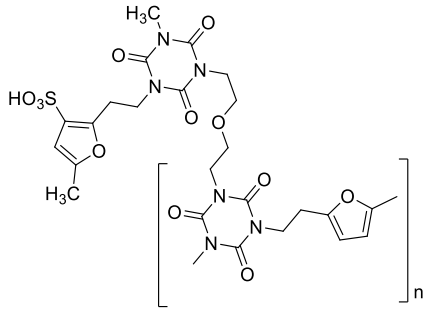

PEP: Trade name :P PEC-1000

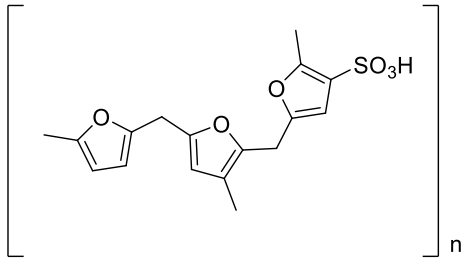

PF: Trade name: NS 200

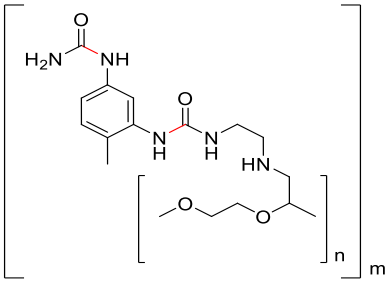

PAPEAMI: Trade name:

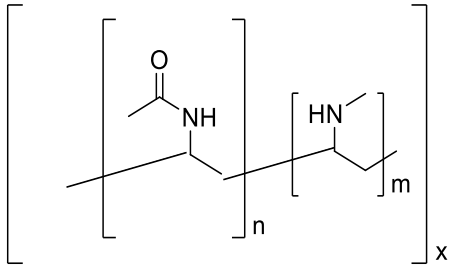

PA-300 RC-100

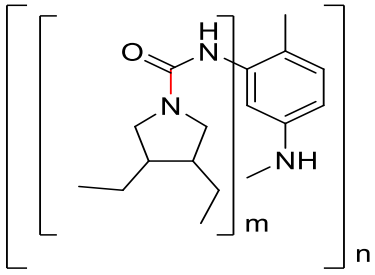

PVA: Trade name: WFX-X006

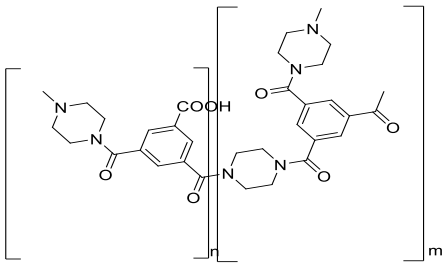

PPAM: Trade name: NS-300

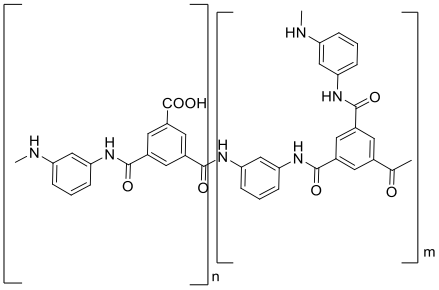

PP CFAP-1: Trade name: FT-30

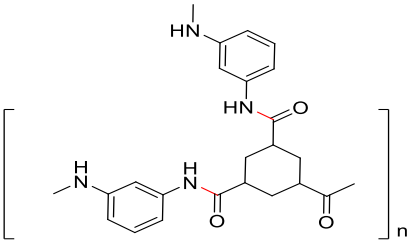

CFAP-2: Trade name: UTC series

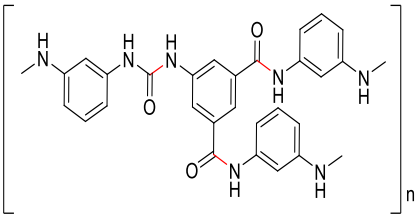

CAP: Trade name A-15

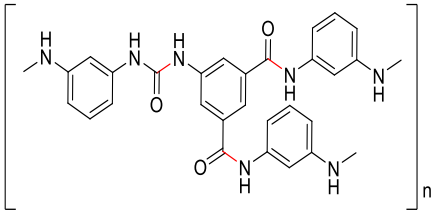

CFAP-3: Trade name: X-20C F A P-3

Fig. 5. Chemical structures of key TFC RO membranes: Polyamide via polyethyleneimine:(PAP), Sulfonated Polysulfone (PSU), Polyether Polyfuran (PEPF), Polyfuran (PF), Polyamide via polyepiamine (PAPEAMI), Polyvinylamine (PVA), Polypyrrolidine (PP), Polypiperazine-amide (PPAM), Crosslinked Fully Aromatic Polyamide-1(CFAP-1), Crosslinked Fully Aromatic Polyamide-2 (CFAP-2), Crosslinked Aralkyl Polyamide (CAP), Crosslinked Fully Aromatic Polyamide-3(CFAP-3). [Ref. 25, 40].

Note: The chemical structure shown is a representative segmental structure of this type of material. It does not cover all variations, e.g. the NS-100 structure shown is the polyamide version, although the polyurea version is also grouped into the same category.

The spiral wound membrane module configuration is most extensively used in RO desalination. The suppliers which provide RO membranes for large scale desalination plants are: DOW, Hydronautics, Toray, Toyobo etc. [25, 40, 50]. The state of the art-seawater desalination RO membrane modules for each supplier is given in Table 2. The following procedures have been used for the synthesis of TFC membranes presented in Figure 5 and Table 2. The use of polysulfone as a support layer opened the way to interfacial polymerization to produce RO membranes, as it could withstand the alkaline conditions created by the use of caustic as an acid acceptor in the interfacial polymerization process. The development of NS- 100, polyethyleneimine reacted with toluene di-isocyanate by Cadotte was a major technological milestone in the history of RO processes [33, 50]. It was the first successful non-cellulosic membrane with comparable flux and monovalent salt rejection. It also demonstrated superior rejection of organic compounds, and good stability in high temperature, acidic and alkaline environments [51, 52]. However, NS-100 membranes have virtually no resistance to chlorine, and they have a pronounced surface brittleness as a result of a highly cross-linked structure.

An alternative commercialized product created using interfacial polymerization of polymeric amines is polyepiamine and specially its two types PA-300 and RC-100 (Figure 5, Table 1) [23, 53, 54]. The PA-300 type membrane had enhanced permeate flux by 42.8% at about 1 $m^3m^{-2}day^1$ and salt rejection 99.4 % at 70 *bar*, as compared to NS-100. This enhancement has led to PA-300 spiral wound modular elements being installed in the TFC SWRO plant at Jeddah the first large RO sea water desalination plant [55]. On the other hand, RC-100 has a high

resistance to bio-fouling which has resulted in successful installation at Umm Lujj II and other desalination plants [56]. There are two other noteworthy interfacial polymerized TFC membranes from polymeric reactants, namely polyvinylamine that offers high flux and polypyrrolidine whose amino/carboxy-groups can be controlled in a way that permits to variable selectivity and amphoteric properties. Initial attempts at interfacial polymerization of monomeric amines, including both aliphatic and aromatic diamines, with terephthaloyl chloride, did not produce membranes with attractive salt rejection performance [32]. Cadotte revisited this case and optimized the polymerization conditions [57]. Nevertheless, this polypiperazine-amide membrane exhibits strong Donnan exclusion effects due to the anionic charged surface via the presence of carboxylic groups, i.e. it can achieve excellent rejection of divalent anions such as sulphate at high flux. This makes it sufficiently attractive for practical usage in nanofiltration (NF) and the membrane has been designated as NS-300. A range of NF membrane based on similar chemistry have been commercialized, e.g. NF-40 series by DOW FILMTEC™ [45, 88], NTR-7250 by Nitto Denko [58], UTC-20 by Toray Industries [59]. Cadotte discovered that membranes with excellent permselectivity can be produced using monomeric aromatic amines and aromatic acyl halides containing at least three carbonyl halide groups, with trimesoyl chloride giving the best results [46, 60, 61]. Unlike other interfacial polymerization methods, heat curing was avoided, and acid acceptor and surfactants were not required because polymerization and crosslinking were both rapid even when acyl halide was supplied at lower concentrations.

Membrane FT-30 was prepared by interfacial reaction between 1,3-benzenediamine with trimesoyl chloride and has resulted in distinct surface characteristics, which has been described as a ‘ridge and valley’ structure. Studies have shown that the rougher ‘ridge and valley’ type of surface contributed to a larger surface area used specifically for water transport and thus water flux [62].

In seawater desalination tests, FT-30 yielded fluxes of nearly 1 $m^3 m^{-2} day^{-1}$ with 99.3 - 99.5 % salt rejection at operating pressure 55 x 10^5 Pa. The aromatic polyamide structure of FT-30 provides a high degree of resistance to compression, thermal and chemical resistance, as well as a wide pH operating range (3-11). Although not completely resistant to chlorine, FT-30 shows a degree of tolerance to chlorine and oxidizing agents than other commercially available polyamide membranes which are sufficient to withstand accidental exposure to this chemical [63], DOW FILMTEC™ has commercialized a number of products based on this membrane [64]. This membrane has a significant impact on the design and cost of RO desalination [65]. It was the first spiral wound membrane element capable of competing with the Du Pont asymmetric hollow fiber polyamide B-9 Permasep membranes, originally produced in 1972. The success of FT-30 led to creating of a number of similar products [66], e.g. CPA2 membrane produced by Hydranautics [67], UTC-70 by Toray Industries [73]. Furthermore, Permasep A-15 TFC membrane (Figure 5 and Table 1) prepared by reacting 1,3- benzenediamine with a saturated cross-linking agent, cyclohexane-1,3,5-tricarbonyl chloride resulting in an aralkyl polyamide membrane gives better flux. [48, 68]. The application of isocyanato aromatic acyl halides (e.g. 1-isocyanato-3,5-benzenedicarbonyl chloride) as cross-linking agents for 1,3-benzenediamine was likewise patented in order to produce a membrane containing both amide and urea linkages that excels in both flux and salt rejection [49]. This latter membrane was designated X-20, showing superior resistance to fouling and chlorine due to its relatively neutral surface charge and stronger polyamide-urea bond linkage [69].

Virtually all organic membranes explored to date have been made of polymeric materials which in general offer a wide variety of structures and properties. The polymeric materials which represents the most widely used current (first generation) organic membrane materials are: Cellulose acetate (CA), cellulose triacetate(CTA) and cellulose nitrates,

[70-72], polysulfone (PSU), polyethersulfone (PES) [73] , polyacrylonitrile (PAN) [74], polyvinylidene fluoride (PVDF) [75,76], polypropylene (PP) [77, 78], polyvinyl alcohol (PVA), polytetrafluoroethylene (PTFE), Polyamide (PA), and polyimide (PI), and Polyamide hydrazide(PH). The chemical structures of these common polymeric materials are given in Figure 6:

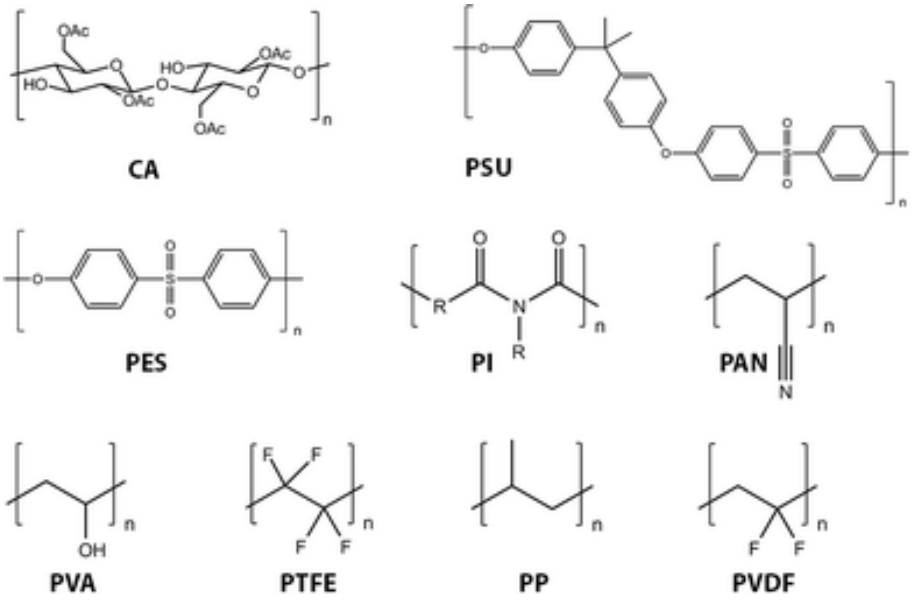

Fig. 6. Chemical structures of commonly used polymeric membrane materials: Cellulose acetate (CA), polysulfone (PSU), polyethersulfone (PES), polyimide (PI), polyacrylonitrile (PAN), poly vinyl alcohol (PVA), polytetrafluoroethylene (PTFE), polypropylene (PP), and polyvinylidene fluoride (PVDF). (Ref. 169)

Polysulfone (PSU) and polyethersulfone (PES) are among the most commonly used for UF and also as supporting substrates for NF and RO processes. These materials exhibit excellent permeability, the selectivity of permeate, mechanical stability, and chemical resistance. For example, the glass transition temperature (T_g) of PES is 225 °C, and

PSU exhibits pH stability and oxidation resistance. For MF applications, PP and PVDF are the most frequently used materials [79].

In general, no single polymeric membrane material mentioned above simultaneously exhibits chemical/thermal stability, oxidation/pH resistance, and mechanical strength. Significant effort has been directed toward enhancing permeation flux, pollution resistance, operation pressure stability, and membrane service life. The main drawback of most of these polymeric membranes is their inherent hydrophobicity resulting in a high fouling tendency, which often leads to higher operation cost, shorter lifetime, irreproducible separation performance, and smaller application range. Fouling is the accumulation of substances on the membrane surface/or within pores, which results in deterioration of membrane performance. The interaction between membrane surfaces and solution components plays an important role in the extent of membrane fouling. Fouling is primarily caused by a buildup of proteins, organics, inorganics, microorganisms, and microbial communities on the membrane surface [80].

After the discovery of the asymmetric membrane by Loeb-Sourirajan 1960, further research was focused on cellulosic membrane materials. However, the susceptibility of the acetate group to hydrolysis, limited the durability and application. The alternative polymers with chemical stability were needed. The fully cross-linked polyamide TFC RO membranes (1970-1980) and controlling morphological changes by monitoring polymerization reactions (the 1990s), the revolutionary improvement of this commercial RO membrane has been rather slow during the first decade of this century. Current products of RO desalination membranes are still based on the original chemistry discovered during the 1980s, i.e. interfacial polymerization of monomeric aromatic amines and conventional CA materials. Despite the fact that no new polymeric membranes have been commercialized recently, the performance of RO membranes has still improved, i.e. water permeability has been at least doubled, and the recovery of fresh water can be over 60 %. These improvements are the results of surface modification, as well

as closer monitoring of interfacial polymerization reaction parameters, as well as the more effective design of the module structure [25, 81, 82].

Surface Modification

Surface modification is an excellent method to introduce hydrophilic properties and functional groups to the membrane surface. To modify membrane surface properties various chemical and physical methods (techniques) have been developed. The performance of polymeric materials in many applications relies largely upon the combination of bulk (e.g. mechanical) properties with the properties of their surfaces. However, polymers very often do not possess the surface properties or mechanical properties that are critical for their successful application.

Hydrophilicity and surface charge are key parameters that affect the fouling propensity of a membrane. A hydrophilic and uncharged surface is considered to be resistant to fouling. Any chemical compound coming in contact with the membrane that is chemically reactive may alter the membrane surface by attaching or detaching some functional moieties, or it introduces a change in the hydrophilicity and surface charge. Moreover, these surface characteristics are related to surface roughness and membrane pore diameter. Given the fact that selective leaching of hydrophilizing polymeric additives is the ultimate change in the membrane, its surface is expected to turn more hydrophobic. But chlorine-exposed membranes turned more hydrophilic, probably owing to the formation of bigger pores and charged species by chain scission. Similarly, exposure of PES membrane to hypochlorite solution was shown to make it more negative owing to the formation of phenyl sulfonate after chain scission and subsequent increase in pore diameter [244]. This could be because the chlorine substitution generated dipole moments and/or gradual dissipation of the surface

coating layer that was applied to modify the membrane [240]. In addition, the amide nitrogen of the membrane is also highly vulnerable to chlorine attack because of electron-withdrawing effect of the carbonyl group. Upon exposure to free chlorine, N-H group is chlorinated to N-Cl group which can reversibly form the initial amid by treatment with reducing agents. The aromatic rings are also susceptible to attack by chlorine because it is an electron-rich region.

Surface modification methods can be divided into six main groups: a) Coating (thin-film composites), b) blending, c) composite, d) chemical, e) grafting and f) combination methods.

a) The coating is a method wherein the coating material forms a thin layer that non-covalently adheres to the substrate. The coating can be done by different methods including physical adsorption by non-covalent bonds. This physical adsorption method involves the attachment of thin hydrophilic layer on the surface of the membrane in order to increase the hydrophilicity of the membrane [83-84, 86]. Adsorption occurs through electrostatic interactions, hydrophobic interactions, hydrogen interactions, and chemical reactions with functional groups that are present on the membrane surface [84, 87]. Coating can be done also with a monolayer using Langmuir–Blodgett or analogous methods, deposition from a glow discharge plasma, and casting between two polymer solutions by simultaneous spinning such as a triple orifice spinneret [85, 88-91]. Several research studies have been used coating techniques to modify the surface of the PES membrane. For instance, the synthesized PES membrane was coated with poly dopamine (DPA) in an alkaline solution of dopamine (DA). DA is oxidized at alkaline pH and then polymerized to form a cross-linked poly dopamine (PDA) arrangement which could adhere onto many solid materials. The results of the study showed that both the hydrophilicity and blood compatibility of the coated PES membrane with PDA enhanced significantly [92].

The PES membrane modification with poly (sodium 4-styrene sulfonate) (PSS) by permeation of PSS solution through PES membranes during 100 min has been possible [86]. Preadsorption of PSS can take place on the surface and inside the pores. This can be determined based on molar mass of PPS polymer in contrast with the membrane pore size. The results of this study showed that the surface-modified PES membranes with PSS have a better antifouling effect than the unmodified membrane. Charged membranes were prepared by coating PES ultrafiltration membranes with sulphonated poly (2, 6-dimethyl-1,4 phenylene oxid) [87]. Recently thermal cross-linking of poly (ethyleneglycol on PES membrane was published using methylene methylacrylate as an accelerator [93]. The coating techniques can be used easily, and it is a way to efficiently improve the PES membrane without deterioration the mechanical property of PES membranes. However, one main drawback of coating techniques is that the layer of hydrophilic polymers and monomers can be degraded with membrane long usage. The coatings have been the preferred method for modification of LFC (Low Fouling Composite) series respectively LFC1(of area 33.9 m^2, flow 37.8 m^3/d, and rejection 99% and LFC_2 (of 33.9 m^2, flow 41.6 m^3/d and rejection 95%). Both membranes have the same durable aromatic polyamide composition as traditional composite RO membrane material. However, unlike negatively surface charged traditional composite RO membranes, the LFC_1 membrane surface has a neutral charge, while the LFC_2 membrane surface has a cationic charge [94]. Recently are introduced the LFC_3-LD type membranes, targeting applications in wastewater treatment/reclamation [95]. Neutrally charged, these membranes are designed to minimize the adsorption of organic foulants. The reported stable performance over time has been [96] attributed to a poly (vinyl alcohol) (PVA) coating on the surface of a conventional fully aromatic polyamide membrane [99]. Coatings of PVA and poly (N,N-dimethylaminoethyl methacrylate) have also shown superior resistance against chlorine attack [97, 100]. Currently hydrophilic dendritic polymers have been reported to have successfully modified a membrane surface

to reduce fouling effects. They are called “Dendrimers” (composed of a large number of monomers units that were chemically linked together similar to linear polymers). A major difference between linear polymers and dendrimers is that a linear polymer consists of long chains of molecules like coils, crisscrossing each other. A dendrimer consists of molecular chains that branched out from a common center and there is no entanglement between each dendrimer molecules. Dendrimer research is still at its early stage, the synthesis of dendrimers is very difficult and expensive [98]. Another study is surface coatings with hydrophilic polymers, and surface segregation methods with amphiphilic block copolymers [101].

b) Blending is a process in which two (or more) polymers mixed to obtain the request properties. Usually, the blending technique, i.e. change the properties (enhance the hydrophilicity) of the PES membrane since new materials are blended with PES. In addition, the polymer blending can be categorized as homogenous or heterogenous [102, 103]. Polymeric blending allows hydrophobic PES membrane which exhibited high chemical and mechanical strength to be blended with hydrophilic polymeric materials such as polyethylene glycol (PEG), polyvinylpyrrolidone (PVP), or (polyethylene oxide-b-polypropylene oxide-b-polyethylene oxide) [104]. PES membrane can be also blended with the inorganic nanomaterials such as silica, silver, aluminum oxide and titanium dioxide [105]. In copolymer blending, for instance, the PES membrane has been blended with the copolymers N,N - dimethyl-N-methacryloxyethyl-N-(3-sulfopropyl), (DMMSA) - butyl methacrylate (BMA) for bovine serum albumin (BSA) separation [106]. In using inorganic nanomaterials blending, for example, the PES was modified with inorganic nanomaterials (TiO_2) to produce PES–TiO_2 membranes which were synthesized from the casting solution that consist of various compositions of polymer solvents (DMF and EtOH) and TiO_2 additive. The modified structure of the PES–TiO_2 membranes has changed from a sponge-like to a finger-like structure after the modification, and enhances the antifouling properties, even inevitable leaching of the

blended hydrophilic materials from the polymeric membranes appears after long-term use [104, 107]. Modifying macromolecules (SMMs-synthesized from (phenyldisocianate), (propylene diol) and fluoro alcohol is used alternatively [108]. The use of branched amphiphilic copolymers (P123-b-PEG) and of an amphiphilic comb-copolymer with polystyrene as hydrophobic part and PEG has also been reported [109, 110]. In the latter case, the hydrophilic PEG segments are spontaneously segregated to the membrane surface during immersion precipitation, which increased hydrophilicity and reduced protein adsorption from 6.8 to 0.5 mg/cm^2, whereas only a slight change in permeation properties was observed. Comparable results were found for PSU-based blended membranes with amphiphilic copolymer shaving PSU backbones and PEG side chains, (PSU-g-PEG). These membranes exhibited good mechanical characteristics, and remarkably reduced protein adsorption (about 72% reduction in protein adsorption with 10 wt., % PSU-g-PEG blending) [111]. Besides, the use of branched amphiphilic PEG, recently amphiphilic copolymers such as phosphoryl chlorine copolymer (i.e. synthesized copolymer composed of 2-methacryloxyethylphosphorylcholine (MPC) and n- butyl methacrylate (BMA) with PES membranes were investigated [112]. Only few of these amphiphilic copolymers such as tetronic have been synthesized on commercial scale. Another work includes homogeneous blending [113-116].

c) Composite membrane of N,O-carboxymethyl chitosan/poly(ethersulfone) (CM-CS/PES) was prepared by immersing PES microfiltration membranes into CM-CS solutions and cross-linking with glutaraldehyde. The (CM-CS/PES) membrane possess a weak positive charge at low pH 3-4 and a rather strong negative charge at high pH 6-8, it means that they resist protein fouling at high pH, and separate proteins by adsorption at low pH. The membrane surface that adsorbs proteins previously can subsequently be the recovered by increasing the pH [117]. Sulfonated poly (ether-ethersulfone)-poly(ether-sulfone) (SPEES-PES) and sulfonated poly(ether-ethersulfone)-

poly(ethersulfone)/poly (vinyl chloride) (SPEES-PES/PVC) composites were used to measure glucose and hydrogen peroxide permselectivity in ampero-metric biosensors. Also, highly charged cation permeable composite membranes were prepared from a blend of sulfonated PES with sulfonated poly (ether ether-ketone) [118, 119].

d) In the chemical modification method, the membrane material is treated with modifying agents to introduce various functional groups on the membrane surface. For example, [-CH_2CH_2 CH_2 SO_3] groups have been coupled onto the surface of PS hollow fibers using the reaction of PS, propane sulfone, and Friedel-Crafts catalysts. The resulting membranes were claimed to show excellent anti-adsorption behavior. Also, a surface modification with propylene oxide and Friedel-Crafts catalyst was carried out. In addition, sulfonation (-SO_3H), hydroxylation (-OH), carboxylation (-COOH), amination (-NH_2), chloromethylation, lithiation reactions were applied to improve the hydrophilicity of PES. More specifically, in sulfonation reaction the negatively charged sulphonic acid groups were introduced to the PES membrane. There are two types of sulfonation that can be used to introduce SO_3H groups to the polymeric chain; it can be done by a heterogeneous treatment using sulfonating agents or a homogenous treatment using pre-sulfonating monomers in the polymerization reaction [120, 121]. Various water-soluble solvents such as acids and alcohols have been used to treat the membrane surface. Mixtures of alcohol (ethanol and isopropanol) and acid (hydrofluoric and hydrochloric acid) in water are also used to improve flux and rejection due to the partial hydrolysis and skin modification initiated by the alcohol and acid [122]. The presence of hydrogen bonding is claimed to encourage interaction between acid and water, which produces more surface charge and eventually enhances the hydrophilicity and water flux remarkably. Also, treatment of a membrane surface with ammonia or alkyl compounds, particularly ethylenediamine and ethanolamine, and achieved both enhanced flux and salt rejection was patented [123]. A 70 % flux improvement is attained by

soaking composite membranes in solutions containing various organic species, e.g. glycerol, sodium lauryl sulphate, and the triethylamine salt of camphorsulfonic acid [124, 125]. Post-treatment of membranes using an aqueous solution of poly (vinyl alcohol) and a buffer solution can effectively improve the abrasion resistance as well as flux stability of the membrane [126, 127]. Vast flow enhancement was achieved by a chemical treatment of FT-30 membrane with hydrofluoric and fluosilicic acids. The membrane was soaked in a 15 % solution of hydrofluoric acid for seven days and exhibited about a 4-fold improvement in flux and slightly higher salt rejection. Membrane surface analysis showed that the fluorine ratio was higher due to the effects of the treatment. In addition, etching of the surface had resulted in a thinner barrier layer. Whilst increasing the flux without altering the chemical structure, this method however suffers from leaching of the hydrophilizing components over time causing the loss of any flux enhancement. [128-129].

e) Grafting is other another surface modification technique. It is a method wherein monomers are covalently bound onto the membrane surface. The surface modification by grafting includes: i) chemical, ii) photochemical, or via high energy, iii) plasma and iv) enzymatic techniques. The choice of the grafting technique depends on the chemical structure of the membrane and the desired characteristics after surface modification.

i) In chemical grafting, free radicals are produced during the activation of chemical species that due to their very high reactivity are attached onto the substrate surface. In the presence of monomer moieties, they enable to initiate polymerization that permits to graft a copolymer. Peroxydisulfate and metabisulfite oxidizing agents were used to initiate free radical polymerization with methacrylic acid, polyethyleneglicol-methacrylate, and sulfopropylmethacrylate agents in aqueous solution at ambient temperature [130]. In general, this technique is simple and available, leading to a membrane that is claimed to be less sensitive to fouling due to the presence of the hydrophilic grafted monomers. The modification of carbon surface with aryl groups derived

from aryldiazonium salts is now a very efficient method that is widely used. The scheme of the method is given in the Figure 7. The key step in this procedure is the electrochemical or chemical reduction of the aryldiazonium cation that enables the formation of aryl radicals that immediately attack the carbon surface and are attached to it [131-132].

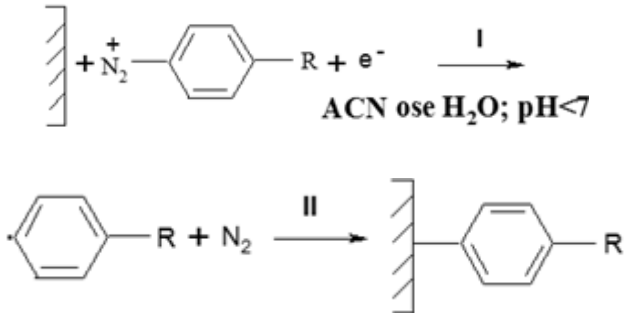

Fig. 7. The modification of the carbon surface with an aryldiazonium salt.

ii) Photochemical grafting and radiation are the initiation techniques for surface grafting. When a chromophore on a macromolecule absorbs light, it is brought in an excited state and one or more bonds may dissociate into radicals that can act as initiation grafting process. Radicals that are generated in this manner on the membrane surface can react with the monomer to form the grafted polymer. If the absorption of light does not lead to the formation of free radicals, this process can be promoted by the addition of sensitizers, which in turn abstract hydrogen atoms from the base polymer surface and produce the free radicals required for the grafting, [133]. The irradiation of macromolecules can cause homolytic fission and thus forms free radicals on the membrane. UV irradiation and UV-assisted graft polymerization are techniques that can selectively alter membrane surface properties without affecting the bulk polymer. The UV irradiation technique is used for

modification of poly(arylsulfone) membranes, and to graft several hydrophilic monomers (e.g. n-vinyl-2 pyrrolidone, n-vinyl caprolactane) onto 10 kDa PES ultrafiltration membranes.

UV-assisted graft polymerization of the same monomer (N-vinyl-2-pyrrolidinone) onto 50 kDa PES membranes create highly wettable PES membranes with high fouling resistance compared to the base membrane [134-136].

Thin-film composite polyamide (PA) membranes for the first time have presented a convenient route to configure their surface charge by gamma-ray induced grafting. This modification resulted in an improved water flux over 55% from 45.9 to up 70 $Lm^{-2}h^{-1}$, whilst NaCl rejection was found to drop by only 1% compared to pristine membranes [137].

iii) Plasma treatment is another surface modification method. When gases receive enough energy, they can be exited into the plasma state, which is a mixture of ions, electrons, excited species, and free radicals. Plasma surface treatment usually refers to a plasma reaction that either results in modification of molecular structure, or atomic substitution. Plasma treatment, which is produced by ionization of a gas or water, is a technique used to modify PES membrane and to generate radicals acting as active sites for graft polymerization [84, 138]. Although this technique is effective it has drawbacks such as time dependency of the induced changes [145]. The hydrophilicity of the membrane surface is increased through the active species that are produced in the plasma keeping the backbone of the polymer unmodified. Depending on the plasma means, this technique provides new functional groups on the surface of the membrane with new characteristics. Gas plasma treatment is also used to induce surface modification: water permeability is improved by oxygen plasma treatment due to the introduction of hydrophilic carboxylate groups, whereas argon plasma treatment can greatly enhance chlorine resistance by increasing the extent of cross-linking at the nitrogen sites [139-140]. Recently is reported that the use of atmos-

pheric gas plasma surface activation on the surface of conventional polyamide TFC membranes can greatly enhance anti-fouling properties [141]. After gas plasma surface activation, a polymeric brush layer is formed by free radical polymerization based on acrylamide monomers or methacrylic acid. This brush layer can effectively reduce the ability of foulants to adhere to the surface, as proven during multiple fouling tests, where this membrane has outperformed the commercial low-fouling membrane LFC_1, particularly in mineral fouling test.

iv) The enzymatic grafting method is quite new. The principle involved is that an enzyme initiates the chemical/electrochemical grafting [142] by converting the substrate (monomer, oligomer or chains) into reactive free radicals that react with the membrane. Enzymatic grafting of chitosan resins and films using tyrosinase and chlorogenic acid and different hydroxybenzoic acids has been reported [143].

Among other surface modification methods one can mention thermal-induced polymerization. This technique is effective and useful to immobilize biomolecule compounds such as enzymes, proteins and amino acids which are covalently attached on the surface of the PES membrane by a chemical reaction. The chemical initiators or cleavage agents have always used the so-called Atom transfer radical polymerization (ATRP) method which permits their activation in the presence of catalyzers like copper (I) and (II) chloride and the reaction with the monomer. [144] This is relatively new technique to graft polymer, and it is considered easy and efficient since it requires reasonably mild conditions and allows different vinyl monomers to be polymerized in a controlled way with a well-defined structure. There are three grafting techniques used for surface-initiated ATRP and so far, enable to modify PES membrane: the grafting-through, the grafting-to, and the grafting-from. However, there are a few research studies that cover the surface-initiated ATRP method used for PES membrane modification [145-147]. All chemical surface modification methods allow the grafting of the organic layer without affecting the material bulk properties when appropriate conditions are selected. The improvement of membrane

performance can also be achieved by optimization of polymerization reactions. This process includes many parameters such as: reactant diffusion coefficients, reaction time, solvent solubility, solution composition, nucleation rate, curing time, polymer molecular weight range, and characteristics of the micro-porous support [148-152]. In addition, the inclusion of additives into the casting solution plays a major role in alteration of monomer solubility, its diffusion, hydrolysis and protonation, and they can also act as scavengers for the inhibitory reaction by-products [153]. The addition of: triethylamine salt of camphorsulfonic acid, N,N-dimethylformamide, alcohols, ethers, Sulphur-containing compounds, water soluble polymers, or polyhydric alcohol to the amine solution can improve membrane permeability without significant change in salt rejection [154-155]. Instead of mixing additives into the amine reactant solutions, the addition of a 'complexing agent' into the acyl chloride solution is possible. Most widely used are phosphate-containing compounds such as triphenyl phosphate, which can modify and eliminate the repulsive interaction of acyl chloride with other compounds by removing the halides formed during amide bond formation [156]. Recently the introduction of active additives, more specifically surface-modifying macromolecules, into the reactants has been reported. In this method the additive can move toward the active surface during the polymerization, and hence alter the surface chemistry which permits to obtain desirable properties. For example, the participation of hydrophilic surface-modifying macromolecules, such as poly (ethylene glycol) end-capped oligomers, in the interfacial polycondensation reaction has improved the membrane flux and stability of salt rejection over time [157]. The surface treatment methods proposed here may have significant implications for the development of high flux reverse osmosis membranes in the future.

Novel Desalination RO Membranes

Advanced membranes with superior selectivity and permeability are essential for the development of membrane-based separation technology. Since the operation of the first RO desalination plant, only polymeric membranes have been employed for the industrial use. The advances in conventional polymeric RO membranes have been rather limited since the late 1990s, especially concerning the membrane permeability. Recently, advances in nanotechnology have led to the development of nano-structured materials (polymeric, inorganic carbon nanotubes, and biomimetic which may form the basis for new RO membranes [158]. A nanofiltration membrane based on rigid star amphiphiles (RSA) has been reported recently [159-160]. The membranes were prepared by direct percolation of methanol solutions of the RSAs through an asymmetric polyethersulfone support that had been previously conditioned with methanol and cross-linked poly-vinyl alcohol. These membranes have shown an extremely smooth surface with an overage roughness in the range of 1-2 *nm* as compared with higher values for commercial NF membranes (20-70 *nm*). The composite multilayer dendrimer structure allows the control of narrower pore size distribution. In respect to commercial NF membranes, these membranes showed comparable contaminants rejection performance with double the flux. Considering the similarity of polymeric NF and RO membrane morphology, this new route of polymeric membrane synthesis may offer a better alternative in tuning membrane structure. Tunable C_2N Membrane for highly efficient water desalination recently were reported. Through molecular dynamic simulations, first-principles calculations, and recent experiments based on graphene-like carbon nitride (g-C_2N) monolayer with highly efficient filters look promising for water desalination. It was found that the water permeability of g-C_2N is significantly higher than that reported for graphene filters by almost one order of magnitude [161-162]. However, further investigation is needed to verify the suitability for RO process; in particular its salt rejection is yet unknown. Recent

reports addressed the other materials for production of composite membranes with CA, CA nanofibers, amphiphilic block copolymers, such as Pluronic F 127, conductive polymers to improve antifouling properties. [163, 169].

Biomimetic RO Membranes

Membranes incorporating bacterial Aquaporin Z proteins have been reported to show superior water transport efficiency relative to conventional RO membranes [164]. Aquaporins were incorporated into the walls of self-assembled polymer vesicles constituted of tri-block copolymer, poly (2-methyl-2-oxazoline) block - poly (dimethylsiloxane) block- poly (2-methyl-2-oxazoline). An initial permeability test was carried out on the aquaporin-triblock polymer vesicles by stopped-flow light-scattering experiments. The results reported giving at least an order of magnitude improvement in permeability compared to commercially available TFC RO membranes [164-166]. The use of an NF membrane as a biomimetic membrane support has been reported [167]. A continuous phospholipid bilayer was successfully formed on an NTR-7450 membrane and fully covered it, using the vesicle fusion approach. Further study is needed to incorporate aquaporins into the phospholipid bilayer for practical use in water purification. A Danish Company named Aquaporin was founded in 2005 in order to develop these membranes for practical industrial use. The company has recently been awarded a patent on the method of fabricating membranes incorporating aquaporins [168]. Rather than using triblock polymers the aquaporins are reconstituted into lipid bilayers fabricated using the Langmuir-Blodgett method, a vesicle fusion method, or they are spin-coated. The patent also discloses the two different orientations of the membrane: (a) a lipid bilayer incorporating the aquaporins is sandwiched between two hydrophilic porous support layers such as mica, polysul-

fone or cellulose; or (b) a lipid bilayer incorporating aquaporins is assembled over a hydrophobic porous support membrane such as a porous PTFE (Poly tetra fluoro ethylene) film. Although a salt separation test has yet to be reported, extremely high salt rejection is expected from aquaporins since their functional biological performance only allow the passage of water molecules [169]. However, for many practical issues, such as identification of appropriate support materials, understanding of the resistance to membrane fouling, and even identification of an appropriate range of operating conditions must be carried out to develop this membrane for practical use. The reverse osmosis (RO), ultrafiltration (UF), and nanofiltration (NF) membrane materials play an important role in membrane technology development. These materials employed separately or in their integrated form have received increasing attention for a specific application.

Inorganic membranes

Membranes can also be made from inorganic materials such as ceramics or zeolites. The inorganic membranes are composed of a wide range of materials from: Al, Si, Ti, Zr oxide (each oxide has a different surface charge in solution), mixed oxides of the above elements or additional compounds of minor concentration. The structure of inorganic modules is a flat membrane which contain a microporous support layer and meso or micro-porous active layer. In the following sections, we survey recently developed membrane materials, their characteristics, synthesis /fabrication. Details of traditional membrane formation and operation processes can be found in the literature [5, 170 - 172]. Inorganic membranes such as zeolites show required desalination properties, are tolerant to waters which readily foul polymer membranes and can withstand more cost-effective cleaning methods [173 - 174].

Ceramic materials for production of ceramic membranes are one of the inorganic membranes used in high operating temperatures, radioactive heavily contaminated feeds, and highly reactive environment [175]. They are mostly made from alumina, silica, titania, zirconia, or any mixture of these materials. Generally ceramic membranes are made up of a macro-porous support layer and a meso- or microporous active layer. The state-of-the-art ceramic membrane preparation techniques include pasting extrusion for supports, and slip-casting of powder suspensions or sol-gel processing of colloidal suspensions for deposition of the active layer. Membrane elements have been developed from simple tubular modules to monolithic honeycomb-type structures which offer higher packing efficiency. Currently commercial ceramic membranes are widely used in micro- and ultra-filtration applications whereas ceramic membranes for nano-filtration are under development [176]. The industrial use of ceramic membranes in domestic water production is rare but their process robustness has attracted the attention of researchers for both membrane distillation and pervaporation [177-179]. A group of researchers has been reported results on the use of ceramic membranes for RO desalination. The use of Si ZK-4 zeolite membranes for NaCl solution desalination, as well as oil filled water, 100 % of ion rejection was achieved [180]. This group has experimentally investigated the RO separation mechanism and feasibility of application of ceramic membranes. Zeolites are natural crystalline aluminosilicate materials with uniform sub-nanometer macropores and an active layer of micropores 0.3- 0.8 *nm*. Zeolite crystals are natural or can be synthesized in a laboratory. In Figure 8 are shown the sub-nm intercrystalline pores within the zeolite structure that allow the passage of water molecules and reject the salt [181].

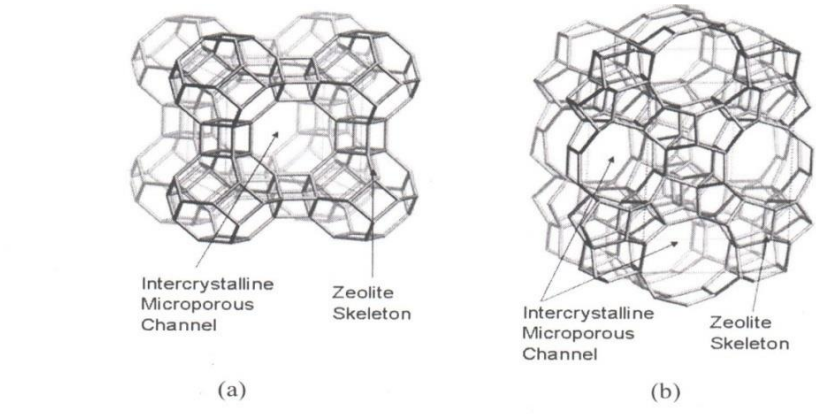

Fig 8. Micro-porous ceramic membrane structure: micro-porous channel in the crystalline structure (a) Type A Zeolite; and (b) MFI Zeolite. (Reprinted with permission from Ref. 181).

Currently inorganic membranes are widely used in micro and ultrafiltration, whereas inorganic membranes for nanofiltration are under development. Theoretical calculations have shown that ions can be completely excluded by zeolite membranes with pore sizes smaller than the size of the hydrated ion. A-type zeolite membranes exhibit 0.4 *nm* pores and MFI (mordenite framework inverted)-type membranes 0.56 *nm*. The first experimental attempt at RO of a NaCl solution using a MFI silicalite-1 zeolite membrane showed 77 % salt rejection and a water flux as low as 0.003 m^3 m^{-2} day^{-1} at $21x10^5$ Pa. It is also reported that rejection of bivalent cations is higher than for monovalent ions, in a test using a feed containing mixed ion species. In other words, the rejection of sodium ions in a mixed positive ion solution is lower than that for a pure solution of NaCl. The lower rejection is attributed to ion transport across nanometer-sized interstitial defects created during the membrane synthesis process. These results show that the filtration mechanism is not only dependent on size exclusion, but also on Donnan exclusion due to the charged double layer induced by adsorbed ions on the pore or the intercrystalline walls as presented Figure 8 [182-183]. It was stated that the salt rejection depends on the formation and size of

the electric double layer (EDLs) at the surface of the intercrystalline defects [184]. The thickness of this layer decrease with an increase in ion concentration: the electric double layer can overlap and prohibit the transport of salt ions, while, in high salt concentration, (EDLs) become thinner and no longer overlap, allowing ions to pass through the intercrystalline defects. All these experimental results showed that nanometer-sized intercrystalline defects controlled the majority of ion transport and represent a challenge for the fabrication of zeolite membranes [184]. In fact, it was stated that polycrystalline zeolite membranes inevitably contain nanometer-scale intercrystalline pores, which decrease the efficiency of ion rejection especially for high concentration feed solutions containing multivalent cations. Recently it was reported that typical zeolite membranes are prepared by the hydrothermal deposition method on porous inorganic or stainless-steel support. Supporting material must provide the physical durability to the membrane, but no effect on fluid flow and salt rejection than the zeolite separation layer [185]. Although the first RO test with a zeolite membrane was unsuccessful, i.e. both salt rejection and water flux were too low to be of practical use, subsequent work has been conducted to improve both by modifying the zeolite structure. The Si / Al ratio, which dominates the wettability and membrane surface charge, has been optimized to give improved flux and salt rejection. The Al content in the membrane can alter the surface hydrophilicity and therefore affinity with water [186]. Defects in the crystal structure are minimized by secondary growth of a zeolite layer on zeolite seeded onto a porous α-alumina substrate [187]. This combined effort generated a remarkable improvement, with a 2 μm thick zeolite membrane with 50: 50 Si / Al ratio rejecting 92.9 % of sodium ions with a water flux of (0.11 $Lm^{-2}\ h^{-1}$) at 2.7 MPa [188]. In a recent report from the same group, the thickness of the membrane has been further reduced to 0.7 μm, providing excellent organic (> 99 %) and salt rejection (97.3 %) as well as nearly 4 times improvement in water flux [189-190]. Although the improvement of zeolite membranes

has been tremendous in the past 10 years, their performance and economics are still no match for polymeric membranes. The zeolite membrane thickness is still at least 3 times higher than the current state of the art polymeric RO membranes, causing higher resistance to water flux. Consequently, ceramic membranes require at least 50 times higher membrane area than polymeric ones to achieve an equivalent production capacity. Another candidate for the formation of sub–nm porous material with controlled pore size distribution is carbide-derived carbon materials [191]. The performance of zeolite membranes may be affected by pressure, ion concentration and composition of the feed salt solution. An increasing of feed temperature has e greater influence on the ion permeation than on the water permeation, resulting in a decline of the ion rejection. On the contrary increasing the transmembrane pressure can enhance both the water flux and ion rejection rates because the ion flux is much less affected by pressure compared to water flux. The RO zeolite membranes possess excellent thermal and mechanical stability, operating pressure and temperature are desirable for enhancing the separation efficiency. Increasing feed ion concentration results in an exponential increase of ion flux because of both the driving force for ion transport and effective pore size increase with the increase of ion concentration due to the diminishing of the electric double layer at increased ion concentration [184-185]. Zeolite membranes have shown higher permeability and selectivity than polymeric membranes. They exhibit better resistance to harsh chemical conditions and can withstand high pressure and temperature, which constitute advantages for desalination [185] but their performance and economics are still no match for polymeric membranes, because the membrane thickness is still at least 3 times higher than polymeric RO, causing higher resistance to water flux. As a result, inorganic membranes require at least 50 times higher membrane area than polymeric ones to achieve the same productivity. As it is mentioned before despite the organic materials, exists also UF and NF inorganic membrane materials with improved properties. For example: TiO_2, TiO_2/Al_2O_3 (photocatalytic decomposition of azo-dye

under UV irradiation), Ag/TiO_2 nanofiber, TiO_2 nanowire and TiO_2 nanotube, (bacterial inactivation, anti-fouling, anti-bacterial concurrent rejection, and photocatalytic oxidation), Al_2O_3/SiC (reduction of defect density on the surface), and NF inorganic materials such as TiO_2-SiO_2 (chemical and thermal stability pollutant adsorption capacity),TiO_2 hollow fiber at temp.(900^oC) [improved membrane properties],and graphene oxide (GO) [10 times higher flux and high retention than commercial membranes], respectively. However, large-scale applications of these inorganic materials are limited due to high operation cost and inherent mechanical fragility thus far.

Inorganic–organic hybrid membrane materials

Although the concept of combination of organic and inorganic material, is not new, the incorporation of inorganic materials into organic RO TFC membranes only started in the early 2000's. Inorganic–organic hybrid membrane membranes are also called mixed matrix membranes (MMM) [192]. The main objective of MMM is to combine the benefits offered by each material, i.e. the high packing density**,** good permselectivity, and long operational experience of polymeric membranes, coupled with the superior chemical, biological and thermal stability of inorganic membranes [193]. The latest development in membrane material design is the use of hybrid (inorganic–organic) materials in order to try to overcome the limitations associated with polymeric membrane systems. MMM is known also as composite membranes, produced by dispersing fillers in a polymeric matrix. Inorganic materials that have been explored are metal oxides (*e.g.*, Al_2O_3, TiO_2, SiO_2, ZnO, Fe_2O_3), metals (*e.g.*, Cu, Ag) and carbon-based materials (*e.g.*, graphene and carbon nanotubes). Introducing inorganic moieties into a polymeric matrix system can offer multi-functionality beyond separation alone and can enhance hydrophilicity, mechanical strength, water permeability, rejection rate, and antifouling properties. This is, in part, because such additives can modify the

kinetics and thermodynamics of the formation process of the polymeric membrane such that the membrane surface and pore structure can be altered. Various fabrication methods have been developed to incorporate these nanomaterials in a polymer matrix. These include blending, phase inversion methods (resulting in well-mixed nanomaterials in the matrix), interfacial polymerization (resulting in a thin layer of nanocomposite on the surface of the membrane or a thin layer with nanocomposite membrane substrates), self-assembly of nanoparticles, surface coatings, layer-by-layer processing, and surface grafting [194]. The behavior of various nanomaterials in polymeric matrices during the phase-inversion process and their structural performance during filtration were recently reviewed [195]. The membranes consisting of nanomaterials in a polymer matrix were used for water treatment [195-196]. Recent developments in thin-film composite membrane have received increasing attention as these systems exhibit superior performance compared with asymmetric membranes for desalination [197 - 199]. Modifying the membranes by blending organic and inorganic materials (especially nanoparticles) may offer advantages such as excellent filtration performance, thermal and chemical stability, as well as membrane forming ability. Currently, NPs such as oxide species (*e.g.*, SiO_2, TiO_2, Al_2O_3, ZnO) and metal particles such as Ag have been used to modify organic membranes. Widely used polymeric membranes such as PES and PVDF with improved antifouling property were realized by incorporating various NPs [169, 200 - 202]. In one of the earlier reports on hydrophilic modification of PES membranes with NPs was presented zinc oxide (synthesis of ZnO/PES membranes and ZnO NPs/glycerol) as an alternative to TiO_2 as it offers lower cost material [203-204]. Halloysite ($Al_2Si_2O_5(OH)_4 \cdot 2H_2O$) nanotubes (HNTs) have recently been used as catalyst supports, nanoreactors, and filler for the polymer to improve the mechanical and thermal properties of the composites [205]. Another report addressing the bio-fouling issue was carried out by modifying PSU membranes with Ag NPs synthesized using various ionic surfactants (silver sulfadiazine, dodecyltrimethylammonium bromide, benzalkonium chloride, or sodium dodecylbenzene sulfonate) [206].

Nano-particle / Polymeric Membranes

Another important development of TFC membrane technology is the incorporation of nanoscale particles into a composite membrane structure. The titanium oxide (TiO_2) nanoparticles have been added into PA thin-film composite membranes frequently used for water treatment process [207]. The top thin layer of PA-TiO_2 was prepared by interfacial reaction between MPD and TMC in the presence of TiO_2 nanoparticles in the organic phase solution. Results revealed that membrane water flux enhanced with increasing TiO_2 concentration as a result of increasing the surface hydrophilicity. The rejection of $MgSO_4$, however, was reported to decrease sharply upon TiO_2 addition. The significant changes in salt rejection can be explained by the significant reaction interference of TiO_2 in the polymerization process, leading to a lower degree of polymerization. Self-assembly of TiO_2 nanoparticles on the TFC membrane was also investigated and serve to reduce membrane biofouling [208]. It is little probable that TiO_2 might wash away from membrane surface during operation, owing to the bidentate coordination of carboxylate to Ti^{4+} and H-bonding interaction between COOH functional group and TiO_2 nanoparticles, as shown in Figure 9.

As TiO_2 could be hybridized with membrane top structure by simply dipping the neat composite membrane in the TiO_2 colloidal solution, a new type of TFC membrane demonstrating great potential on microbial fouling prevention could be easily produced. Apart from TiO_2 addition, there have been other attempts to modify transport properties of RO membranes by employing different types of molecular sieve nanoparticles in PA film [209, 210]. In Figure 10 is depicted the new concept of embedding molecular sieve nanoparticles in the top selective layer in the preparation of thin film nanocomposite (TFN) membrane.

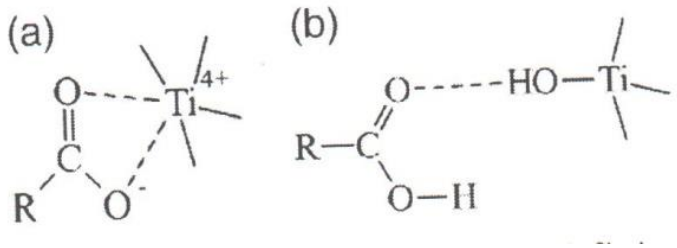

Fig. 9. The mechanism of self-assembly of TiO_2 onto thin film layer, a) by a bi-dentate coordination of carboxylate to Ti^{4+} and b) by an H- the bond between COOH group and surface hydroxyl group TiO_2 nanoparticles. (Ref. 198)

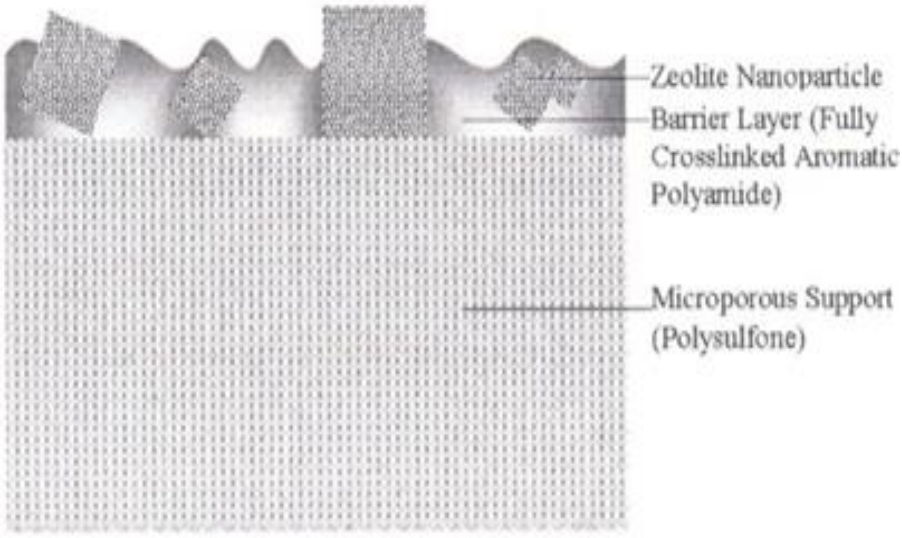

Fig. 10. Schematic cross-section of zeolite nanocomposite membrane (Re-printed with permission from Ref. 209)

The new concept was first started by in early 2007 [209]. In later work, it is experienced that the super-hydrophilic and negatively charged zeolite-A embedded throughout PA thin film was able to dramatically improve the permeability of the TFN membrane and remained

equivalent salt rejection when compared with the pure PA composite membrane. Since the size of the zeolite particles is designed to match the PA film thickness, it thus provides a favorable flow path through each particle incorporated into membrane, leading to high water permeation [210]. This improved membrane water process is just as effective as current technology but more energy efficient and potentially less expensive. In order to further enhance water molecules transport rate, the impregnated bigger pore size of zeolite NaX (0.74 *nm*) was incorporating in the thin film layer with the aim of creating larger molecular tunnels for water to flow [211]. It is found that this particular pore size of zeolite offers preferential flow paths for water molecules of (0.27 *nm*) in diameter but restricts the permeation of hydrated sodium and chloride ions (0.8-0.9 *nm*). Instead of differences in particles' size, controllable design in interfacial chemistry of membrane is also possible using another type of molecular sieves, owing to their tunable functionality with respect to hydrophilicity, charge density and antimicrobial capability. It was recently reported that hydrophilized ordered mesoporous carbons (H-OMCs) modified from pristine OMCs were possible to be used as nano-filler in making thin-film polymer matrix of improved properties [212). It was found that H-OCMs prepared from silica template and argon atmospheric pressure plasma (APP) could be well dispersed in the aqueous solution which was likely to minimize large aggregate particles which appeared on the substrate surface during IP process, leading to high quality of thin film layer formed and considerably improved membrane performances with respect to water permeability and bovine serum albumin adsorption. The incorporation of the very small size of silica particles (20 nm) into PA film was tried in an effort to develop TFN membrane with improved separation performance and enhanced thermal stability [213]. Both water permeability and solute selectivity were reported to increase upon the addition of 1–2 wt. % silica. As experienced by the authors, proper control of particle loading is necessary because membranes prepared at high silica loading tend to display

thicker top film, accompanied with larger pore size and higher pore number density.

Carbon Nano - tube / Polymeric Membranes

In order to overcome the limits of current polymeric membranes, new types of the membrane with higher permeability and salt rejection have been developed. Carbon nano-tubes (CNTs) have caught the attention of many researchers due to the similarity between their fluid transport properties and those of water transport channels in biological membranes [214]. Experimental results of fluid flow in a CNT membrane was first reported in 2004 [215]. These membranes use carbon nanotubes (CNTs) as membrane pores. These membranes are an allotrope of carbon consisting of rolled-up sheets of graphitic layers [216]. An earlier model of mixed CNT membranes which was mainly designed to upgrade a UF membrane with nanotubes was described earlier [217]. The Multi Wall Nano Tubes (MWNTs) (up to 5% by weight volume) were blended with polysulphone (PS), and were tested under operating pressure of 1- 4 $x10^5$ Pa [218]. The MWNTs membranes revealed two pieces of conflicting data according to the molecular weight of solute. For an aqueous solution of poly(ethylene oxide) (MW 100.000) the solute rejection efficiency was (>95% and water flux 14-17 $Lm^{-2}\ h^{-1}$. In contrast to an aqueous solution of polyvinylpyrrolidone (PVP) 55000 the flux was increased to 40 $Lm\text{-}^{2}h^{-1}$ [217]. It was postulated that the plugging effect between both sizes of nanopores and the soluble molecule might contribute to differences and the solute rejection efficiencies and according to them, it seemed to be a dilemma to accomplish a higher permeability and rejection rate at the same time with the mixed-CNT membrane [217-218]. A patent which disclosed the blending of CNTs into solutions, preferably cross-linking agent solutions (trimesoyl of isophthalic chlorides), for the formulation of composite polymeric membranes was realized [219]. In this way CNTs can be effectively embedded into the barrier layer

formed by conventional interfacial polymerization on a micro-porous polyethersulfone support. It was reported that CNTs need to be functionalized to obtain better solubility inorganic solvents. The CNTs membranes can be classified into two categories according to their fabrication methods: i) vertically aligned CNT membranes (VA-CNTs) and ii) mixed (composite CNTs membranes). The first ones are arranged straight up, and perpendicular to the membrane surface and bound each other by an organic or inorganic filler material. Their development is very important because the water flux would be very rapid due to short nano-channel length and compactness of the nanotube forest. The future of VA-CNTs are the following: CNT are aligned vertically, water flux is supposed to be fast dramatically, functional group can be attached at the tip of CNTs or on the membrane surface conveniently, whereas fabrication procedures are complicated, and need specially adjusted operating system [217]. The cylindrical shape of single walled nanotubes (SWNTs) can be imagined virtually by wrapping them in a layer of graphite called graphene [217]. It seems that CNT membranes outperform existing membranes providing higher water flux and lower energy consumption, but they are not yet commercially available. In order to improve the membrane performances, the recent trend in polymer-based membrane research has been to investigate various types of nanocomposite films as an active layer of RO membrane, so-called nanocomposite membranes, in which these films are fabricated using a nanosized filler such as MWCNT, graphene and graphene oxide. Graphene is a carbon-based material considered as a potentially selective material for membranes. Graphene is a single layer of graphite with atomistic thickness, consisting of a lattice of hexagonally arranged sp^2 bonded atom, which exhibits a high breaking strength and impermeability to molecules as small as standard gases including helium [216, 220-221]. These properties suggest that created graphene ultrathin high flux membranes can act as molecular sieves [222]. Furthermore, the roll-to-roll production of graphene on ultra large copper has been developed, which indicates the feasibility

of large-scale membrane fabrication [223]. Some recent studies have explored the transport of ions through pores in graphene membranes [224-225]. For small diameter membranes, the water flux lower through the graphene membrane compared to that of CNT membrane, but for large diameter pores, water flux is higher through the graphene. Thus the graphene membranes can be used as an ultra-efficient water transporter, compared to thin CNT membranes, whenever the diameter is larger than 0.8 *nm* using classical dynamic simulations, the difference in desalination dynamics related to pore size, pore chemistry and hydrostatic pressure applied was examined, but more measurements could be done for water transport and salt rejection in connection with this parameters [222]. The most common graphene-based material is graphene oxide (GO). GO nanosheet additives offer good chemical stability and high surface area. GO-doped PSU polymer matrix exhibits enhanced hydrophilicity, water flux, and salt rejection [226]. Cross-linked GO nanosheets on a polydopamine-modified PES support displayed 4–10 times higher flux 80 and 276 $Lm^{-2}\ h^{-1}\ MPa^{-1}$ (LMH/MPa) than that of most commercial nanofiltration membranes [227]. The schematic illustration of a GO membrane fabrication procedure and reaction mechanisms is shown in the Figure 11.

A high performance of RO thin composite membranes using MWCNT and aromatic polyamide (PA) was successfully prepared by interfacial polymerization. In this regard, MWCNT PA-based membranes have been prepared by several groups and in general, these membranes have exhibited some level of improved performance [228 - 234], see Figure 12. The advantages claimed for these membranes range from increased salt rejection, large fluxes, greater durability, and even antimicrobial properties. MWCNT synthesized by catalytic chemical vapor deposition [235-236] have been widely studied due to their fascinating chemical and physical properties, and among all nanocarbon materials, they can be mass- produced for commercially available applications [237]. The structure of the fully aromatic PA-based RO membrane derived from *m*-phenylendiamine (MPD)-

trimesoyl chloride (TMC) is constrained due to its stoichiometry; the addition of MWCNT can significantly vary their performance due to their unique features such as dispersability diameter, length, straightness, and chemical functionalities, among many others. The SEM of MWCNT-PA nanocomposite membranes are shown in the Figure 12.

Although these past reports acknowledge the key role of MWCNT in aromatic PA nanocomposite membranes, still little attention has been devoted to the mechanisms related to the improvement of flow rate, selectivity and chlorine tolerance [238]. Carbon nanotubes inducing chlorine tolerance are particularly interesting because chlorine sensitivity has been recognized as a major drawback of PA-based RO membranes. Recently the addition of MWCNT to rubber reduce the chlorine-induced degradation of the polymer matrix [239 - 241]. Although the degradation mechanism of rubber by chlorine is different from that of PA, particularly due to the lack of hydrolysis, covalent chlorination is a common problem for both polyamide and rubber. For these reasons, MWCNT are not only promising composite fillers with chlorine protective properties, but might also help to provide mechanical robustness to PA-based RO membrane. The incorporation of MWNTs throughout the superselective thin film layer was also explored as a facile approach to produce superior hydrophilic membrane with fast water molecules transport [242]. As MWNTs were not well-dispersed in the nonpolar solvent of organic phase, a modified IP process was proposed by immersing support membrane into organic phase first prior to the conventional IP process. The TFN membranes have shown to increase both permeability and selectivity (~4.5 $Lm^{-2}\ h^{-1}$ at 0.6 *MPa*, ~78% at 5 *mmol*/L Na_2SO_4) when compared with TFC membrane without MWNTs (~1.6 $Lm^{-2}\ h^{-1}$, ~70%) and TFN membrane prepared by the conventional IP (~2.6 $Lm^{-2}\ h^{-1}$, ~74%). Recent reports on CNT incorporation include the fabrication of multi-walled CNT-blended PES composite membrane *via* the phase-inversion method, and amine functionalized multi-walled CNTs/PES composite membranes, which showed improved hydrophilicity and antifouling properties [105, 243 -244].

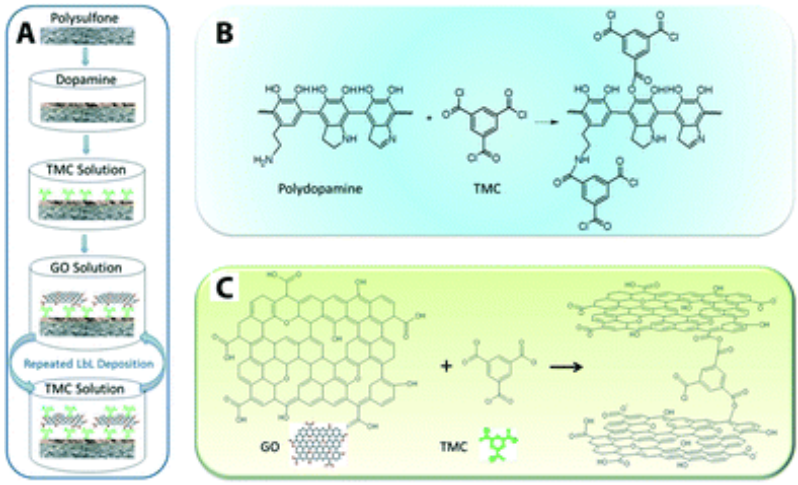

Fig.11. Schematic illustration of (A) GO membrane fabrication procedure, (B) the mechanism of reactions between polydopamine and TMC (cross-linker: 1,3,5-benzenetricarbonyl trichloride), and (C) reaction mechanism between GO and TMC. Reprinted with permission from ref. [245].

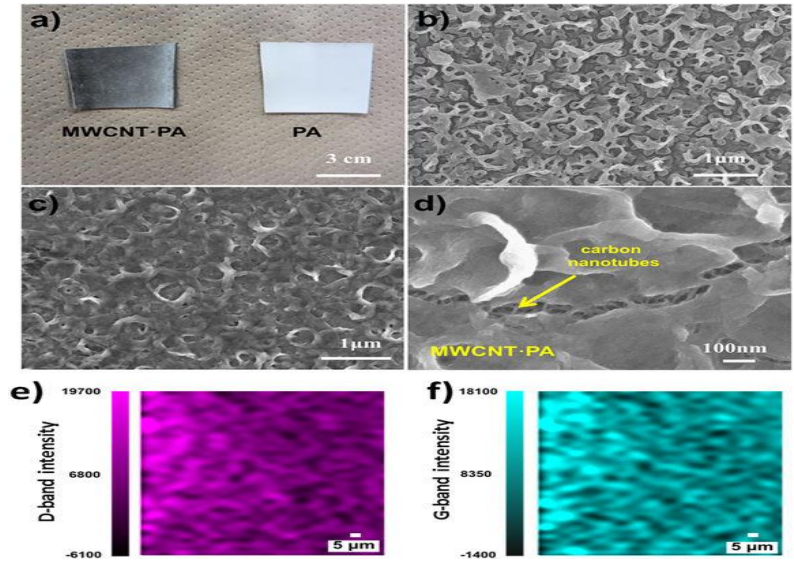

Fig.12. SEM images of MWCNT-PA nanoparticle RO membranes: (**a**) Photographs of a plain PA and a MWCNT·PA nanocomposite (**b**) RO membranes. SEM images of the surface of the plain PA membrane and the (**c**) MWCNT·PA nanocomposite membrane. (**d**) Detail showing the reinforcing nanotubes through a fracture. Raman mapping of the nanocomposite MWCNT·PA membrane showing the intensity of the (**e**) D-band and (**f**) G-band characteristic of carbon nanotubes [228].

This review is expected to benefit the desalination industry by lowering energy and membrane cost, simplifying pre-treatment processes; providing lower membrane maintenance cost; potentially achieving single pass RO desalination; and increasing plant capacity. In this regard, nowadays over the world are installed RO desalination plants of large capacities. For example the Island of Aruba has a large desalination plant of capacity 42.000m^3 per day, Ras Al Khai (Saudi Arabia) 728 million L per day, Sorek (Israel) the largest desalination plant in the world: 627.000m^3 per day, Carlsbad (California) 227304.5 m^3 per day, and 50-75 significant desalination projects per year in USA with an overage capacity of approximately 4546,09 m^3 per day etc.

Conclusions

The advancement of conventional and development of novel membrane materials has made RO the most efficient technology and one of the best performing technologies for desalting sea and brackish water. The development of polymeric materials for RO membranes has been rather slow during the first decade of this century. Current products from major manufacturer of RO desalination membranes are still based on the original chemistry (interfacial polymerization of monomeric aromatic amines, while, asymmetric membrane products are still based on the concept of conventional CA materials. Although the TFC membranes show excellent selectivity and high flux, they are faced with degradation by chlorine and excessive pressure to overcome resistance arising of fouling. Polymeric membranes made via rigid star–shaped amphiphilic molecules, have been a break-through since interfacially polymerized RO/NF membrane has been dominating for years. Despite the high permeability and comparable rejection performance the biomimetic materials membranes are relatively unstable, with particularly severe fouling having been observed. In order to improve the performance, the various modification methods of

conventional membrane materials and fabrication of novel ones has been established. Remarkable progress has been made in establishing new fabrication methods for tailoring membrane pore structures, surface properties, and morphology. The studies on substrate surface properties e.g. pore dimension, surface roughness, hydrophilicity, porosity) could match perfectly with interfacial synthesized PA layer and also to a strong adhesion between active and support layer to overcome the swelling problem which might limit the operations of composite membranes to certain applications. In this regard, composite membrane materials such as GO, CNTs, inorganic NP-based materials and antifouling multifunctional hybrid membranes represent the next generation of progress in membrane technology. Despite recent advances in synthesis of novel membrane materials, surface modification/functionalization methods, and optimization of operating design with designed characteristics especially toward addressing membrane fouling (biofouling, scaling, organic, and colloidal fouling) issues remain urgent need to develop the reliable membranes. The prevention of fouling remains an unsolved problem in water treatment leading to high operational costs and low product efficiency. A high cost of nano-membrane manufacturing process still exists. The further search of these factors may possibly bring to membrane performance and desalination industry advancement in the future.

References

[1] N.H. Afgan, Sustainability concept for energy, water and environment systems, Springer, 2008, pp25-49.

[2] N. L. Le, S. P. Nunues, *Sustainable Materials and Technologies*, 2016, 7, 1-28.

[3] S. Sourirajan and T. Matsuura, Reverse Osmosis /Ultrafiltration Processes Principles, N.R.C. Canada, 1985, Chapter 2.

[4] H. Strathmann, Synthetic membranes and their preparation, in Synthetic Membranes Science, Engineering and Application,

P.M. Bungay et al. (Eds)., Dreidel Publishing Company, Dordrecht, 1986, 181. 1-39.

[5] Baker, Richard: "Membrane Technology and Application", 2nd ed., John Wiley & Sons, Ltd, Chichester, 2004.

[6] T. Uemura and M. Henmi, Advanced membrane technology and Applications, Norman N. Li et al.(eds), Wiley, New Jersey, 2008, pp 3-19.

[7] D. Bargeman and C.A. Smolders, Synthetic membranes and their preparation, in Synthetic Membranes Science, Engineering and Application, Eds by Bungay et al., Dreidel Pub. Company, Dordrecht, 1986, pp 567-579.

[8] C. E. Reidid, E. J. Breton. *J. Appl. Polym. Sci.*, 1959, 1333-143

[9] D. Klemm, B. Heublein, H.-P. Fink and A. Bohn. l *Angew. Chem., Int. Ed.*, 2005, 44, 3393.

[10] E. Saljoughi, T. Mohammadi. *Desalination*, 2009, 243, 1–7.

[11] A. Kumano, N. Fujiwara, Cellulose Triacetate Membrane Technology and Application, John Wiley and Sons Inc., New Jersey, 2008, pp.21

[12] W. M. King, P. A. Cantor, L.W. Schoellenback, C. R. Canon, High-Retention, Reverse Osmosis Desalination Membranes from Cellulose Acetate, in: A. F. Turbak (Ed) Membranes from Cellulose Derivatives, Interscience Publisher, New York 1970.

[13] K. J. Edgar, C. M. Buchanan, J. S. Debenham, P. A. Rundquist, B. D. Seiler, M.C. Shelton, D. Tindall. *Prog. Polym. Sci.*, 2001, 26, 1605-1688

[14] L. Credali, G. Baruzzi, V. Guidotti. Reverse Osmosis Anisotropic Membranes Based on Polypiperazine Amides, Patent Application No. 41295559, (1978)

[15] Y. E. Kirsh, Y. M. Popov. *Russian Chemical Reviews*, 1988, 57, 566.

[16] L. Credali, P. Parrini. *Polymer*, 1971,12, 717-729.

[17] L. Credali, A. Chiolle, P. Parrini. *Desalination*, 1974, 14, 137-150.

[18] J. Glater, S.-k. Hong, M. Elimelech, *Desalination*, 1994, 95, 325-345.

[19] P. Parrini. *Desalination*, 1983. 48, 67-78.

[20] C. Brousse, R. Chapurlat, J.P. Quentin. *Desalination*, 1976,18; 137-153.

[21] M.D. Guiver, A.Y. Tremblay, C.M. Tam, Method of Manufacturing a Reverse Osmosis Membrane and the Membrane So Produced, Patent Application No. 4894159, 1990.

[22] M.K. A.Y. Himeshima. *Polymer Journal*, 1991, 23, 513-520.

[23] S. Hara, K. Mori, Y. Taketani, T. Noma, M. Seno. *Desalination*, 1977, 21, 183-194.

[23] J. Cucera "Reverse Osmosis" Design, Processes, and Applications for Engineers, Wiley, New Jersey, 2010.

[24] H. Sekiguchi, F. Sato, K. Sadamitsu, K. Yoshida, Solute –separating Membrane, Patent Application No.4067804,1978.

[25] K. P. Lee. T. C. Arnot, and D. Mattia, *J. of Membr. Sci.*, 2011,370, 1-22.

[26] F. S. Francis, Fabrication and Evaluation of New Ultra-Thin reverse Osmosis membranes in National technical information Services, 1966.

[27] L. T. Rozelle, J. E. Cadotte, R. D. Corneliussen, E. Erikson, Final Report on Development of New Reverse Osmosis Membrane,1968.

[28] Li D, Wang H. *Journal of Material Chemistry*, 2010, 20, 4551-4566.

[29] B. J. A. Tarboush, D. Rana, T. Matsuura, H. A. Arafat, R. M. Narbaitz. J. *Membr. Sci*., 2007, 289, 258-267.

[30] L. Li, S. Zhang, X. Zhang. *J. Membr. Sci*., 2007, 286, 258-267.

[31] R. J. Petersen, J.E. Cadotte. Thin film Composite Reverse Osmosis membranes, in: M.C. Porter (Ed) Handbook of Industrial Membrane technology, Noyes Publication, New Jersey, 1990.

[32] R. J. Petersen. *J. Membr. Sci.*, 1993, 83, 81-150.

[33] J.E. Cadotte, Reverse osmosis Membranes, Patent Application No.4039444o,1997.

[34] B. Khorshidi,Th. Thundat, B. A. Fleck, M. Sadrzadeh. Scientific Reports, 2016, 6, Article number: 22069.

[35] R.L. Riley, H.K. Lonsdale, C.R. Lyons. *J. Appl. Polym. Sci.*, 1971, 15, 1267-1276.

[36] M. Kurihara, N. Kanamaru, N. Harumiya, K. Yoshimura, S. Hagiwara. *Desalination*, 1980, 32, 13-23.

[37] H. Yasuda, M.O. Bumgarner, H.C. Marsh, N. Morosoff. *Journal of Polymer Science*, 1976, 14, 195-224.

[38] H. Yasuda, H.C. Marsh. *J. Appl. Polym. Sci.*, 1975, 19, 2981-2990.

[39] D.T. Tran, S. Mori, M. Suzuki. *Thin Solid Films*, 2008, 516, 4384-4390.

[40] Amira Abdelrasoul, H, Doan and Ali Lohi, Development of Conventional RO Membranes, Intech, Chapt.2 2017.

[41] Schiffer D.K., Davis R.B., Coplan M.J. Development of Composite Hollow Fiber Reverse Osmosis Systems, 1979.

[42] R.L. Riley, R.L. Fox, C.R. Lyons, C.E. Milstead, M.W. Seroy, M. Tagami. *Desalination*, 1976, 19 , 113-126.

[43] A.J. Naaktgeboren, G.J. Snijders, J. Gons. *Desalination*, 1988, 68, 223-242.

[44] T. Kawaguchi, H. Minematsu, Y. Hayashi, S. Hara, F. Ueda, Amphoteric Ion Permeable Composite Membrane, Patent Appl. No. 4360434, 1982.

[45] P. Eriksson. *J. Membr. Sci.*, 1988, 36, 297-313.

[46] J.E. Cadotte, Interfacially Synthesized Reverse Osmosis Membrane, Patent Appl. No. 4277344, 1981

[47] T. Uemura, Y. Himeshima, M. Kurihara, Interfacially Synthesized Reverse Osmosis Membrane, Patent Appl. No. 4761234, 1988.

[48] S.A. Sundet, Production of Composite Membranes, Patent Appl. No. 4529646, 1985.

[49] S.D. Arthur, Multilayer Reverse Osmosis Membrane of Polyamide-Urea, Patent Application No. 5019264, 1991.

[50] A. Kumano, N. Fujiwara, Cellulose Triacetate Membranes for Reverse Osmosis, in: N.N. Li, A.G. Fane, W.S.W. Ho, T. Matsuura (Eds.) Advanced Membrane Technology and Application, John Wiley & Sons, New Jersey, 2008, pp. 39.

[51] C.R. Bartels. *J. Membr. Sci.*, 1989, 45, 225-245.

[52] K.J. Mysels, W. Wrasidlo. *Langmuir*, 1991, 7, 3052-3053.

[53] W.J. Wrasidlo, Semipermeable Membranes and the Method for the Preparation Thereof, Patent Appl. No. 4005012, 1977.

[54] R.L. Riley, C.E. Milstead, A.L. Lloyd, M.W. Seroy, M. Tagami. *Desalination*, 1966, 23, 331-355.

[55] C.E. Hickman, I. Jamjoom, A.B. Riedinger, R.E. Seaton. *Desalination*, 1979, 30, 259-281.

[56] W.G. Light, J.L. Perlman, A.B. Riedinger, D.F. Needham. *Desalination*, 1988, 70, 47-64.

[57] J.E Cadotte, Reverse Osmosis Membrane, Patent Appl. No. 4259183, 1981.

[58] Y. Kamiyama, N. Yoshioka, K. Matsui, K. Nakagome. *Desalination*, 1984, 51, 79-92.

[59] M. Kurihara, Y. Himeshima. *Polymer Journal*, 1991, 23, 513-520.

[60] J.Y. Koo, R.J. Petersen, J.E. Cadotte, California Meeting., ACS, Anaheim, CA, USA, 1986, pp. 391-392.

[61] J.E. Cadotte, R.J. Petersen, R.E. Larson, E.E. Erickson. *Desalination*, 1980, 32, 25-31.

[62] S.Y. Kwak, S.G. Jung, Y.S. Yoon, D.W. Ihm. *J. Polym. Sci., Part B*: *Polym. Phys.*, 1999, 37, 1429-1440.

[63] J. Glater, M.R. Zachariah, S.B. McCray, J.W. McCutchan. *Desalination*, 1983, 48, 1-16.

[64] R.E. Larson, J.E. Cadotte, R.J. Petersen. *Desalination*, 1981, 38, 473-483.

[65] F. Crowdus. *Ultrapure Water*, 1984, 1, 29-30.

[66] W.G. Light, H.C. Chu, C.N. Tran. *Desalination*, 1987, 64, 411-421.

[67] J.E. Tomaschke. Patent Appl. No. 4948507, 1990

[68] S.A. Sundet, S.D. Arthur, D. Campos, T.J. Eckman, R.G. Brown. *Desalination*, 1987, 64, 259-269.

[69] M. Jenkins, M.B. Tanner. *Desalination*, 1998, 119 ,243-249.

[70] J. J. Qin, Y. Li, L. S. Lee and H. Lee. *J. Membr. Sci.*, 2003, 218, 173–183.

[71] T. Shibutani, T. Kitaura, Y. Ohmukai, T. Maruyama, S. Nakatsuka, T. Watabe and H. Matsuyama. *J. Membr. Sci.*, 2011, 376, 102–109.

[72] F. Soyekwo, Q. G. Zhang, C. Deng, Y. Gong, A. M. Zhu and Q. L. Liu. *J. Membr. Sci.*, 2014, 454, 339–345.

[73] E. Saljoughi and S. M. Mousavi. *J. Environ. Health Sci. Eng.*, 2015,13,42.

[74] A. L. Ahmad, A. A. Abdulkarim, B. S. Ooi and S. Ismail. *Chem. Eng. J.*, 2013, 223, 246–267.

[75] H. R. Lohokare, M. R. Muthu, G. P. Agarwal and U. K. Kharul. *J. Membr. Sci.*, 2008, 320, 159–166.

[76] I. C. Kim, H. G. Yun and K. H. Lee. *J. Membr. Sci.*, 2002, 199, 75–84.

[77] E. Yuliwati and A. F. Ismail. *Desalination*, 2011, 273, 226–234.

[78] F. Liu, N. A. Hashim, Y. Liu, M. R. M. Abed and K. Li. *J. Membr. Sci.*, 2011, 375, 1–27.

[79] G.-D. Kang and Y.-M. Cao. *J. Membr. Sci.*, 2014, 463, 145–165

[80] D. Rana and T. Matsuura. *Chem. Rev.*, 2010, 110,4, 2448–2471

[81] B. Antrim, R. Lesan, B. Liu, A. von Gottberg. *Desalination*, 2005, 178, 313-324.

[82] C. Bartels, M. Hirose, H. Fujioka. *Desalination*, 2008, 221, 207-214.

[83] B. S. Lalia, V. Kochkodan, R. Hashaikeh and N. Hilal, A. *Desalination*, 2013, 326, 77–95

[84] Van der Bruggen B. *J. Appl. Polym. Sci.*, 2009, 114, 630–642.

[85] N. Nady, M.C. Franssen, H. Zuilhof, M. Mohy Eldin, R. Boom, K. Schroen. *Desalination*, 2011, 275, 1-9.

[86] Reddy AVR, Mohan DJ, Bhattacharya A, et al. *J. Membr Sci.*, 2003, 214, 211–221.

[87] Childress AE, Elimelech M. *J. Membr. Sci.*, 1996,119, 253–268.

[88] Kim KJ, Fane AG, Fell CJD. *J. Membr Sci.*, 1989, 43, 187–204.

[89] Ulbricht M, Belfort G. *J. Appl. Polym. Sci.*, 1995, 56, 325–343.

[90] Duarte LT, Habert AC, Borges CP. *Desalination*, 2002, 145, 53–59.

[91] Duarte LT, Pereira CC, Habert AC, et al. *J. Membr Sci.*, 2008, 311, 12–22.

[92] Cheng C, Li S, Zhao W, et al. *J. Membr Sci.*, 2012, 417–418, 228–236.

[93] Lj. Mu, W.Z. Zhao. *Appl. Surf. Sci.*, 2009, 255, 7273-7278.

[94] R. Gerard, H. Hachisuka, M. Hirose, New Membrane Developments Expanding the Horizon for the Application of Reverse Osmosis Technology, Desalination, 1998,119, 47-55.

[95] Hydranautics' Lfc3-Ld Makes Its Début, Membrane Technology, 2005 ,3-3.

[96] M. Wilf, S. Alt. *Desalination*, 2000, 132, 11-19.

[97] G.-D. Kang, C.-J. Gao, W.-D. Chen, X.-M. Jie, Y.-M. Cao, Q. Yuan. *J. Membr. Sci.*, 2007, 300, 165-171.

[98] A. Sarkar, P.I. Carver, T. Zhang, A. Merrington, K.J. Bruza, J.L. Rousseau, S.E. Keinath, P.R. Dvornic, *J. Membr. Sci.*, 2010, 349, 421-428.

[99] C.Y. Tang, Y.-N. Kwon, J.O. Leckie. *Desalination*, 2009, 242, 168-182.

[100] C.Y. Tang, Y.-N. Kwon, J.O. Leckie. *J. Membr. Sci.*, 2007, 287, 146-156.

[101] J.S. Louie, I. Pinnau, I. Ciobanu, K.P. Ishida, A. Ng, M. Reinhard. *J. Membr. Sci.* 2006, 280, 762-770.

[102] Mulder J. Basic principles of membrane technology. Enschede; Netherlands: Springer Science & Business Media; 2012.

[103] Nady N, Schroën K., Franssen M.C.R., et al. *J. Colloid Interface Science*, 2012, 378, 191–200.

[104] Méndez ML, Romero AI, Rajal VB, et al. *Polym. Eng. Sci.*, 2014, 54, 1211–1221.

[105] Vatanpour V, Esmaeili M, Farahani MHDA. *J. Membr. Sci.*, 2014, 466, 70–81.

[106] Wang T, Wang YQ, Su YL, et al. *J Membr Sci.*, 2006, 280, 343–350.

[107] Sotto A, Boromand A, Zhang R, et al. *J. Colloid Interface Sci.*, 2011,363(2):540–550.

[108] L. Zhang, G. Chowdhury, C. Feng, T. Matsuura, R. Narbaitz. *J. Appl. Polym. Sci*., 2002, 88, 3132-3138.

[109] Y.Q. Wang, Y.L. Su, Q. Sun, X.L. Ma, Z.Y. Jiang. *J. Membr. Sci.*, 2006, 286, 228-236.

[110] X. Ma, Y. Su, Q. Sun, Y. Wang, Z. Jiang. *J. Membr. Sci.* 2007, 292, 116–124.

[111] J.Y. Park, M.H. Acar, A. Akthakul, W. Kuhlman, A.M. Mayes. *Biomaterials*, 2006, 27, 856–865.

[112] Y. Su, C. Li, W. Zhao, Q. Shi, H. Wang, Z. Jiang, S. Zhu. *J. Membr. Sci*. 2008, 322,171177.

[113] X. Fan, Y. Su, X. Zhao, Y. Li, R. Zhang, J. Zhao, Z. Jiang, J. Zhu. *J. Membr. Sci.*, 2014, 464, 100–109.

[114] M. K. Sinha and M. K. Purkait. *J. Membr. Sci.*, 2013, 437, 7–16.

[115] W. R. Bowen, T. A. Doneva and H. B. Yin. *J. Membr. Sci.*, 2001, 181, 253–263.

[116] N. Pezeshk, D. Rana, R. M. Narbaitz and T. Matsuura. *J. Membr. Sci.*, 2012, 389, 280–286.

[117] Z. Zhao, Z. Wang, N. Ye, S. Wang, *J. Membr. Sci.*, 2003, 217, 151-158.

[118] Y. Benmakroha, I. Christie, M. Desai, P. Vadgama. *Analyst*, 1996,121, 521-526.

[119] G.S. Gohil, R.K. Nagarale, V.V. Binsu, V.K. Shahi. *Journal of Colloid Interface Science*, 2006, 298, 845-853.

[120] A. Higuchi, N. Iwata, M. Tsubaki, T. Nakagawa. *J. Appl. Polym. Sci.* 1988, 36, 1753-1768

[121] A. Higuchi, N. Iwata, M. Tsubaki, T. Nakagawa. *J. Appl. Polym. Sci*., 1990, 40, 709-717

[122] W.E. Mickols, Method of Treating Polyamide Membranes to Increase Flux, Patent Application No.5755964, 1998.

[123] M.A. Kuehne, R.Q. Song, N.N. Li, R.J. Petersen, Flux Enhancement in TFC RO Membranes, Environ. Prog. 2001, 20, 23-26.

[124] I. Pinnau, B.D. Freeman, ACSSymp. Ser., 1999,744, 1-22.

[125] C.N. Tran, A.C. Maldonado, R. Somanathan, Thin-Film Composite Membrane, Patent Application No. 5234598, 1993.

[126] H. Hachisuka, K. Ikeda, Patent Appl. No. 6177011, 2001.

[127] R. Gerard, H. Hachisuka, M. Hirose. *Desalination,* 1998, 119, 47-55.

[128] P.R. Dvornic, D. A. Tomaslioua. Current opinion in Colloid and Interface Science, 1996, 1, 221-235.

[129] A. Hamza, G. Chowdhury, T. Matssura, S. Sourirajan, J. Appl. polym. Sci. 1997, 129(1) 55-64

[130] N. Nady, M.C. Franssen, H. Zuilhof, M. Mohy Eldin, R. Boom, K. Schroen. *Desalination*, 2011, 275, 1-9.

[131] Gashi S.T., Daci N.M., F Podvorica. I., Selimi T., Thaçi B.S. *Desalination*, 2009, 240, 1-8.

[132] B. Thaçi, S.T. Gashi, F. Podvorica, *Desalination and Water Treatment*, 2018, 118, 96-102.

[131] Pinson, J and Podvorica, F. *Chemical Society Reviews*, 2005, 34, 429-439.

[132] Belanger, D. and Pinson, J. *Chemical Society Reviews*, 2011, 40, 3995-4048.

[133] K.B. Hvid, P.S. Neielsen, F.F. Stengaard. *Membr. Sci.*, 1990, 53, 189-202.

[134] M. Ulbricht, M. Riedel, U. Marxs. *J. Membr. Sci.*, 1990, 120, 239-259.

[135] J. Pieracci, J.V. Crivello, G. Belfort. *J. Membr. Sci.*, 1999, 156, 223-240.

[136] J. Pieracci, J.V. Crivello, G. Belfort. Chem. Mater., 2010, 12, 2123-2133.

[137] R. Reis, M.C. Duke, B.L. Tardy, D. Oldfield, R.R. Dagastine, J.D. Orbell, L. F. Dumee, *Scientific Reports 7*, 2017, Article no. 4426.

[138] Buonomenna MG, Lopez LC, Favia P, d'Agostino, R, Gordano A, Drioli E. *Water Research*, 2007, 41, 4309.

[139] S. Wu, J. Xing, C. Zheng, G. Xu, G. Zheng, J. Xu. *Journal of Appl. Poly. Sci*., 1997, 64, 1923-1926.

[140] A.B. Gil'man. *High Energ. Chem.*, 2003, 37, 17-23.

[141] N.H. Lin, M.-M. Kim, G.T. Lewis, Y. Cohen. *Journal of Materials Chemistry*, 2010, 20, 4642-4652.

[142] Y. Tsujii, K. Ohno, S. Yamamoto, A. Goto, T. Fukuda. *Adv. Polm. Sci.* 2006, 197, 1-45.

[143] G. Kumar, P.J. Smith, G.F. Payne. *Biotechnol. Bioeng*., 1999, 63, 154–165

[143] T. Chen, G. Kumar, M.T. Harris, P.J. Smith, G.F. Payne. *Biotechnol. Bioeng.*, 2000, 70 564–573.

[144] Matyjaszewski, K.; Tsarevsky, N. V. Nature Chemistry, 2009, 1, 276-288)

[145] Zhao C, Xue J, Ran F. and Sun S. *Prog Mater Sci.* 2013, 58, 76–150.

[146] Su.B, Sun S, Zhao C. Progress in hemodialysis –from emergent biotechnology to clinical practice: In Tech; 2011

[147] Xiang, T., Yue WW., Wang, R., Liang, S., Sun, S.D., Zhao, C.S. *Colloids surfaces*, 2013, 110, 15-21.

[148] Y. Song, P. Sun, L.L. Henry, B. Sun. *J. Membr. Sci.* 2005, 251 67-79.

[149] S.K. Karode, S.S. Kulkarni, A.K. Suresh, R.A. Mashelkar. *Chem. Eng. Sci.* 1998, 53, 2649-2663.

[150] S.S. Dhumal, S.J. Wagh, A.K. Suresh. *J. Membr. Sci.* 2008, 325, 75-771.

[151] A. K. Ghosh, B.-H. Jeong, X. Huang, E.M.V. Hoek. *J. Membr. Sci.* 2008, 311, 34-45.

[152] A. K. Ghosh, E.M.V. Hoek. *J. Membr. Sci.*, 2009, 336,140-148.

[153] M. M. Chau, W.G. Light, H.C. Chu. Patent Application No. 4983291, 1991.

[154] J.-y. Koo, N. Kim, Patent Appl. No. 6015495, 2000.

[155] M. Hirose, K. Ikeda. Patent Appl. No. 5576057, 1996.

[156] W.E. Mickols. Patent Appl. No. 6878278, 2005.

[157] B.J.A. Tarboush, D. Rana, T. Matsuura, H.A. Arafat, R.M. Narbaitz. *J. Membr. Sci.* 2008, 289, 166-175.

[158] M.S. Mauter, M. Elimelech. *Sci. Technol.*, 2008, 42, 5843-5859.

[159] Y. Lu, T. Suzuki, W. Zhang, J.S. Moore, B.J. Mariñas. *Chem. Mater.*, 2007, 19, 3194-3204.

[160] T. Suzuki, Y. Lu, W. Zhang, J.S. Moore, B.J. Mariñas. *Environ. Sci. Technol*. 2007, 41, 6246-6252.

[161] Y. Yang, W. Li, H. Zhou, X. Zhang and M. Zhao. Scientific Reports 6, 2016, Article no: 29218.

[162] Nicolai A, Sumpter BG, Meunier V. *Phys. Chem. Chem. Phys.*,2014, vol.16, Issue 18, 8646-8654.

[163] E. M. Van Wagner, A.C. Sagle, M.M. Sharma, Y-H. La and B.D. Freeman. *J. Membr. Sci.* 2011, 367, 273-287.

[164] M. Kumar, M. Grzelakowski, J. Zilles, M. Clark, W. Meier. *PNAS*, 2007, 104, 20719-20724.

[165] A. Gonzalez-Perez, K.B. Stibius, T. Vissing, C.H. Nielsen, O. G. Mouritsen. *Langmuir*, 2009, 25, 10447-10450.

[166] A. Taubert. *PNAS*, 2007, 104, 20643-20644

[167] L. Lia, J. Dong, T.M. Nenoff, R. Lee. *Desalination*, 2004, 170, 309-316.

[168] P. H. Jesen, D. Kelleer, C.H. Nielsen, Membrane Filtering of water, Patent Appl. OEP18854 77,2010.

[169] Anna Lee, J.W. Elam and S.B. Darling. *Environ. Sci. Water Res. &Technol.* 2016, 2, 17-42

[170] M. C. Porter, Handbook of industrial membrane technology, Noyes publication, Westwood, New Jersey, USA,1990

[171] W. S. Winston Ho and K. K. Sirkar, Membrane Handbook, Springer Science & Business Media, New York, 1992

[172] Comprehensive Membrane Science and Engineering, ed. E. Drioli and L. Giorno, Elsevier B.V., 2010.

[173] Duke MC, O' Brien-Abraham J, Milne N, Zhu B, Lin JYS et al, *Sep. and Purif. Technol*., 2009,68,343 -350

174] Lin J, Murad S, *An international Journal at the Interface between Chemistry and Physics*, 2001,99,1175-1181

[175] C.A.M. Siskens, Chapter 13, in: A.J. Burggraaf, L. Cot (Eds.) Membrane Science and Technology, Elsevier, 1996, pp. 619-639.

[176] A.K. Pabby, S.S.H. Rizvi, A.M. Sastre, Handbook of Membrane Separations: Chemical, Pharmaceutical Food and Biotechnological Applications, in, CRC Press, Boca Raton, 2009.

[177] L. Gazagnes, S. Cerneaux, M. Persin, E. Prouzet, A. Larbot, *Desalination*, 2007, 217, 260-266.

[178] M.C. Duke, S. Mee, J.C.D. da Costa, *Water Res*. 2007, 41, 3998-4004.

[179] W. Kujawski, S. Krajewska, M. Kujawski, L. Gazagnes, A. Larbot, M. Persin, *Desalination*, 2007, 205, 75-86.

[180] L. Lia, J. Dong, T. M. Nenoff, R. Lee, *Desalination*, 2004, 170, 309-316.

[181] C. Baerlocher, L.B. McCusker, D.H. Olson, Atlas of Zeolite Framework Types, 6th ed., Elsevier, Amsterdam, 2007.

[182] L. Li, J. Dong, T.M. Nenoff, R. Lee. *J. Membr. Sci*. 2004, 243 401-404.

[183] A. Rodrigez-Calvo et al, *Hydrology Current Research*, 2004, 5, 167.

[184] Kaufman, Y., Berman, A. and Freger, V. *Langmuir*, 2010, 26, 7388-7395.

[185] Kurihara M, Fusaoka Y, Sasaki, T, Bairinii R and Uemura T, Desalination (1994a), 96,133.

[186] F. Jareman, J. Hedlund, J. Sterte. *Sep. Purif. Technol.* 2003, 32, 159-163.

[187] M.C. Duke, J. O'Brien-Abraham, N. Milne, B. Zhu, J.Y.S. Lin, J.C. Diniz da Costa. *Sep. Purif. Technol*. 2009, 68, 343-350.

[188] L. Li, N. Liu, B. McPherson, R. Lee, *Industrial & Engineering Chemistry Research*, 2007, 46, 1584-1589.

[189] N. Liu, L. Li, B. McPherson, R. Lee, *J. Membr. Sci.* 2008, 325,357-361.

[190] J. Lu, N. Liu, L. Li, R. Lee. *Sep. Purif. Technol*. 2010, 72, 203.

[191] Y. Gogosti, A. Nikitin, H. Ye, W. Zhou, Je. Fisher, B.Yi, H.C.Foley, M. Barsoum. *Nat Mater*, 2003, 2, 591-594.

[192] E. Okumus, T. Gurkan, L. Yilmaz. *Sep. Sci. Technol*. 1994, 29, 2451 -2473.

[193] A.F. Ismail, P.S. Goh, S.M. Sanip, M. Aziz. *Sep. Purif. Technol.* 2009, 70, 12-25

[194] J. Yin and B. Deng. *J. Membr. Sci.*, 2015, 479, 256–275.

[195] P. Wang, J. Ma, F. Shi, Y. Ma, Z. Wang and X. Zhao. *Ind. Eng. Chem. Res.*, 2013, 52, 10355–10363

[196] P. S. Goh, B. C. Ng, W. J. Lau and A. F. Ismail. *Sep. Purif. Rev*. 2015, 44, m216–249

[197] W. J. Lau, A. F. Ismail, P. S. Goh, N. Hilal and B. S. Ooi. *Sep. Purif. Rev*. 2015, 44, 135–156.

[198] W. J. Lau, A. F. Ismail, N. Misdan and M. A. Kassim. *Desalination*, 2012, 287, 190–199

[199] A. F. Ismail, M. Padaki, N. Hilal, T. Matsuura and W. J. Lau. *Desalination* 2015, 356, 140–148.

[200] T.V. Ratto, J.K. Holt, A.W. Szmodis, Patent Appl. No. 20100025330, 2010.

[201] P. Agre. *Biol. Cell*, 2005, 97, 355-356.

[202] M. Kumar, M. Grzelakowski, J. Zilles, M. Clark, W. Meier. PNAS, 2007, 104, 20719-20724.

[203] M. L. Luo, J. Q. Zhao, W. Tang and C. S. Pu. *Appl. Surf. Sci*., 2005, 249, 76–84

[204] S. Balta, A. Sotto, P. Luis, L. Benea, B. Van der Bruggen and J. Kim. *J. Membr. Sci.*, 2012, 389, 155–161

[205] M. Liu, Z. Jia, D. Jia and C. Zhou, *Prog. Polym. Sci.*, 2014, 39, 1498–1525

[206] P. C. Bernardes, N. J. de Andrade, L. H. M. da Silva, A. F. de Carvalho, P. E. Fernandes, E. A. Araujo, C. A. Lelis, P. C. G. Mol and J. P. N. de Sa. *J. Nanosci. Nanotechnol.*, 2014, 14, 6355– 6367

[207] Lee HS, Im SJ, Kim JH, Kim HJ, Min JP, et al, *Desalination*, 2011, 219, 48-56

[208] S.H. Kim, S.-Y. Kwak, B.-H. Sohn, T.H. Park. *J. Membr. Sci*. 2003, 211, 157-165

[209] B.-H. Jeong, E.M.V. Hoek, Y. Yan, A. Subramani, X. Huang, G. Hurwitz, A.K. Ghosh, A. Jawor, J. *Membr. Sci.* 2007, 294 1-7.

[210] M.L. Lind, A.K. Ghosh, A. Jawor, X. Huang, W. Hou, Y. Yang, E.M.V. Hoek, *Langmuir*, 2009, 25, 10139-10145.

[211] M. Fathizadeh, A. Aroujalian, A. Raisi. *J. of Membr. Sci.* 2011, 375, 88-95.

[212] E.-S. Kim, B. Deng. *J. of Membr. Sci.* 2011, 375, 46-54.

[213] G.L. Jedah, P.S. Singh, *J. Membr. Sci.* 2009, 328, 257-267

[214] A. Noy, H.G. Park, F. Fornasiero, J.K. Holt, C.P. Grigoropoulos, O. Bakajin. *Nano Today*, 2007, 2, 22-29.

[215] B.J. Hinds, N. Chopra, T. Rantell, R. Andrews, V. Gavalas, L.G. Bachas. *Membr. Sci.* 2004, 3, 62-65.

[216] Humplic T, Lee J, O'Hern Sc, Fellman BA, Baig Ma et al, Nanotechnology, 2011, 22, 1-19.

[217] Ahn C., Baek Y, Lee C, Kim So et al, *J. of Industrial and Engineering Chemistry*, 2012 ,18, 1551-1559.

[218] Choi JH, Jegal J, Kim WN. *J. of Membr. Sci*, 2006, 284, 406-415.

[219] T. V. Ratto, J. K Holt, A. W. Szmodis. Patent application No.20100025330, 2010.

[220] Lee C, Wei X, Kysar JW, Hone, J. *Science*, 2008, 321, 385-388.

[221] Bunch J.S, Verbridge SS, Alden JS, van der Zande AM, Parpia JM, et al. *Nano Letters*, 2008, 8, 2458- 2462.

[222] Cohen-Tanugi D, Grossman JC. *Nano Letters*, 2012, 12, 3602-3608.

[223] Bae S, Kim H, Lee Y, Xu X, Park JS, et al. *Nature Nanotechnology*, 2010, 5, 574-578.

[224] Sint K, Wang B, Kral P. *Journal of the American Chemical Society*, 2008, 130, 16448- 16449.

[225] Suk ME, Aluru NR. *The Journal of Physical Chemistry Letters* 2010,1, 1590-1594.

[226] B. M. Ganesh, A. M. Isloor and A. F. Ismail. *Desalination*, *313*, 199–207 (2013)

[227] M. Hu and B. Mi. *Environ. Sci. Technol.*, 2013, 47, 3715-3723.

[228] Sh. Inukai, R. Cruz-Silva, J. Ortiz-Medina, A. Morelos-Gomez, K. Takeuchi, T. Hayashi, A. Tanioka, T. Araki, S. Tejima, T. Noguchi, M. Terrones, M. Endo. *Scientific Reports*, 2015, 5, 13562. Doi: 10.1038/srep13562 .

[229] H. Y. Zhao, S. Qiu,' L.Wu', L. Zhang, H. Chen, C. Gao. *J. of Membr. Sci.* 2014, 450, 249–256.

[230] H. J. Kim. K. Choi, Y. Baek, D.G. Kim, J. Shim, Je. Yoon, J.C. Lee. *ACS Applied Materials & Interfaces*, 2014, 6, 2819–2829.

[231] W. F. Chan. H. Chen,'A. Surapathi, M. G. Taylor, X. Shao, E. Marand, J. K. Johnson. ACS Nano, 2013, 7, 5308–5319.

[232] A. Tiraferri, C.D. Vecitis, M. Elimelech. *ACS Applied Materials & Interfaces*, 2011, 3, 2869–2877.

[233] J. N. Shen, C. C. Yu, H. M. Ruan, C. J. Gao & B. Van der. Bruggen. *J. of Membr. Sci.* 2013, 442, 18–26.

[234] L. Zhang, G. Z. Shi, S. Qiu, L. H. Cheng and H. L. Chen. Desalination and Water Treatment, 2011, 34, 19–24.

[235] Oberlin, M. Endo & T. Koyama. *J. of* Crystal Growth, 1976, 32, 335–349.

[236] M. Endo. Grow carbon fibers in the vapor phase. *Chemtech*,1988, 18, 568–576.

[237] M. Endo, T. Hayashi and Y. A. Kim. *Pure and Applied Chemistry*, 2006.78, 1703–1713.

[238] J. Glater, S.K. Hong, M. Elimelech. *Desalin*, 1994, 95, 325–345.
[239] G. D. Kang, C.J. Gao, W.D. Chen, X.M. Jie, Y.M. Cao and Q. Yuan. *J. of Membr. Sci.* 2007,300, 165–171.
[240] Y. N. Kwon & J. O. Leckie. *J. of Membr. Sci.* 2006, 283, 21–26.
[241] M. Endo. *et al.* Industrial & Engineering Chemistry Research, 2010, 49, 9798–9802
[242] H. Wu, B.T ang, P. Wu. *J. Phys. Chem. C*, 2010, 114, 16395-16400.
[243] A. Rahimpour, M. Jahanshahi, S. Khalili, A. Mollahosseini, A. Zirepour and B. Rajaeian. *Desalination*, 2012, 286, 99–107.
[244] E. Arkhangelsky, D. Kuzmenko, V. Gitis. *J. of Membr. Sci.*, 2007, 305, 176-184.
[245] M. Hu, B. Mi. *Environ. Sci. Technol.* 2013, 47, 3715-3723.

ZHVILLIMI I MATERIALEVE TË MEMBRANAVE TË OSMOZËS SË KUNDËRT DHE PROGRESI I TYRE NË TË ARDHMEN: PUNIM REVIAL

Salih T. Gashi

Përmbledhje

Përsosja e materialeve konvencionale dhe zhvillimi i materialeve të reja e ka bërë osmozën e kundërt (OK) një ndër teknologjitë më efikase dhe më së shumti të përdorur për shkripëzimin e ujit të detit dhe në përgjithësi ujërave të njelmët. Zhvillimi i materialeve polimerike të membranave të OK ka qenë disi i ngadalshëm gjatë dekadës së parë të këtij shekulli. Produktet aktuale nga prodhuesit më të mëdhenj të membranave të OK ende bazohen në polimerizimin ndërfaqësor të aminave aromatike ndërsa ato të membranave asimetrike bazohen në konceptin e materialeve konvencionale të acetatit të celulozës. Megjithëse membranat kompozite me film të hollë tregojnë selektivitet të shkëlqyeshëm dhe fluks të lartë, ato degradohen nga klori dhe shtypja e tepërt që përdorët për ta mposht rezistencën që zakonisht rritet gjatë shtupimit. Membranat polimerike të gatitura përmes molekulave amfifilike në formë të yllit kanë qenë zbulim i rëndësishëm, meqë membrana RO/NF e gatitur me polimerizim ndërfaqësor ka dominuar më vite. Përveç permeabilitetit të lartë dhe performancës krahasuese të separimit, materialet membranat biomimetike janë relativisht jostabile, në veçanti te ato është vërejtur shtupim i madh i membranës. Me qëllim të përmirësimit të performancës së materialeve konvencionale dhe të reja, janë studjuar metoda të ndryshme të modifikimit dhe fabrikimit. Progres i dukshëm është bërë në zhvillimin e metodave të reja për të cilat mundësojnë

ndikimin në formimin e strukturës poroze, të vetive sipërfaqësore dhe të morfologjisë të membranave. Studimet e vetive sipërfaqësore të substratit p.sh. dimenzioni i poreve, vrazhdësia e sipërfaqës, hidrofiliciteti dhe poroziteti përputhen në mënyrë perfekte me shtresën e sintetizuar ndërfaqësisht të PA dhe gjithashtu me adhesionin e fortë midis shtresës aktive dhe mbajtëse për të kapercyer problemet e mufatjës që mund të kufizojnë operacionet e membranave kompozite në zbatime të caktuara. Nga ky veshtrim materialet e membranave kompozite siç janë: oksidi i grafitit, nanotubat e karbonit, materialet inorganike të bazuara në nanogrimca dhe membranat hibride multifunksionale antishtupuese paraqesin gjeneratën e ardhëshme të progresit të teknologjisë së membranave. Pavarësisht përparimeve në sintezat e materialeve të reja membranore dhe në metodat e modifikimit të sipërfaqës së tyre me molekula të ndryshme organike si dhe optimizimi i konstruksionit të operimit të tyre, zgjidhja e problemit të shtupimit të membranes (bioshtupimi, shtresimi, shtupimi organik dhe koloidal) mbetet kërkesë urgjente për zhvillimin e membranave të sigurta. Parandalimi i shtupimit ngel problem i pazgjidhur në trajtimin e ujit duke rritur shpenzimet operacionale dhe zvogëluar rendimentin. Kostoja e lartë e prodhimit të nanomembranave ende ekziston. Studimi i mëtutjeshëm i këtyre faktorëve mund të çoj në përmirësimin e performancës së membranes dhe industrisë shkripëzuese në të ardhmen.

KDU 53 (081)

TRANSFORMATIONAL APPROACH SPACE-TIME VARIANT MAGNETIC AND ACOUSTIC FIELD ANALYSIS

Myzafere Limani[a, b]

Abstract

The degree, to which the concept of transformational analogy of electromagnetic field can be applied to other fields such as acoustics and optics, remains an open question. In this paper, the analogy between the acoustic and magnetic field is shown by the action of Lorentz's force. The Lorentz's force (the force acting on currents in a magnetic field) plays an increasingly larger role in techniques applied to visualize current and conductivity in several applications including magneto-acoustic imaging of current, "Hall effect" imaging, ultrasonically-induced Lorentz force imaging of conductivity, magneto-acoustic tomography with magnetic induction, and imaging using magnetic resonance. Based on the experimental laws (Coulomb's law and the law of acoustic pressure action) using the fundamental postulates of the special theory of relativity and Lorentz's transformations, this transformational approach describes the genesis of the acoustic field as entirely analogous to the magnetic field. This analogy is based on the mathematical relations used to describe these phenomena, not on the phenomena themselves. According to this approach, the propagation velocity of acoustic waves depends only from the characteristics of the

[a] Akademia e Shkencave dhe e Arteve e Kosovës, Rr. "Agim Ramadani" nr 305, 10000 Prishtina, Kosovë myzaferelimani@ashak.org

[b] FIEK, Universiteti i Prishtinës, Rr. "Nëna Terezë" nr. 5. 10000 Prishtina, Kosovë

medium, and the influence of the relative velocity between the source and the observer defines the source frequency shift according the Doppler's effect. Defining the pure physical argument of the acoustic field *A* as the analogue of the magnetic field *B*, and in other hand the acoustic pressure *P* and electric field *E*, it is shown that this "dependence" cannot represent limitation to the full extent of the formal analogy between these fields.

Keywords: *transformational approach, magnetic field, acoustic field, electrostatic field, acoustic pressure, Lorentz's force, formal analogy*.

Introduction

Information, like energy, has a wonderful feature that can change its shape from time to time without losing its content. "Signal" is usually understood as encoded information, such as time varying amplitude in time or frequency modulated in electromagnetic or acoustic waves, acting as "carriers". Information travels along with the wave, with velocity of light or sound, and is decoded at a later stage in the receiver. But this movement is not completely free, because the electromagnetic and acoustic waves are limited by physical laws of propagation and scattering. The effects of these laws on communications are usually ignored when it comes to signal analysis and processing. But, physical laws are in some sense the codes themselves, and are indeed unchangeable, absolute codes. Therefore, a co-existence and interaction of these two codes (physical laws and encoded information) should be sought.

At the transmission stage it is possible to suggest a preferred choice of carrier and code, while in the receiving phase better decoding methods can be suggested, taking to account the full advantages of the carrier's nature and using them for precise understanding of the impact of the "medium" in the "message". Medium impact is of particular importance in the case when the medium itself presents a "message" e.g. in optics, radar, sonar and biomedical diagnostics. In these cases, the

initial signal is usually trivial (for example, light or sound beam) and the information required by the receiver is the distribution and nature of the reflectors and absorbers [1].

To explain and mathematically formulate the relation between signal analysis and physics, they must first be formulated both in the same language or code. For signals, this means any choice of the scheme for analysis and synthesis. For electromagnetic waves, the "code" is very limited in choice, and consists of the physical laws of propagation and scattering. It makes sense, then, to start with physics and use appropriately formulated electromagnetic laws. The analysis of electromagnetic signals is based on space-time analysis, and therefore the propagation of acoustic waves can be formulated very naturally through the generalized space-time analysis [2].

Space-time electromagnetic analysis is a natural choice for these fundamental reasons: Maxwell's free space equations are invariant for a set of transformations, called the conformal group *c*, which includes space-time translation and expansion. This means that if any solution is translated for an arbitrary amount in space or time, it remains a solution. Similarly, the solution can be uniformly scaled in space-time, and again remain the solution. Since these operations are used for electromagnetic analysis, it is very reasonable to expect a similar analysis to be used in acoustics and this is the basis of the transformational approach [7].

Transformational approaches have revolutionized the way of designing contemporary equipment. Using the analogy of the basic equations of a certain class of physical fields, high reliability devices can be constructed. In recent years, these approaches have been successfully applied in optics. Transformational optics is an emerging field (first proposed in 2006) [8, 9] that enables the creation of curved light geometry by adapting the optical message it conveys through the medium [10]. Thus, with the help of the transformational optics, a new arena for the creation of optical devices is provided at the level which is difficult to achieve with classical design methods.

Recently, there have been attempts to implement transformational approaches to acoustic systems. Following the transformational optics procedure, a correspondence between medium parameters and coordinate transformations is applied to the acoustics. Transformational acoustics are based on the invariance of the acoustic wave equation under a certain set of coordinate transformations [12, 13]. Another prediction of this approach includes "external acoustic enclosure" where hidden object and resources are located in the same domain and the object is exposed to external sound (diagnostic sonography or ultrasonography).

Lorentz's Transformations and Space-Time Variant Fields

At the beginning of the twentieth century, Einstein, Bohr and Born worked on advancing the mathematical model of Maxwell's equations and exposed some limitations of these equations regarding quantum theory and theory of relativity. Based on Einstein's special theory of relativity, Page, in 1912, derived all Maxwell's equations from Coulomb's law. Such an approach in extracting Maxwell's equations displaces the ambiguity of the origin of the magnetic field and improves the understanding of these equations. This approach will be used in this work to extract the acoustic field's origin in order to show the full extent of formal analogy between the acoustic and magnetic fields.

The proposed transformational method in this approach, entails as an essential prerequisite the existence of an auxiliary abstract relativistic system (we use ''relativistic'' in the general relativity sense of form-invariance under any space-time coordinate transformation) which is analogue to (i.e., possesses the same mathematical structure) the relevant coordinate system (e.g., Cartesian). There is no need for the analogue model to have any direct physical meaning. In many cases, the equations under consideration are form-invariant only under a certain subset of transformations, limiting the technique to this subset.

The Lorentz force action will be explained with the system of two observers located in reference frames *O* and *O'* as shown in Fig.1. In order to be more explicit, we will assume that the Cartesian coordinate system axes of the two observers are parallel and that the reference frame (*O'*) slides along the axis *z* regarding to the reference frame (*O*) with constant velocity **u**.

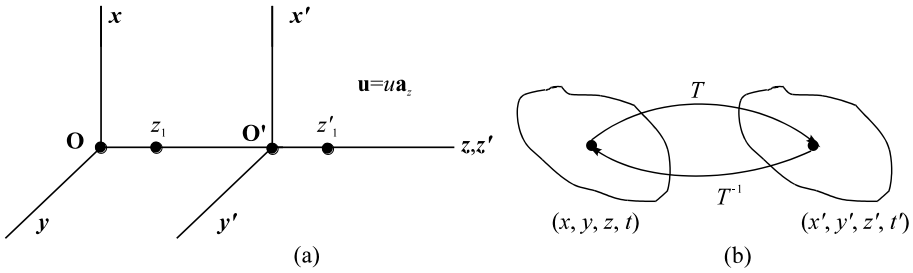

Fig.1. Observers *O* and *O'* are fixed in coordinate systems moving with relative constant velocity **u**.

(a) Orientation of the coordinate system. (b) Transformations *T* and *T '*.

Linear mathematical transformations between these two systems is also assumed, such that each point in the coordinate system (*x*, *y*, *z*, *t*) (Fig. 1. b), under transformation *T* is transformed to a point in the system (*x'*, *y' z'*, *t'*). Transformation *T* should be unequivocal for a given instant of time, such that the point z_1 will be transformed to the point z'_1 in the second coordinate system. Transformation T^{-1} has the same properties. Since there is no relative movement along the *x* or *y* axes, the corresponding transformations are equal to 1. For the observer in the reference frame *O*, any static force field in the *O'* frame will be space-time variant due to the frame movement with relative velocity **u**. One of the fundamental laws of physics, Newton's second law, yields the two forces **F** and **F'** acting in the respective reference frames. To define these forces, we consider material point *p* associated with the reference frame *O'* moving with relative velocity **v** with respect to the frame *O*

(Fig.2). The complete derivation of the relations of ***F*** and **F'** due to Lorentz's force transformations are not given here [14], but they will be applied for solutions of magnetic and acoustic fields. For observer *O* Lorentz's transformation of **F** components to **F'** components are given with following expressions:

$$F'_x = k\,gF_x$$

$$F'_y = k\,gF_y \tag{1}$$

$$F'_z = F_z - \frac{gu}{c^2}\left(v_x F_x + v_y F_y\right)$$

Constant *k* represents the contraction constant given by $k = \sqrt{1-\frac{u^2}{c^2}}$, *c* is the velocity of wave propagation in the medium (acoustic wave velocity and electromagnetic wave velocity) and constant *g* represents the relation between the relative velocities of the frame and the velocity *c* and is expressed as $g \equiv \frac{1}{1-\frac{uv_z}{c^2}}$. For this study case it is assumed that:

$u \ll c$ And $v_z \ll c \rightarrow g = 1$

The inverse transformation of the force components is given by:

$$F_x = \frac{1}{kg}F'_x$$

$$F_y = \frac{1}{kg}F'_y \tag{2}$$

$$F_z = F'_z + \frac{u}{kc^2}\left(v_x F'_x + v_y F'_y\right)$$

The orientations of coordinate axes and relative velocity **u** are the same. Note that the components of velocity **v** are given also in Cartesian coordinate system (*x*, *y*, *z*, *t*).

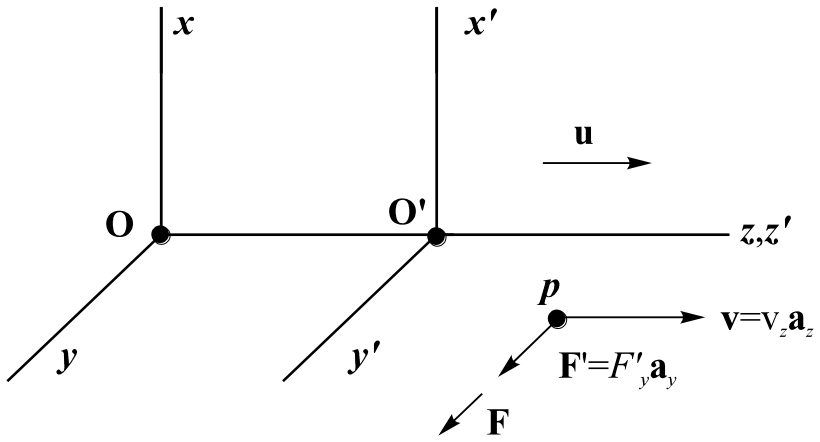

Fig.2 Observers *O* and *O′* experience different forces in the particle *p*.

Force **F** experienced from observer *O* can be obtained applying Lorentz's transformations in **F'**. Assume that the force **F** expressed in vector terms is:

$$\mathbf{F} = F_x \mathbf{a}_x + F_y \mathbf{a}_y + F_z \mathbf{a}_z \tag{3}$$

Using expressions (1) and (2) and applying those in (3) yields to formulations of **F**, in following form:

$$\mathbf{F} = \left(\frac{1}{k} F'_x \, \mathbf{a}_x + \frac{1}{k} F'_y \, \mathbf{a}_y + F'_z \, \mathbf{a}_z \right) + \left[\frac{u}{kc^2} \mathbf{v} \times \left(\mathbf{a}_z \times \mathbf{F}' \right) \right] \tag{4}$$

The advantage of this expression lies in its simplicity of usage in formulating the origins of the magnetic and acoustic fields. The velocity

of particle **v** appears only as vector product with other terms inside the brackets.

Space-Time variant Electric and Magnetic fields

Consider two systems of observers *O* and *O'* as is shown in Fig.3., Assuming reference frame of observer *O'* sliding along *z* axis with respect to the reference frame of observer *O*, and relative velocity between the two referent frames is **u**.

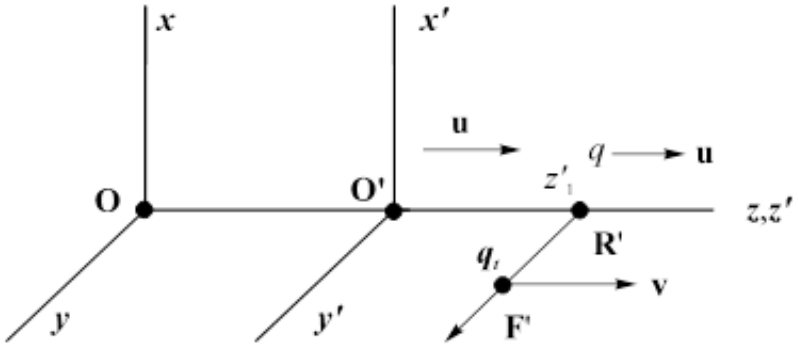

Fig.3 Moving charge *q* acts in testing charge q_t according to the Coulomb's law.

Assume there is an electrostatic field **E'** across the whole region. This electrostatic field can be caused by an electric charge fixed at the point z'_1 of the coordinate system (*x', y', z', t'*). Since the charge is fixed regarding the observer *O'*, the electrostatic field is also fixed. If there is a test charge q_t in this region, then force **F'** caused by *q*, will act on the

testing charge. Considering the charge q fixed to reference frame of observer *O'*, the only force detected from observer *O'* in the test charge will be Coulomb's force given by:

$$\mathbf{F'} = \frac{q\, q_t}{4\pi\, \varepsilon_0} \frac{\mathbf{R'}}{(R')^3} = q_t \mathbf{E'} \tag{5}$$

The electrostatic field **E'** detected by observer *O'* can be obtained from:

$$\mathbf{E'} = \frac{F'_x}{q_t}\mathbf{a}_x + \frac{F'_y}{q_t}\mathbf{a}_y + \frac{F'_z}{q_t}\mathbf{a}_z \tag{6}$$

The force field is given in Cartesian coordinates as:

$$\mathbf{F'} = F'_x\, \mathbf{a}_x + F'_y\, \mathbf{a}_y + F'_z\, \mathbf{a}_z \tag{7}$$

For the observer *O'*, both the force field and the electric field are static fields and therefore the theory of electrostatic fields can be applied here. For observer *O*, the charge is sliding along the *z* axis and consequently the force field and the electric field appear as space-time variant. If we assume the definition of force field by the Coulomb's law for the static case, as is seen by observer *O'*, using Lorentz's transformations, the dynamic force field (space-time variant field) can be assigned. It is also assumed that the charge is invariant to Lorentz's transformations. In this way, the acting force in the particle q_t detected by observer *O*, according to the equation (4) will be

$$\mathbf{F} = \left(\frac{1}{k} F_x'\, \mathbf{a}_x + \frac{1}{k} F'_y\, \mathbf{a}_y + F'_z\, \mathbf{a}_z\right) + \frac{u}{k\, c^2}\left[\mathbf{v} \times \left(\mathbf{a}_z \times \mathbf{F'}\right)\right] \tag{8}$$

In the Equation (8) the velocity **v** is the particle q_t velocity with respect to the observer *O*, and *k* is the contraction factor. Under assumption that the velocity **v** is zero, the observer *O* will detect a force field **F** and an electric field **E** given by:

$$\mathbf{F} = \frac{1}{k} F'_x \mathbf{a}_x + \frac{1}{k} F'_y \mathbf{a}_y + F'_z \mathbf{a}_z \tag{9}$$

$$\mathbf{E} = \frac{\mathbf{F}}{q_t} = \frac{1}{k} E'_x \mathbf{a}_x + \frac{1}{k} E'_y \mathbf{a}_y + E'_z \mathbf{a}_z \tag{10}$$

Equation (10) represents the transformation of electric field as seen by *O'* to the field as seen by observer *O*. Individual transformed components of this field are:

$$E_x = \frac{E'_x}{k}, \qquad E_y = \frac{E'_y}{k}, \qquad E_z = E'_z \tag{11}$$

It should be noted that if the relative velocity **u** between two reference frames is equal to zero, the contraction factor *k* is equal to 1, and thus the electric fields in both frames are identical. The force **F** measured by the observer *O* in the fixed test charge q_t (when **v** = 0) is called the electric field force or Coulomb's force, and it's given by:

$$\mathbf{F} = q_t \mathbf{E} = \mathbf{F}_{coul} \tag{12}$$

As long as the test charge is in rest, observer *O* will detect only the Coulomb's force, even though the source charge *q* is moving. This conclusion is derived from Equation (8). For the moving source charge, the Coulomb's force in q_t will be time variant.

Let's now consider the most general case of Equation (8), when velocity **v** is not zero. In this case, Equation (8) expressed in terms of electric field **E** and **E'**, yields

$$\mathbf{F} = q_t\mathbf{E} + \frac{u}{kc^2}\left[\mathbf{v} \times \left(\mathbf{a}_z \times q_t\mathbf{E}'\right)\right] \tag{13}$$

With rearrangement of the variables inside the square brackets, the last equation can be expressed as:

$$\mathbf{F} = q_t\mathbf{E} + q_t\left[\mathbf{v} \times \left(\frac{u}{kc^2}\mathbf{a}_z \times \mathbf{E}'\right)\right] \tag{14}$$

As indicated in the last expression, the total force seen by observer *O* is the sum of Coulomb's force and a force described by the variables within the brackets. - The part inside the brackets represents the vector product of velocity vector **v** and a field depending from **u** and **E'**. This field is called the magnetic field and is defined as:

$$\mathbf{B} \equiv \frac{u}{k\,c^2}\mathbf{a}_z \times \mathbf{E}' \tag{15}$$

This is the expression of the magnetic field for the case of special axes and charge orientation, and shows that this field is independent from test charge or test charge velocity **v**, and is given in terms of field **E'** and velocity **u**. It also indicates that the magnetic field is caused by the electric field in motion **E'**, seen by an observer **O**, and does not represent a new phenomenon.

If we express force **F** in terms of the new defined magnetic field as follows:

$$\begin{aligned}\mathbf{F} &= q_t\mathbf{E} + q_t\mathbf{v} \times \mathbf{B} \\ \mathbf{F} &= q_t\left(\mathbf{E} + \mathbf{v} \times \mathbf{B}\right)\end{aligned} \tag{16}$$

the standard form of Lorentz's force expression is obtained. So, Lorentz's force represents the sum of the Coulomb's force and the force due to the magnetic field.

$$\mathbf{F} = \mathbf{F}_{coul} + \mathbf{F}_{mag} \tag{17}$$

This approach of expressing the force fields can be used to extract Maxwell's equations, starting from a single experimental law (Coulomb's law) and applying Lorentz's transformations. Representing the causality of time variant electric and magnetic fields is one of the advantages of this approach.

Space-Time variant Acoustic field

To show the formal analogy between the magnetic field and the acoustic field, as in the previous described case of the magnetic field, the model of force transformation will be followed. In this way, starting from an experimental law and using relativity and Lorentz's force definition, the origin of the acoustic field will be derived.

Assume observers *O* and *O*' measure the sound velocity *c* and conclude that this velocity is constant. Assume also the validity of Lorentz's transformations for observed system. The coordinate axes of two observers are located as in Fig. 4.

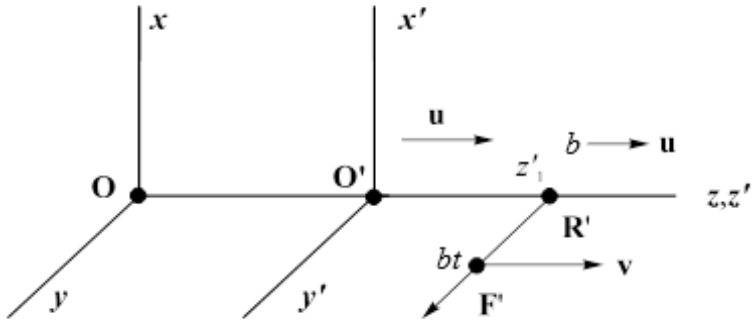

Fig.4. Static pressure from source *b* influence force on the surface of the punctual test body b_t.

Let us also assume the presence of acoustic pressure field *Ps'* in the entire region of reference frames of two observers. This pressure field may be caused by a punctual acoustic source *b* fixed at the point z'_1 of reference frame (*x', y', z ', t'*). Since the source is fixed with respect to the observer, the pressure field is also fixed. If in this region is a testing body b_t, fixed with reference frame (*x', y', z ',* t'), observer *O'* will detect only force *F'* acting on surface S_0 of b_t due to static pressure from source *b*. This force is given as:

$$\mathbf{F}' = \mathbf{S_0} p'_s \tag{18}$$

Since the force **F'** is a vector perpendicular to S_0, the expression for **F'** can be written as:

$$\begin{aligned} \mathbf{F}' &= \mathbf{S}_0\, p'_s = \mathbf{S}_0(\mathbf{a}_x + \mathbf{a}_y + \mathbf{a}_z)\, p'_s \\ &= S_0(p'_s\mathbf{a}_x + p'_s\mathbf{a}_y + p'_s\mathbf{a}_z) = S_0\,\mathbf{p}'_s \end{aligned} \tag{19}$$

where S_0 is the test body surface, and p'_s static pressure detected by the observer *O'*. In addition, in this case, field of force is also given in Cartesian coordinates, using:

$$\mathbf{F}' = F_x\mathbf{a}_x + F'_y\mathbf{a}_y + F'_z\mathbf{a}_z \tag{20}$$

From which the pressure field components can be set as well:

$$\mathbf{p}'_s = \frac{F'_x}{S_0}\mathbf{a}_x + \frac{F'_y}{S_0}\mathbf{a}_y + \frac{F'_z}{S_0}\mathbf{a}_z \tag{21}$$

For the observer *O'* the force field and the pressure field are static. For observer *O* these fields are time variant and may be determined using the Lorentz's transformations. We should bear in mind the essential assumption that surface S_0 is invariant under Lorentz's transformations.

From the force **F**' and its components (Fig.4) and also from Equation (8), the force **F** detected on the testing body b_t by observer *O* can be expressed with:

$$\mathbf{F} = \left(\frac{1}{k} F_x^{'} \mathbf{a}_x + \frac{1}{k} F_y^{'} \mathbf{a}_y + F_z^{'} \mathbf{a}_z \right) + \frac{u}{k\,c^2} \left[\mathbf{v} \times \left(\mathbf{a}_z \times \mathbf{F}' \right) \right] \tag{22}$$

Where *k* represents the contraction factor for the sound velocity *c*, and **v** is the velocity of b_t with respect to reference frame of the observer *O*. If$v = 0$, the fields detected by the observer *O* are:

$$\begin{aligned} \mathbf{F} &= \frac{1}{k} F_x^{'} \mathbf{a}_x + \frac{1}{k} F_y^{'} \mathbf{a}_y + F_z^{'} \mathbf{a}_z \\ \mathbf{p}_s &= \frac{\mathbf{F}}{S_0} = \frac{1}{k} p_s^{'} \mathbf{a}_x + \frac{1}{k} p_s^{'} \mathbf{a}_y + p_s^{'} \mathbf{a}_z \end{aligned} \tag{23}$$

Equation (23) actually represents Lorentz's transformation of pressure field $\mathbf{p_s}$**'** to $\mathbf{p_s}$ as observer *O* sees it. If $u = 0$ (relative velocity of two reference frames), the contraction factor *k* is equal to1 and the pressure fields in both frames will be the same. Force **F** measured by the observer *O* is called the force of static pressure, and is given by:

$$\mathbf{F} = S_0 \, \mathbf{p}_s \tag{24}$$

As long as is v = 0, the force of static pressure is the only force detected by observer *O*. Although the static field is sliding across z axis ($u \neq 0$), this force will only appear as time variant force field.

Now consider the most general case of Equation (4), when velocity is $\boldsymbol{v \neq 0}$. In this case, Equation (4) expressed in terms of pressure field $\mathbf{p_s}$ and $\mathbf{p'_s}$, yields to:

$$\mathbf{F} = S_0 \, \mathbf{p}_s + \frac{u}{k\,c^2} \left[\mathbf{v} \times \left(\mathbf{a}_z \times S_0 \, \mathbf{p}_s^{'} \right) \right] \tag{25}$$

With rearrangement of variables within the square brackets, for the acting force in this case, the expression analogue to Equation (14) can be obtained:

$$\mathbf{F} = S_0 \mathbf{p}_s + S_0 \left[\mathbf{v} \times \left(\frac{u}{k c^2} \mathbf{a}_z \times \mathbf{p}_s^{'} \right) \right] \tag{26}$$

The Equation (26) shows the total acting force in b_t as a sum of force due to static pressure and another force which depends on the velocity **v**, movement of the static field **u** and the static pressure $\mathbf{p'}_s$. The term inside the square brackets represents vector product of vector **v** and a new field vector. This new field, in analogy to the magnetic field defined in previous section, represents the acoustic field and is defined as:

$$\mathbf{A} \equiv \frac{u}{kc^2} \mathbf{a}_z \times \mathbf{p}_s^{'} \tag{27}$$

This is an acoustic field for the case of special orientation of the axes and the S_0 as assumed at the beginning of this approach. The acoustic field, defined in this way, is independent of the test surface and its velocity **v**, but is expressed in terms of static pressure field $\mathbf{p'}_s$ and the velocity of movement of this field **u**. The definition of the acoustic field according to (27) shows that this acoustic field is not caused by any new phenomenon, but rather is a consequence of the relative movement of the static pressure field with respect to the reference frame of the observer.

Force equation expressed in terms of recently defined acoustic field yields to:

$$\begin{aligned} \mathbf{F} &= S_0 \mathbf{p}_s + S_0 \left(\mathbf{v} \times \mathbf{A} \right) \\ \mathbf{F} &= S_0 \left(\mathbf{p}_s + \mathbf{v} \times \mathbf{A} \right) \end{aligned} \tag{28}$$

The Equation (28) represents Lorentz's force expression for the acoustic field. According to this formulation, this force is sum of static pressure force and acoustic force acting on test body surface S_0.

$$\begin{aligned} &\mathbf{F} = \mathbf{F}_s + \mathbf{F}_a \\ \text{or} \quad &\mathbf{F} = S_0 \left(\mathbf{p}_s + \mathbf{p}_a \right) \end{aligned} \tag{29}$$

Where $\mathbf{p}_a$ is the acoustic pressure defined by

$$\mathbf{p}_a = \mathbf{v} \times \mathbf{A} \tag{30}$$

We have introduced the acoustic pressure or sound pressure, which is usually denoted by *p*. Unlike in electromagnetism, where the magnetic field **B** is treated separately from the velocity **v** of testing body, in acoustics product $\mathbf{v} \times \mathbf{A}$ is always treated as acoustic pressure.

Using Lorentz's transformations and based on analogy of Lorentz's force for electromagnetic fields, we obtained the basic similar expression of the acting force for pressure and acoustic fields. This force is expressed in terms of static pressure and acoustic pressure, showing full analogy of acoustic and magnetic fields. From Equation (28) all propagation and scattering laws of acoustic waves can be derived.

Transformational approach for describing the origin of the acoustic field by the Lorentz's force offers several advantages. First, based on this analogy and with the derivation of the acoustic field origin, it is proved that the acoustic phenomena occur with the displacement of medium particles from their stationary position, as consequence of the movement of the test body (regarded as a source of acoustic waves) and hence, that the acoustic phenomena are inevitable because of the motion of propagation medium (the static pressure field movement velocity **u**).

Secondly, this paper shows that the propagation velocity of the acoustic wave *c* does not depend on the relative velocity between the source and the observer in the sense that it does not pose any limitations

to the extension of the analogy between the acoustic field and the electromagnetic field. Rather it shows complete analogy between acoustic and magnetic phenomena.

Conclusion

In the theory of fields and waves in general, a fundamentally difficult and complex problem is the prediction of the field in the presence of any structure described with a wide range of possible variations in geometry or composition. The correlation of these variations is the genesis of the difficulties in solving the problems of wave propagation and scattering. From the mathematical point of view, difficulties arise due to nonlinearity of system response equations and associated coefficients.

In the case of electromagnetic and acoustic wave propagation and scattering, the complexity of the problem is characterized by the effects of heterogeneity of the structure extended throughout the physical domain to the resulting field. Traditional formulations require the complete response of the structure. For such an approach, a complete description of the structure is needed, so any partial description or approximation is a source of difficulty due to the large number of operations required to numerically solve the problem and unsuitability of use, as a consequence. In addition, any change introduced in the structure or in the incident wave (space-time variant field) formally causes such circumstances that require a completely new formulation of the problem.

The first goal in this paper was to mathematically prove the tenets of transformational approaches to acoustic field. Following the transformational electromagnetic procedure, compatibility between magnetic field and acoustic field parameters and coordinate transformations is shown. Transformational acoustics are based on the expression for Lorentz's, force, which is derived applying the same approach as in electromagnetics. Although the idea of the existence of such an analogy

is not new at all, problems with the differences in the nature of the two fields in the literature are briefly overlooked without any mathematical formulation.

The transformational approach to problem solving in the acoustic fields has a natural physical interpretation expressed by definition of the genesis of acoustic field based on Lorentz's force derivation. Based on the experimental laws (Coulomb's law and the law of static pressure action) using the fundamental postulates of the special theory of relativity and Lorentz's transformations, this paper shows that these two fields, in the description of their geneses are completely analogous. This analogy is based solely on the mathematical relationships that describe these phenomena, not the phenomena themselves.

Based on the obtained expressions for the magnetic and acoustic field defined through Lorentz's force, a solid approach for full extension of analogies is provided. The complex acoustic problems can be solved using well-processed methods of electromagnetic fields. Such an approach, in the general case, does not eliminate the essential difficulties in the theoretical solution of the problem, but it significantly facilitates them in the case of acoustics because of the possibility to implement the electromagnetic solving methods without any need of verifying them. These methods are well-defined and advanced so their direct application to solving analogous acoustic problems is undoubtedly a major advantage.

References

[1] Roth, J. B., The role of magnetic forces in biology and medicine. Exp Bio Med, 236(2), 132-137, 2011.

[2] Garcia-Meca, C., Carlani S., Barcelo C., Jannes G., Sanche-Deheza J., Martinez A., Analogue transformations in physics

and their application to acoustics. Science Report, 3, 157-182, 2009.

[3] Cummer A. S., Rahm M., Schuring D., Material parameters and vector scaling in transformation acoustics. New Journal of Physics 10, 1367-2360, 2008.

[4] Wang Z., Zhang W., Huang W., Feng S., Li F., Optics Express, vol. 23, No. 19, 1140-1148, 2015

[5] Garcia-Meca, C., Carlani S., Barcelo C., Jannes G., Sanche-Deheza J., Martinez A., Analogue transformations in physics and their application to acoustics. ESA, Report, 2012.

[6] Qian K., Ren Z., Pandit V., Schuller B., Wavelets revisted for the classification of acoustic scenes. Detection and Classification of Acoustic Scenes and Events, 2017.

[7] Kaiser G., "A friendly guide to wavelets", Birkohouser, Boston, Basel, Berlin, 1994.

[8] Pendry, J. B., Schurig, D. &Smith, D. R. Controlling electromagnetic fields. Science 312, 1780–1782 (2006).

[9] Leonhardt, U. Optical conformal mapping. Science 312, 1777–1780 (2006).

[10] Schurig, D. et al. Metamaterial Electromagnetic Cloak at Microwave Frequencies. Science 314, 977–980 (2006).

[11] Kaiser G., Quantum Physics, Relativity, and Complex Spacetime, North Holland, Amsterdam.1990

[12] Zhang, S., Genov, D. A., Sun, C. & Zhang, X. Cloaking of Matter Waves. Phys. Rev.Lett. 100, 123002 (2008).

[13] McCall, M. W., Favaro, A., Kinsler, P. & Boardman, A. A spacetime cloak, or a history editor. J. Opt. 13, 024003 (2011).

[14] John M., Electromagnetic field theory, John Wiley & Sons, 1976.

[15] Patrick H. J., Kersey A. D., Buchollz F., Analysis of response of long period fibber grating to external index of refraction, IEEE for Lightwave Technolog. Vol. 16, Sept. 1998.

[16] Elengav A., Gupta K., Motion prediction of moving object based on Autoregressive model, IEEE Trans. Sys. Man. Gyb. Vol. 28, Nov. 1998.

[17] Cummer S., The futures of transformations and metamaterials, Photonics and Nanostructures – Fundamentals and Applications, Vol.15, 10-23, 2010.

[18] Zhang J., Pendry J. B., Luo Y., Transformation Optics from macroscopic to Nanosclae regimes. Advanced Photonics, open Access, 2019.

[19] Konofagou E. E., Localized harmonic motion imaging: theory, simulations and experiments. Ultrasound in Medicine & Bilology, Vol. 29, 10, 1405-1413, 2003.

[20] Edwards R., Trushkevych o., Eriksson T. J. R., Ramadas S. N., Ultrasound visualization using polymer dispersed liquid crystal sensors. AIP Conference Proceedings 1806, 020021 (2017); https://doi.org/10.1063/1.4974562 Published online: 16 February 2017.

[21] Chambers D. H., Berryman J. G., Analysis of the time reversal operator for a small spherical scatterer in an electromagnetic field. IEEE Transactions on Antennas Vol. 52 Issue: 7, 2011.

QASJA TRANSFORMACIONALE E ANALIZËS SË FUSHAVE MAGNETIKE DHE AKUSTIKE TË NDRYSHUESHME HAPËSIRË-KOHË

Myzafere Limani

Përmbledhje

Kohët e fundit ka pasur përpjekje për zbatimin e qasjes transformacionale në sistemet akustike. Duke ndjekur procedurën e optikës transformacionale, në akustikë është aplikuar një korrespondencë midis parametrave të mediumit dhe transformimeve të koordinatave. Akustika transformacionale bazohet në invariancën e ekuacionit të valës akustike nën një grup të caktuar të transformimeve të koordinatave. Një tjetër parashikim i kësaj qasjeje përfshin "mbështjellje të jashtme akustike", ku objekti i fshehur dhe burimet janë të vendosura në të njëjtën fushë (domen) dhe objekti është i ekspozuar ndaj tingullit të jashtëm (te dignastifikimi me ultratingull).

Shkalla në të cilën koncepti transformacional në analogji me fushën elektromagnetike mund të zbatohet në klasat e fushave tjera si akustika dhe optika, ende mbetet një pyetje e hapur. Duke u nisur nga ligjet eksperimentale (ligji i Coulomb-it dhe ligji i veprimit të presionit akustik) me anë të postulateve themelore të teorisë speciale të relativitetit dhe transformimeve të Lorentz-it, në këtë punim nxjerret shprehja eksplicite për gjenezën së fushës akustike si analoge me atë magnetike. Kjo analogji bazohet vetëm në relacionet matematikore që përshkruajnë këto dukuri, e jo në vetë dukuritë.

Bazuar në disa publikime të viteve të fundit [18], [15], kjo qasje ka filluar të ndryshoj. Në punimin [18], autori e përkrah plotësisht shtrirjen e analogjisë në mes të këtyre dy fushave dhe këtë e argumenton matematikisht me anë të valëzave. Në punimin dytë [15] autori fare nuk ndalet në këtë

çështje dhe heshtazi zbaton analogjinë e kundërt. Pra, problemin e difraksionit elekromagnetik në një strukturë e zgjidhë duke zbatuar zgjidhjet e problemit analog akustik, dhe rezultatet e fituara janë të kënaqshme.

Përfundim tjetër i rëndësishëm nga ky trajtim është se në këtë mënyrë tregohet se shpejtësia e përhapjes së valëve akustike është e pavarur nga shpejtësia relative në mes të burimit dhe vëzhguesit dhe se kjo shpejtësi varet vetëm nga karakteristikat e mediumit. Në bazë të shprehjeve të fituara ofrohet një qasje solide për zbatimin e plotë të analogjive në zgjidhjen e problemeve komplekse akustike duke shfrytëzuar metodat e përpunuara mirë nga fushat elektromagnetike. Qasja e këtillë në zgjidhjen e problemit të përhapjes dhe shkapërderdhjes së valëve akustike, në rastin e përgjthshëm, nuk eliminon vështirësitë esenciale në zgjidhjen teorike të problemit, por nga aspekti akustik në praktikë, dukshëm i lehtëson ato, me zbatimin e metodave të përpunuara mirë nga elektromagnetika. Zbatimi i drejtëpërdrejtë i tyre në zgjidhjen e problemeve analoge akustike padyshim paraqet përparësi të madhe dhe është frytëdhënës.

KDU 541.2

THE ADSORPTION OF ARYLDIAZONIUM SALTS ONTO THE (8,8) SINGLE WALL CARBON NANOTUBES – AN "AB INITIO" AND MONTE CARLO STUDY

Avni Berisha [a, *]
Fetah I. Podvorica[a, b, *]

Abstract

The adsorption behavior of several aryldiazonium salts (bearing -H, $-NO_2$ or $-N(CH_3)_2$ in para positions) toward the (8,8) Single Walled Carbon Nanotube (SWCNT) were evaluated using "ab initio'' and Monte Carlo Calculations. The adsorption energies onto the SWCNT were evaluated at three distinctive adsorption sites using three aryldiazonium cations bearing electron- donating or -withdrawing groups. The highest adsorption energies for the studied systems were found in the case when the aryldiazonium cation were hosted inside the SWCNT with the adsorption energy value of -71 kcal/mol. The Monte Carlo calculations permitted in semi-quantitative manner to have the adsorption geometry and the energy of the substituted aryldiazonium tetrafluoroborate molecules in simulated adsorption media.

[*] Department of Chemistry, FNMS, University of Prishtina "Hasan Prishtina", 10000 Prishtina, Republic of Kosova. Email: avni.berisha@uni-pr.edu.
[a] Department of Chemistry, FNMS, University of Prishtina "Hasan Prishtina", 10000 Prishtina, Republic of Kosova. Email: fetah.podvorica@uni-pr.edu.
[b] Academy of Science and Arts of Kosova.

Introduction

Aryldiazonium salts are now widely used as precursors for tailoring material surfaces with organic film of different thickness and composition. [1] The key species for the modification of the material surfaces are aryl radicals derived from their corresponding aryldiazonium salt. The activation of aryl diazonium salts is made in several ways: electrochemically, chemically, by solvolysis, thermally or by the light. Once created, the aryl moieties are able to attach on many surfaces like (carbon of various types including graphene and carbon nanotubes), metals, semiconductors and insulators.[2] The modification of single and Multiwall CNT surfaces with aryl moieties permits the creation of new assemblies that have interesting properties in the field of transistors. [3]

Carbon Nanotubes (CNT) are produced in different ways: the arc discharge method [4], laser ablation [5] and chemical vapor deposition. [6] Due to their long one-dimensional structure (diameter in the nm range and the length several hundred up to μm] and their physio-chemical properties like excellent electrical conductivity and very good thermal stability the CNT are exploited for many purposes in micro nanoelectronics and other domains like composite materials, biomedicine, sensors etc. [7]

Prior to their chemical or electrochemical reduction, the aryl diazonium salts are adsorbed physically on the substrate surface through weak interactions that may include π-stacking and different hydrophobic interactions. The existence of such two-step mechanism aryldiazonium grafting mechanism is described first by Strano et al. [8] They have observed by transient Raman Spectroscopy and photoluminescence measurements during the grafting of the 4-chlorobenzene diazonium salt in aqueous solution onto SWCNT surface: a selective adsorption step where a long-lived intermediate is physically adsorbed onto the CNT surface succeeded by a covalent grafting step.

The same group has proposed a model for the modification of swcnt with 4-hydroxybenzene diazonium salt where the adsorption step

that precedes the grafting step is considered the rate determining step. [9] the model has been confirmed by experimental results.

The adsorption properties of aryldiazonium salts onto swcnt surface were enhanced by the use of surfactants sdbs (sodium dodecyl sulfate), sdc (sodium deoxycholate) and stc (sodium taurocholate) that have a bridge role and enables the better interaction between diazonium ion and charged surfactant heads. [10]

The aim of the present paper is to put in evidence the existence and the strength of such interactions of aryldiazonium salts onto the carbon surface.

Computational details

DFT calculations

First principles DFT calculations were carried out using the DFT code implemented in the Dmol^3 software (BIOVIA). The Generalized Gradient Approximation (GGA) in the form of Perdew et al. (PBE) [using all electron core treatment / DNP 3.5 basis set / energy convergence criteria of 1.0e-5 Ha and 1.0e-6 SCF tolerance] in combination with the Tkatchenko-Scheffler (TS) dispersion correction schemes was used to compute the adsorption energies.

Monte Carlo Calculations

The Materials studio 7.0 has been used to construct the slab models and other molecular structures. The Monte Carlo (MC) calculations of the interaction between the aryldiazonium tetrafluoroborate molecules and the SWCNT were carried out in the simulation box of 20 Å^3 using periodic boundary conditions (PCB). The SWCNT structure used in DFT and Monte Carlo calculations was a (8,8) SWCNT model with a length of 13.18 Å and an inner diameter of 10.85 Å. The adsorption

media effect was approximated in the MC by packing 30 water molecules, 10 hydronium ions (geometrically optimized using Universal forcefield) onto the simulation box together with two substituted aryldiazonium tetrafluoroborate molecules (using the same optimization algorithm). Prior to the MC calculations the charges for all of the optimized molecules (using PBE/GGA) were assigned using the Gasteiger method [11] (Figure 1). The MC calculation was applied using 5 cycles of simulated annealing with 50000 steps for each process. The temperature of the annealing process was set automatically at 10^5 to 10^2 K for each cycle. Possible adsorption configurations were obtained as the temperature was slowly decreased.

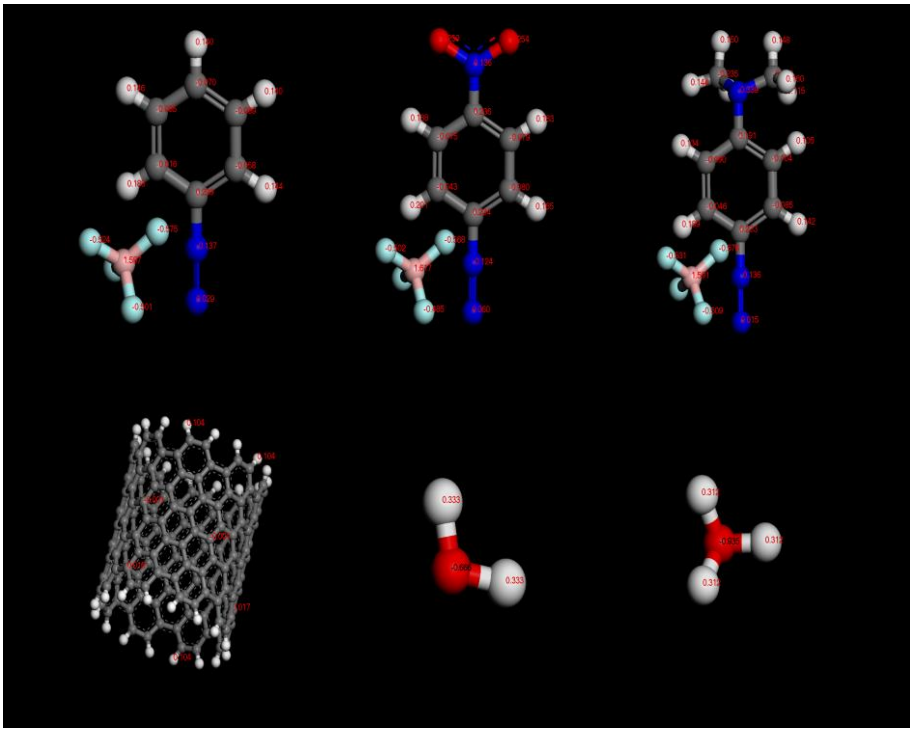

Fig. 1. Optimized **s**tructures and the Gasteiger assigned atom charges for the molecules used in the Monte Calculations.

DFT results

The adsorption energy (Eads.) [12,13] was calculated as:

$$E_{(ads)} = -(E_{SWCNT/aryldiazonium\ cation} + E_{aryldiazonium\ cation} - E_{SWCNT})$$

For the adsorption energy three different adsorption + 3 different aryldiazonium cations were explored, namely: 1. Adsorption of the aryldiazonium cations inside the SWCNT cavity (Figure 2 A1-C1); 2. Adsorption of the aryldiazonium cations planar oriented toward surface (Figure 2 A2-C2) and 3. Adsorption of the aryldiazonium cations perpendicularly oriented to the SWCNT surface (Figure 2 A3-C3).

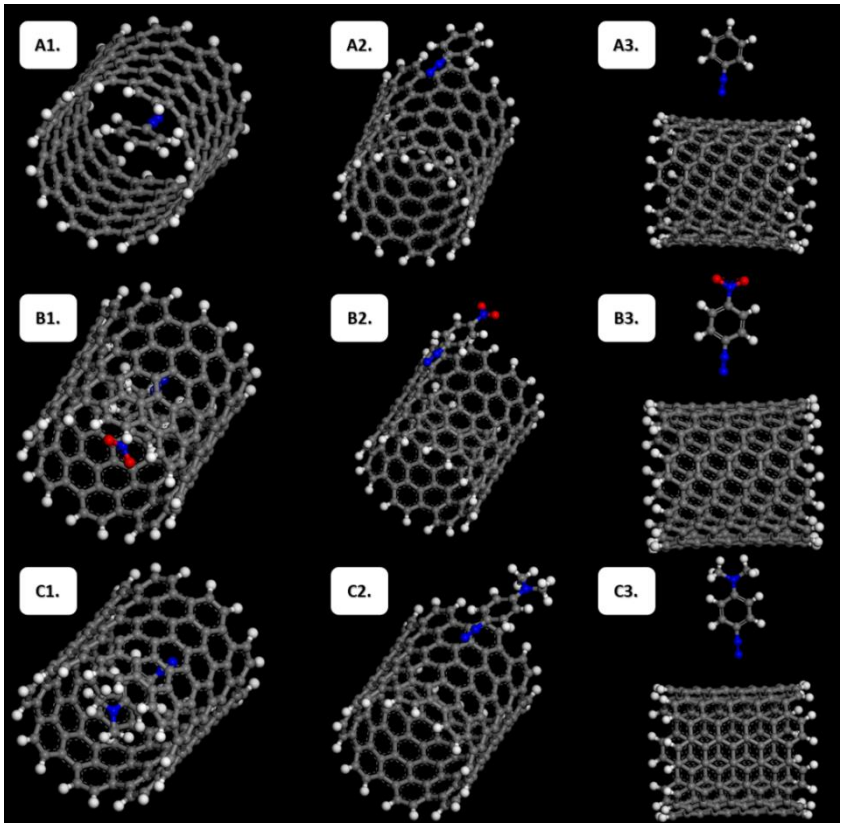

Fig. 2. Optimized **s**tructures (GGA/PBE/TS) for the adsorption of aryldiazonium cations onto three distinctive adsorption positions onto the SWCNT surface.

The adsorption energies are presented in the Figure 3. The highest adsorption energies for all of the studied aryldiazonium cations were found in the case when the cations are adsorbed inside the SWCNT cavity. The adsorption energies follow the order: NO_2-Ph-N_2^+ (-71.4 kcal/mol) > Ph-N_2^+ (-54.32 kcal/mol) > $(CH_3)_2$-N-Ph-N_2^+ (-53.82 kcal/mol). These results imply that the strongly deactivating groups favor the adsorption inside the SWCNT cavity. The second most favored adsorption positions are when the aryldiazoniums are planar oriented to the surface plane, this increases the possibility for π-π stacking between the SWCNT surface and the phenyl moiety of the aryldiazonium cation.

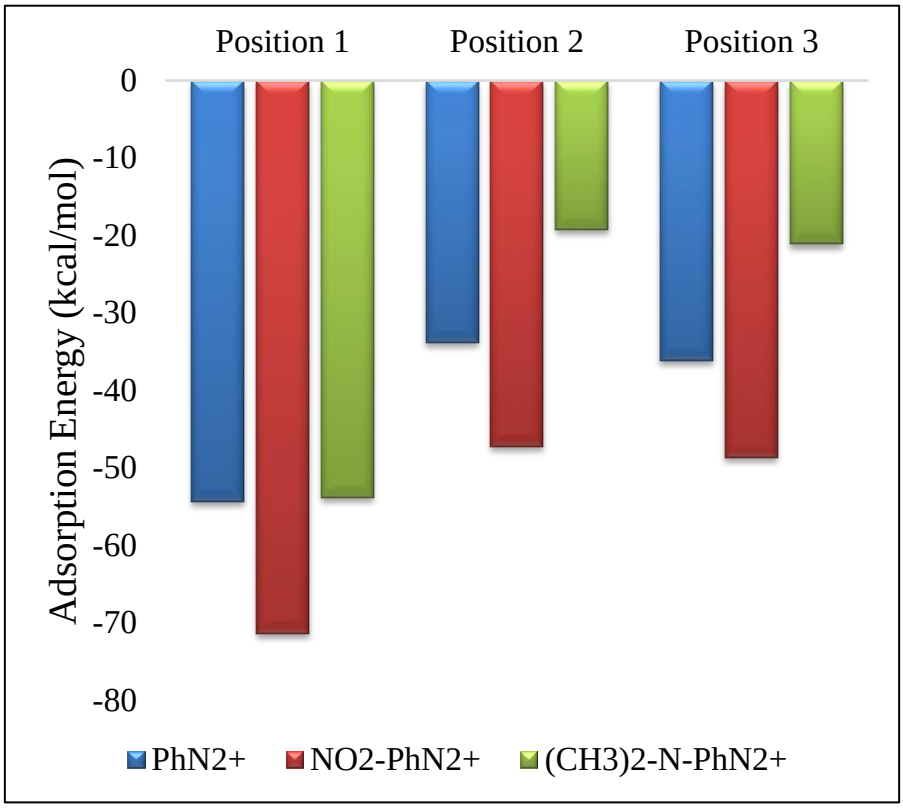

Fig. 3. Adsorption energies for the interaction of the aryldiazonium cations with the SWCNT surface.

The adsorption geometry and energy are important parameters to elucidate the grafting of these salts when applied to surface modification – the results support the fact that in this case the first step prior to the grafting reaction is the adsorption/orientation of these molecules to the SWCNT surface.

Monte Carlo Results

The most stable adsorption configuration of aryldiazonium tetrafluoroborate molecules onto the (8,8) SWCNT surface obtained by simulated annealing using the Adsorption Locator module are presented in Figure 4. As it is evident from the Figure A1 and A2 the adsorption of benzendiazonium tetrafluoroborate is done on the side and the edge of the SWCNT, the nitrobenzendiazonium salt (Figure 4, B1 and B2) has a similar adsorption tendency although in case of the edge adsorption the orientation of the diazonium group is oriented away from the SWCNT surface. In the case of the adsorption of the N-dimethylbenzendiazonium is evident a tendency of this molecule to be hosted in the inner tubular cavity of the SWCNT (Figure 4, C2).

The results of the adsorption energies during the Monte Carlo simulation are presented in Figure 5 A-C. In the case of the adsorption of two PhN_2^+ molecules, the adsorption energy is in the range of -445 to -715 kcal/mol and the value of the maximum energy distribution probability is at -483 kcal/mol. For the NO_2- PhN_2^+, the adsorption energy is in the range of -507 to -823 kcal/mol and the value of the maximum energy distribution probability is at -601 kcal/mol. The adsorption energy range for $(CH_3)_2$-N-Ph-N_2^+ is located in the region between -515 to -780 kcal/mol and the value of the maximum energy distribution probability in this case is at -661 kcal/mol. The adsorption of the diazonium molecules decreases in the order: $(CH_3)_2$-N-Ph-N_2^+ (-661 kcal/mol) > NO_2-PhN_2^+ (-601 kcal/mol) > PhN_2^+ (-483 kcal/mol).

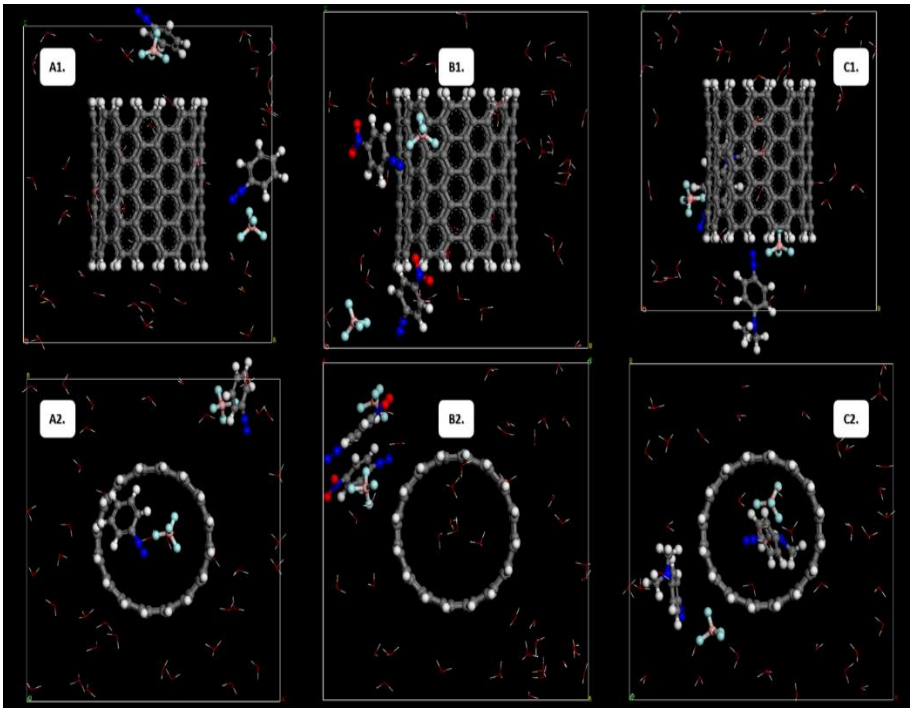

Fig. 4. Side (A1,B1,C1) and Top (A2,B2,C3) view for the most stable energy adsorption configurations for the: A. phenyldiazonium- and B. nitrophenyldiazonium- and C. N-dimethyldiazonium tetrafluoroborate molecules in presence adsorption media (30 water molecules and 10 hydronium ions) onto the (8,8) SWCNT surface attained by the adsorption locator module.

The highest adsorption energy in the case of $(CH_3)_2$-N-Ph-N_2^+ is reflected from the fact that during the MC calculations one of the molecules enters the cavity of the SWCNT.

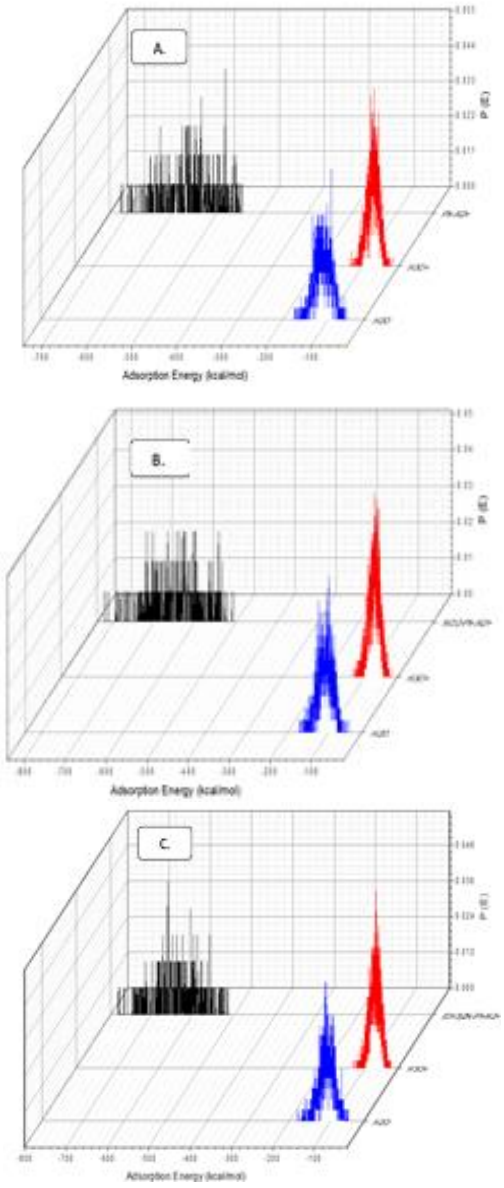

Figure 5. The adsorption energy distribution of the adsorbate: A. 2 phenyldiazonium tetrafluoroborate, B. nitrophenyldiazonium tetrafluoroborate and C. N-dimethylbenzenediazonium tetrafluoroborate onto (8,8) SWCNT) surface in presence of simulated adsorption media (30 water molecules and 10 hydronium ions).

Conclusions

The adsorptive behavior of three substituated aryldiazonium salts bearing +I and -I substituents has been explored using ‘’ab initio’’ and Monte Carlo calculations. The DFT calculations show that the highest adsorption energies are obtained when the aryldiazonium cations are inside the cavity of the SWCNT. When the effects of the substituents are compared, the highest adsorption energies are obtained for the nitro substituted aryldiazonium cation which is a strong deactivating group. This study presents the first example to our knowledge that applies the Monte Carlo calculation jointly in conjunction with the simulation of the adsorption media to elucidate the adsorption mechanism of the aryldiazonium salts onto the SWCNT surface - a mandatory step to understand the grafting mechanism of these molecules onto SWCNT.

Conflict of Interest Statement

The authors declare that the research was conducted in the absence of any commercial or financial relationships that could be construed as a potential conflict of interest.

Acknowledgments

The authors gratefully acknowledge also the support from Ministry of Education, Science and Technology of Kosova (Nr.2-5069) for providing them with the computing resources.

References

[1] Berisha, A., Chehimi, M.M., Pinson J. and Podvorica, F.I. Book chapter "Electrode Surface Modification Using Diazonium Salts" in Electroanalytical Chemistry, A Series of Advances: Volume 26, Edited by Allen J. Bard and Cynthia G. Zoski, CRC Press, 2015, 115–224, DOI: 10.1201/b19196-4.

[2] Pinson, J. and Podvorica, F. Attachment of organic layers to conductive or semiconductive surfaces by reduction of diazonium salts. Chemical Society Reviews 2005, 34, 429 - 439.

[3] Wang, C., Cao, Q., Gaur, A., Rogers, J.A. and Shim, M. Electronically Selective Chemical Functionalization of Carbon Nanotubes: Correlation between Raman Spectral and Electrical Responses. *J. of Am. Chem. Soc*., 2005, 127, 11460-11468.

[4] Journet, C., Maser, W.K., Bernier, P., Loiseau, A., Lamy de la Chapelle M., Lefrant, S., Denlard, P., Lee, R. and Fischer, J.E. Large-scale production of single-walled carbon nanotubes by the electric-arc technique. *Nature*, 1997, 388, 756-758.

[5] Yadasaka, M., Komatsu, T., Ichihashi, T. and Iijima, S. Single-wall carbon nanotube formation by laser ablation using double-targets of carbon and metal. *Chem. Phys. Lett.* 1997, 278, 102-106.

[6] Kong, J., Cassell, A.M. and Dai, H. Chemical vapor deposition of methane for single-walled carbon nanotubes. *Chem. Phys. Lett.* 1998, 292, 567-574.

[7] Chehimi, M.M. and Pinson, J. Applied Surface Chemistry of Nanomaterials. Nova Sciences Publishers, Book. New York, 2013.

[8] Usrey, M., Lippmann, E.S., and Strano, M.S. Evidence for a two-step mechanism in electronically selective single-walled carbon nanotube reactions. *J. of Am. Chem. Soc*., 2005, 127, 16129-16135.

[9] Nair, N., Kim, W.-J., Usrey, M.L. and Strano, M.S. A Structure-Reactivity Relationship for Single Walled Carbon Nanotubes Reacting with 4-Hydroxybenzene Diazonium Salt. *J. of Am. Chem. Soc*., 2007, 129, 3946-3954.

[10] Lin, S., Hilmer, A.J., Mendenhall, J.D., Strano, M.S. and Blankschtein, D. Molecular Perspective on Diazonium Adsorption for Controllable Functionalization of Single-Walled Carbon Nanotubes in Aqueous Surfactant Solutions. *J. of Am. Chem. Soc*., 2012, 134, 8194-8204.

[11] Gasteiger, J.; Marsili, M. A New Model for Calculating Atomic Charges in Molecules. *Tetrahedron Lett.* 1978, *19* (34), 3181–3184.

[12] Mehmeti, V. V.; Berisha, A. R. Corrosion Study of Mild Steel in Aqueous Sulfuric Acid Solution Using 4-Methyl-4h-1,2,4-Triazole-3-Thiol and 2-Mercaptonicotinic Acid-an Experimental and Theoretical Study. *Front. Chem.* 2017.

[13] Berisha, A.; Combellas, C.; Kanoufi, F.; Médard, J.; Decorse, P.; Mangeney, C.; Kherbouche, I.; Seydou, M.; Maurel, F.; Pinson, J. Alkyl-Modified Gold Surfaces: Characterization of the Au-C Bond. *Langmuir* 2018, *34*, 11264-11271.

ADSORBIMI I KRIPËRAVE TË ARILDIAZONIUMIT NË NANOTUBAT E KARBONIT NJË SHTRESOR (8,8) – NJË STUDIM "AB INITIO" DHE MONTE CARLO

Avni Berisha

Fetah I. Podvorica

Përmbledhje

Në këtë punim është studjuar aftësia e adsorbimit të disa kripërave arildiazonium (me substituentë (H, -NO_2 dhe –$N(CH3)_2$ në pozitën para) në nanotubat e karbonit një shtresor (8,8) janë llogaritur duke përdorur llogaritjet me metodën "Ab initio" dhe Monte Carlo. Energjitë e adsorbimit në nanotubat e karbonit një shtresor në tri vende të ndryshme të adsorbimit duke përdorur tri kripëra arildiazonium që kanë grupe elektron donore ose akceptore. Energjitë më të mëdha të adsorbimit për sistemet e studiuara janë gjetur në rastin kur kripërat janë vendosur brenda murit të nanotubit të karbonit një shtresor me vlerë të energjisë së adsorbimit – 71 kcal/mol. Llogaritjet Monte Carlo kanë mundësuar që në mënyrë gjysmë kuantitative të gjenden gjeometria e adsorbimit dhe energjia e kripërave të arildiazoniumit në mjediset e simuluara të adsorbimit.

KDU 577.16(082)

β- CAROTENE UNDER OXIDATIVE STRESS INDUCES GENOTOXICITY

Alija, A. J.[a]
Bresgen, N.[b]
Langhans C.D.[c]
Sommerburg, O.[d]
Siems, W.[e]
Eckl, P.M.[b]

Abstract

In previous investigations we demonstrated that oxidative β-carotene cleavage products (CPs) induce genotoxic effects even at nanomolar concentrations in primary hepatocyte cultures. Since it is known that β-carotene under oxidative stress undergoes cleavage, we further tested the effects of β-carotene under oxidative stress. Primary cultures of rat hepatocytes were treated with DMNQ (2,3-dimethoxy-1,4-naph-

[a] Department of Biology, University of Prishtina, Xhorxh Bush, n.n., Prishtina 10000, Kosova. *E-mail: avdulla.alija@uni-pr.edu*
[b] Department of Biosciences, University of Salzburg, Hellbrunnerstr.34, A-5020 Salzburg, Austria
[c] Metabolic Laboratory, Center for Metabolic Diseases, University Children's Hospital, Heidelberg, Germany
[d] University of Heidelberg, Department of Pediatrics, Division of Pediatric Pulmonology and Allergy and Cystic Fibrosis Center, Heidelberg, Germany.
[e] Lesimed Institute of Physiotherapy and Gerontology, Crusiusstraße 5, 38690, Goslar, Germany

thoquinone). Thereafter, the cultures were analyzed for cyto and genotoxic effects. The endpoints evaluated were: the mitotic index, the percentage of apoptotic and necrotic cells, the percentage of micronucleated cells (MN), and the numbers of chromosomal aberrations (CA) and sister chromatid exchanges (SCE). Furthermore, the formation of apocarotenals was analyzed. DMNQ applied at a concentration of 40 µM induced significant increases of MN, CA and SCE compared to the untreated control. In the presence of 1 and 5µM β-carotene a further increase of MN, CA and SCE was observed. Statistically significant increases of MN and SCE were observed at 50µM β-carotene. At this concentration elevated levels of apo-carotenals were found. Based on these data it can be concluded that β-carotene undergoes cleavage under conditions of oxidative stress and exerts genotoxic effects, which most likely can be attributed to the formation of cleavage products.

Key Words: β-carotene, DMNQ, oxidative stress, genotoxicity, hepatocytes

Introduction

Due to antioxidant and antimutagenic properties [1-3], β-carotene is widely used in the prevention of diseases associated with oxidative stress [4-8], but unexpectedly, the Alpha-Tocopherol Beta-carotene-Cancer prevention (ATBC) study and the Beta-Carotene and Retinol Efficacy Trial (CARET) showed an increased risk of lung cancer in smokers [9,10].

The effect of β-carotene can be modified under certain conditions and concentrations [11] showing antioxidant or prooxidant effects, dependent upon oxygen tension and the concentration of β-carotene applied, i.e.β-carotene shows concentration dependent antioxidant effects at low oxygen tensions (15 torr), but at higher oxygen tensions (760

torr) the effect becomes prooxidant. The same authors [12] also observed an increase of protein oxidation by β-carotene under high oxygen tensions. Similar data were obtained by Palozza et al. [13] under high oxygen tension, high carotenoid concentration and unbalanced redox status. Under these conditions β-carotene exhibited prooxidant properties causing damage to DNA, proteins or lipids [13].

Free radical attack on carotenoids results in the formation of numerous cleavage products which have been shown to be mitochondriotoxic [14]. A mixture of these products as well as one of the major cleavage products formed, apo-8'-carotenal(apo-8), induced genotoxic effects in primary rat hepatocytes [15]. Furthermore, a mixture of CP enhanced the genotoxic effects of oxidative stress induced by DMNQ or hypoxia/reoxygenation [16]. Hurst et al. [17], showed that these cleavage products are formed at physiologically or pathophysiologically relevant concentrations of β-carotene (2 and 6 μM) under the conditions of cigarette smoke induced oxidative stress. Interestingly, β-carotene has also been demonstrated to stimulate lipid peroxidation at high oxygen tensions [18]. It has further been reported that retinal and apo-8, two β-carotene oxidation products, significantly increased the levels of 1, N(2)-etheno-2'-deoxyguanosine and 8-oxo-7,8-dihydro-2'-deoxyguanosine in calf thymus DNA. These lesions are believed to be important in the development of human cancers [19]. In addition, it has been reported that oxidized β-carotene products facilitate the formation of benzo[a]pyrene (BaP) metabolites that bind to DNA [20]. Apo-8 additionally has been shown to act as a strong inducer of cytochromes P450 [21]. On the other hand, β-carotene itself showed a powerful effect on phase I carcinogen bioactivating enzymes associated with the generation of oxidative stress in the lung [22] which appears to be associated with pro-oxidant and potentially co-carcinogenic effects [23].

Smoking causes a decrease of the levels of antioxidants such an ascorbate and alpha tocopherol that have a stabilizing effect on the unoxidized β-carotene [22]. As a consequence, the oxidation of β-carotene

by cigarette smoke generates various products, including 4-nitro-β-carotene, β-apo-carotenals, and β-carotene epoxides [24], and these cleavage products appear to be responsible for the carcinogenic response in the lungs of cigarette smokers.

Furthermore, β-carotene oxidation products increase the amount of binding of benzo[a] pyrene metabolites, an important cigarette smoke carcinogen [20]. β-Carotene and cigarette smoke also showed a potential detrimental effect causing oxidative damage and modifying p53-related pathways of cell proliferation and apoptosis induction [25].

Paolini and co-workers [26] showed that β-carotene produces a significant increase in carcinogen metabolizing enzymes in the lungs of rat, including activators of polycyclic aromatic hydrocarbons, and this induction was associated with the generation of oxidative stress.

Previous investigations [15, 16] demonstrated that the supplementation of β-carotene to the medium did not induce any genotoxic effect. For this reason, the study described here was initiated to evaluate *in vitro* whether β-carotene under conditions of oxidative stress exhibits a genotoxic potential. Primary hepatocytes were therefore treated with increasing β-carotene concentrations during exposure to oxidative stress by DMNQ (2,3-dimethoxy-1,4-naphthoquinone) as a source of free radicals [27, 28]. The cyto-toxicological endpoints evaluated were: the mitotic index, the percentage of apoptotic and necrotic cells, the percentage of micronucleated cells (MN), and the numbers of chromosomal aberrations (CA) and sister chromatid exchanges (SCE).

Materials and Methods

Chemicals

MEM with Earle`s salts and non-essential amino acids, and antibiotics were obtained from Life Technologies, Vienna, Austria. Plastic culture dishes were from Sarstedt, Austria. EGF, collagenase and other

cell culture chemicals - unless otherwise specified - were purchased from Sigma Chemical Company via Biotrade, Vienna.

Since crystalline β-carotene is not water soluble the carotenoid had to be emulsified in a soybean carrier oil to enable physiological activity. The water-dispersible β-carotene in soybean suspension (2 % w/v) and the soybean suspension used as blank matrix in the experiments were a gift of Cognis Australia Pty Limited (Australia). The carotenoid emulsion was made from a starting material of 30 % β-carotene (derived from an algal extract) in soybean oil which was emulsified in a 30 % water and 70 % glycerol aqueous phase using a glyceryl mono-oleate emulsifier. The fine emulsion provides the carotenoid in a lipid globule size of around 1 micron or less so that interaction can occur at the cellular level.

Animals

Experiments were carried out at the former Department of Cell Biology, now Department of Biosciences, University of Salzburg. Eight weeks old female Fischer 344 rats, weighing approximately 100 g, were obtained from HARLAN, Winkelman (Germany) and were kept in a temperature (20-24°C) and humidity (55% rH) controlled room, with a 12 h light-dark cycle. The diet was a commercial autoclavable rat/mouse chow obtained from Ssniff, Germany. Water was provided ad libitum. The animals were allowed to acclimate for at least two weeks prior to hepatocyte isolation. The experimental work is conducted in accordance with the European Community Guidelines and is approved by the Austrian Ministry of Education, Science and Research (BMWFW-66.012/0037-WF/V3b/2016).

Hepatocyte isolation and culture

Hepatocytes were isolated from female Fischer 344 rats by the in-situ two-step collagenase perfusion technique as described by Michalopoulos et al. [29], plated at a density of 20 000 viable cells/cm² on

collagen-coated 60-mm diameter plastic culture dishes. Hepatocytes were plated in 5 ml of serum free Minimum Essential Medium (MEM) containing 1.8 mM calcium supplemented with non-essential amino acids, pyruvate (1 mM), aspartate (0.2 mM), serine (0.2 mM) and penicillin (100 U)/streptomycin (100 µg/ml) [30,31]. The cultures were incubated at 37°C, 5% CO_2 and 95% relative humidity. The medium was exchanged for fresh MEM after an incubation period of 3 hours and the cultures were returned to the incubator.

Treatment

Approximately 48 hours after the first exchange of the medium, DMNQ (dimethoxy-1,4-naphtoquinone; Sigma) at a concentration of 40 µM (made up freshly for each experiment) alone and in combination with β-carotene at concentrations of 1, 5, and 50 µM was added and the cultures were incubated for further 3 hours. Thereafter, the medium was aspirated and the plates were washed twice with fresh medium to completely remove the applied substances. Fresh MEM containing 0.4 mM Ca^{2+}, supplemented as described above with the further addition of insulin (0.1 µM) and EGF (40 ng/ml) was added. To determine SCE induction, BrdU (10 µM) was added to 3 dishes of each concentration. Thereafter, cells were incubated for an additional 48 h.

Analysis of the formation of the long chain CPs

HPLC of the reaction mixtures was carried out for detection of longer-chain molecular products, such as β-apo-carotenals. The HPLC system consisted of a Beckman System Gold 126 pump equipped with an UV-detector Beckman System Gold 167, and an injector Spark Promis II. Chromatographic separation was achieved on an Ultrasphere ODS column 5 µm, 4.6 mm × 25 cm (Beckman). CPs were separated applying the method of Hess et al. [32] with slight modifications. The mobile phase consisted of acetonitrile / tetrahydrofuran / methanol / 1% ammonium acetate (684 / 220 / 68 / 28) and was pumped at 1.5 ml/min.

The UV-detector was set at 450 nm. Prior to analysis the dried samples were dissolved in a mixture of acetonitrile / dioxane / ethanol (3 / 1 / 1) to yield a final concentration of 0.15 mM. A volume of 60 µl was injected. In the chromatograms of the different reaction mixtures peak identification was achieved by comparison of retention times combined with peak overlay after spiking the sample with the standards. Beside β-carotene the following metabolites could be detected by HPLC: apo-4'-carotenal, apo-8, apo-12'-carotenal, and apo-15'-carotenal (retinal).

Fixation, staining and cytogenetic analysis

As described by Eckl et al. [30, 33] colcemide (0.4 µg/ml) was added after forty-eight hours to 3 dishes each (where BrdU was added), and the cultures were incubated for a further 3 hours. No colcemide was added to the cultures for the micronucleus assay.

For the micronucleus assay, cells were fixed in the dishes with methanol: glacial acetic acid (3:1) for 15 minutes, briefly rinsed with distilled water and air dried.

For chromosome preparations cells were harvested by replacing the medium with 2 ml of collagenase solution (0.5 mg collagenase/ml) and incubation for 10 minutes. The detached cells were collected by centrifugation (44 x g), treated with hypotonic KCl solution (0.02M) for 10 minutes at 37 °C and fixed in freshly prepared methanol: glacial acetic acid (3:1) overnight. Preparations were made by dropping the cell suspension on precleaned frosted slides.

For micronucleus determination the fixed cells were stained with the fluorescent dye DAPI (4,6',6-diamidino-2-phenylinol) in McIlvaine buffer (0.2 M Na_2HPO_4 buffer adjusted with 0.1 M citric acid to pH 7.0) for 30 min in the dark at room temperature. After washing with McIlvaine buffer, the dishes were rinsed with distilled water followed by air drying. For microscopic observation fixed and stained cells were mounted in glycerol. To determine the mitotic index, the frequencies of apoptotic and necrotic cells and the number of cells with micronuclei

1000 cells per dish were analyzed under the fluorescence microscope (Leitz Aristoplan).

The slides for determining chromosomal aberrations and SCE induction were stained with Hoechst 33258 (4.5µg/ml) in Sörensen phosphate buffer pH 6.8 for 20 min, rinsed with Sörensen phosphate buffer and exposed to black light (General Electric, F 40 BLB Black light) for 15 minutes on a warming plate kept at 50 °C. After removal of the cover slips the slides were briefly washed with distilled water and stained in 5% Giemsa solution. 20 well spread first division metaphases were analyzed for chromosomal aberrations under the phase contrast microscope (Leitz Laborlux 11). 20 well spread second division metaphases were analyzed for SCE. The number of aberrations is given per diploid cell, i.e. 42 chromosomes. The SCEs are reported per chromosome.

Statistical analysis

Student`s double sided t-test for independent samples was used to calculate the levels of significance.

Results

The controls (matrix in1% DMSO and matrix in1% DMSO + 40µM DMNQ) did not induce any cytotoxic effect (Table I). Interestingly, there were also no cytotoxic effects (necrotic and apoptotic cells) (Table I) in the combined treatment with DMNQ and β-carotene up to a concentration of 50 µM. Similarly, the matrix control did not induce any genotoxic effect (Table II) while DMNQ at a concentration of 40 µM caused a significant increase ($P<0.05$) of micronucleated cells, chromosomal aberrations and SCEs (Table II).

Since 40 µM DMNQ was the lowest concentration which caused genotoxic effects in primary rat hepatocytes, this concentration was applied in combination with different concentrations (1, 5 and 50 µM) of

β-carotene in order to investigate whether β-carotene alters the response of primary hepatocytes to DMNQ.

As demonstrated in Table I, β-carotene had no cytotoxic effect compared to the control (matrix + 40 μM DMNQ), but induced significant increases of genotoxicity (Figure 1).

β-Carotene at a concentration of 50 μM significantly ($P<0.05$) increased the percentage of micronucleated cells (Figure 1A) and SCEs ($P<0.005$) (Figure 1C) compared to the control while the increase of chromosomal aberrations was not significant (Figure 1B).

Furthermore, there was a prominent dose-dependent increase of apo-8 and a less prominent increase of apo-12`-carotenal (Figure 2).

Table I. Cytotoxic effects of combined treatment of primary hepatocytes with β-carotene and DMNQ

	Mitotic index	**Necrotic cells (%)**	**Apoptotic cells (%)**
Negative control (Matrix in1% DMSO[1])	1.05 ± 0.13	0.23 ± 0.15	0.40 ± 0.36
Control (Matrix in1% DMSO[1] +40 μM DMNQ)	0.97 ± 0.15	0.17 ± 0.05	0.13 ± 0.06
DMNQ + 1 μM β-C	1.00 ± 0.17	0.13 ± 0.06	0.17 ± 0.06
DMNQ + 5 μM β-C	0.90 ± 0.26	0.13 ± 0.06	0.13 ± 0.05
DMNQ + 50 μM β-C	1.03 ± 0.31	0.31 ± 0.08	0.30 ± 0.26

[1]represents the concentration of DMSO at the highest β-carotene concentrations applied. Data represent the means ± SD (standard deviation) of three independent experiments.

Table II. Genotoxic effects of DMNQ in primary rat hepatocytes

	Micronucleated	CA/metaphase[2]	SCE/chromosome[3]
Negative control (Matrix in1% DMSO1)	7.63 ± 0.86	0.08 ± 0.02	0.36 ± 0.08
Matrix in 1% DMSO[1] + 40 µM DMNQ	11.50 ± 1.61*	0.21 ± 0.04*	0.68 ± 0.30*

*[1] represents the concentration of DMSO at the highest β-carotene concentrations applied data represent the means ± SD (standard deviation) of three independent experiments. * P≤ 0.05.*
[2]Number of chromosomal aberrations per metaphase
[3]Number of sister chromatid exchanges per chromosome

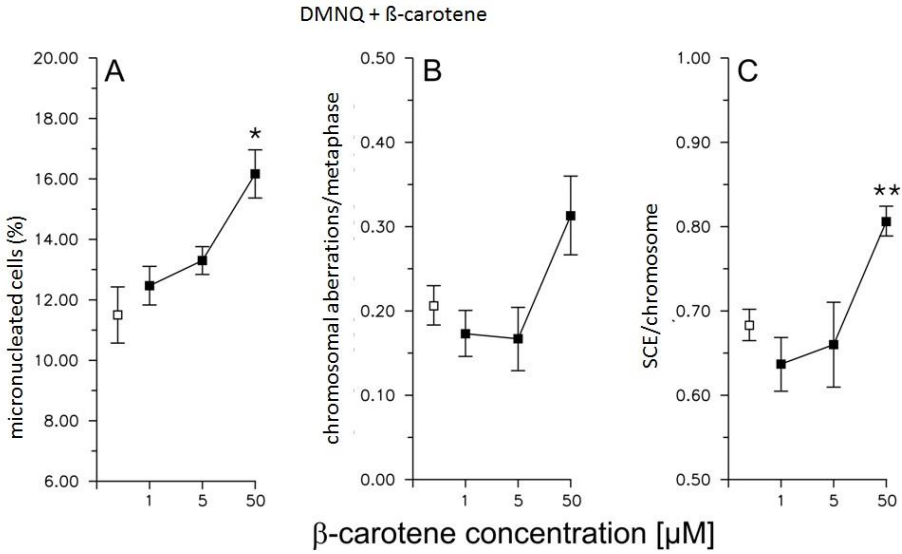

Fig. 1. Frequencies of micronucleated cells (A), chromosomal aberrations (B) and SCE (C) in control cultures (40 µM DMNQ, open squares) and cultures simultaneously treated with β-carotene. Data represent the means ± SEM (standard error of the mean) of three independent experiments. * P≤0.05; **P ≤ 0.005.

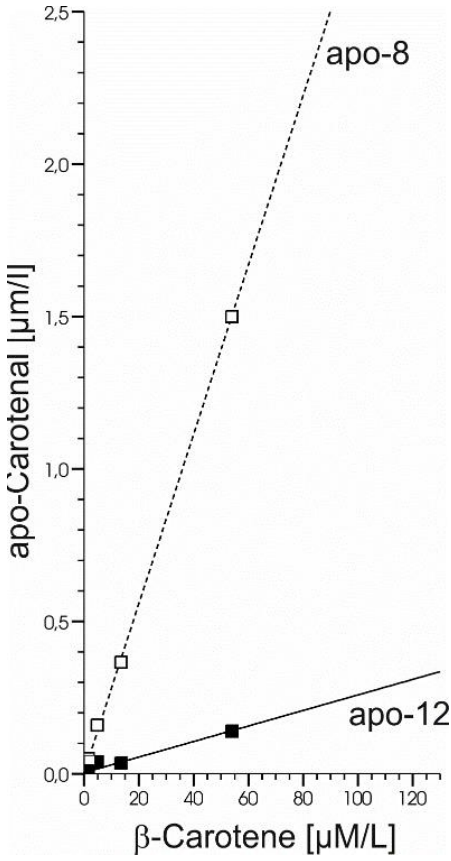

Fig. 2. Long-chain β-carotene cleavage products formed in primary rat hepatocytes cultures after a 3 h supplementation with β-carotene and DMNQ.

Discussion

DMNQ is considered to cause DNA damage and genotoxic effects via the formation of OH-radicals [34]. This genotoxic potential of DMNQ was also observed in this study at the concentration applied (40 µM). Following the addition of β-carotene the effect of DMNQ was further enhanced, and the strongest effect was obtained at a concentration of 50 µM of β-carotene. Similar results were obtained when rat

hepatocytes were exposed to hypoxia/reoxygenation (Hy/Re) [35]. Hy/Re caused a significant genotoxic effect and the application of β-carotene during the reoxygenation phase led to a significant increase of micronucleated cells (at concentrations of 5 and 50 µM β-carotene) and chromosomal aberrations at a concentration of 50 µM β-carotene [35]**.** Therefore, the genotoxic effects observed after the combined treatment with DMNQ or Hy/Re and β-carotene have to be attributed to the dose-dependent formation of cleavage products which either directly (due to their prooxidant properties) [14], or indirectly (involving the metabolism in hepatocytes or other metabolically competent cells such as those in the lung) induce damage to DNA. However, when DMNQ and Hy/Re were applied to rat pneumocyte type II cells the effects were very low compared to those obtained in rat hepatocytes [36]. This observation may be explained by the different metabolic capacities.

Conclusion

The central finding of this investigation is the confirmation that β-carotene under conditions of oxidative stress (DMNQ) induces genotoxicity, and the genotoxic effects observed can be attributed to the formation of CPs. These findings confirm those observed in previous studies [15, 16, 37].

Acknowledgements

The authors thank Lance Schlipalius and Michael Strahan (Cognis Australia Pty Limited) for making the cell line preparations of β-carotene used in this study available.

References

[1] Aidoo, A.; Lyn-Cook, L.E.; Lensing, S.; Bishop, M.E. and Wamer, W. *Carcinogenesis*. 1995, 16(9), 2237-2241.

[2] Rauscher, R.; Edenharder, R. and Platt, K.L. *Mutat. Res.*1998, 413(2), 129–142.

[3] Arriaga-Alba, M.; Rivera-Sanchez, R.; Parra-Cervantes, G.; Barro-Moreno, F.; Flores-Paz, R. and Garcia-Jimenez, E. *Arch. Med. Res.* 2000, 31(2), 156-161.

[4] Sies, H.; Stahl, W. and Sundquist, A.R. *Ann. N. Y. Acad. Sci.* 1992, 669, 7-20.

[5] Olson, J.A. and Krinsky, N.I. *FASEB J.* 1995, 9(15), 1547-1550.

[6] Halliwell, B. *Lancet*. 2000, 355 (9210), 1179-80.

[7] Agarwal, S. and Rao, A.V. *Drug Metabol. Drug Interact.* 2000, 17(1-4), 189-210.

[8] Lu, Q.Y.; Hung, J.C.; Heber, D.; Go, V. L.; Reuter, V.E.; Cordon-Cardo, C.; Scher, H.I.; Marshall, J.R. and Zhang, Z.F. *Cancer Epidemiol. Biomarkers Prev.* 2001, 10(7), 749-756.

[9] Blumberg, J. and Block, G. *Nutr. Rev.* 1994, 52(7), 242-245.

[10] Omenn, G.S.; Goodman, G.E.; Thornquist, M.D.; Balmes, J.; Cullen, M.R.; Glass, A.; Keogh, J.P.; Meyskens, F.L.Jr.; Valanis, B.; Williams, J.H.Jr.; Barnhart, S.; Cherniack, M.G.; Brodkin, C.A. and Hammar, S. *J. Natl. Cancer Inst.* 1996, 88 (21), 1550-1559.

[11] Zhang, P. and Omaye, S.T. *Toxicol. In Vitro*. 2001, 15(1),13-24.

[12] Zhang, P. and Omaye, S.T. *Toxicology*. 2000, 146: 37-48,

[13] Palozza, P.; Calviello, G. and Bartoli, G.M. *Free Radic. Biol. Med.* 1995, 19(6), 887-892.

[14] Siems, W.; Sommerburg, O.; Schild, L.; Augustin, W.; Langhans, C.D. and Wiswedel, I. *FASEB J.* 2002, 16(10), 1289-1291.

[15] Alija, A.J.; Bresgen, N.; Sommerburg, O.; Siems, W. and Eckl, P.M. *Carcinogenesis*. 2004, 25(5):827-31.

[16] Alija, A.J.; Bresgen, N.; Sommerburg, O.; Langhans, C. D., Siems, W. and Eckl, P.M. *Carcinogenesis*. 2006, 27(6):1128-33.

[17] Hurst, J.S.; Contreras, J.E.; Siems, W.G. and Van Kuijk, F.J. *Biofactors*. 2004, 20(1):23-35.

[18] Bast, A. and Haenen, G.R.M.M. *Environ. Toxicol. Pharmacol*. 2002, 11 (3-4), 251-258.

[19] Marques, S.A.; Loureiro, A.P.; Gomes, O.F.; Garcia, C.C.; Di Mascio, P. and Medeiros, M.H. *FEBS Letters*. 2004, 560 ,125-130.

[20] Salgo, M.G.; Cueto, R.; Winston, G.W. and Pryor, W. A. *Free Radic. Biol. Med*. 1999, 26, 162–173.

[21] Gradelet, S.; Leclerc, J.; Siess, M. H. and Astorg, P. O. *Xenobiotica*. 1996, 26(9), 909-919.

[22] Wang, X.D. and Russell, R.M. *Nutr. Rev*. 1999, 57 (9 Pt 1), 263-272.

[23] Paolini, M.; Antelli, A.; Pozzetti L.; Spetlova, D.; Perocco P.; Valgimigli, L.; Pedulli, G.F. and Cantelli-Forti, G. *Carcinogenesis*. 2001, 22(9), 1483-1495.

[24] Arora, A.; Willhite, C.A. and Liebler, D.C. *Carcinogenesis*. 2001, 22(8):1173-8.

[25] Palozza, P.; Serini, S.; Di Nicuolo, F.; Boninsegna, A.; Torsello, A.; Maggiano, N.; Ranelletti, F.O.; Wolf, F.I.; Calviello, G. and Cittadini, A. *Carcinogenesis*. 2004, 25(8):1315-1325.

[26] Paolini, M.; Cantelli-Forti, G.; Perocco, P.; Pedulli, G.F.; Abdel-Rahman, S.Z. and Legator, M.S. *Nature*. 1999, 398(6730), 760–761.

[27] Liu, R.M.; Shi, M.M.; Giulivi, C. and Forman, H.J. *Am J Physiol. 1998*, 274: 330-336.

[28] Bresgen, N.; Karlhuber, G.; Krizbai, I.; Bauer, H.; Bauer, H.C. and Eckl, P.M. *J Neurosci Res*. 2003, 1;72(3):327-33.

[29] Michalopoulos, G.; Cianciulli, H.D.; Novotny, A.R.; Kligerman, A.D.; Strom, S.C. and Jirtle R.L. *Cancer Res.* 1982, 42(11), 4673-4682.

[30] Eckl, P.M.; Strom, S.C.; Michalopoulos, G. and Jirtle, R.L. *Carcinogenesis*. 1987, 8(8), 1077-1083.

[31] Eckl, P.M. and Raffelsberger, I. *Mutat Res.* 1997, 392(1-2), 117-24.

[32] Hess, D.; Keller, H. E.; Oberlin, B.; Bonfanti, R.; Schuep, W. *Int. J. Vitam. Nutr. Res*. 1991, 61: 232-238.

[33] Eckl, P.M.; Whitcomb, W.R.; Michalopoulos, G. and Jirtle, R.L. *J. Cell. Physiol.* 1987, 132(2), 363-366.

[34] Morgan, W.A.; Hartley, J.A. and Cohen, G.M. *Biochem. Pharmacol*.1992, 22;44(2):215-21.

[35] Eckl, P.M.; Alija, A.J.; Bresgen, N.; Bojaxhi, E.; Vogl, C.; Martano, G.; Stutz, H.; Knasmüller, S.; Ferk, F.; Siems, W.G.; Langhans, C.D. and Sommerburg, O. Carotenoids and Mutagenesis In Carotenoids and Vitamin A in Translational Medicine; Sommerburg, O.; Siems, W.G. and Kraemer, K., Eds.; CRC Press, 2013, pp. 155-174.

[36] Haider, C.; Ferk, F.; Bojaxhi, E.; Martano, G.; Stutz, H.; Bresgen, N.; Knasmüller, S.; Alija, A. and Eckl, P.M. *Antioxidants. 2017*, 6(2).

[37] Alija, A.J.; Bresgen, N.; Sommerburg, O.; Langhans C.; Siems, W. and Eckl, P. *Biofactors*. 2005, 24, 159-163.

β- KAROTENA NËN STRES OKSIDATIV INDUKON GJENOTOKSICITET

Alija, A. J.
Bresgen, N.
Langhans C.D.
Sommerburg, O.
Siems, W.
Eckl, P.M.

Abstrakt

Në hulumtimet e mëparshme kemi demonstruar se produktet oksidative të zbërthimit të β-karotenës indukojnë efekte gjenotoksike edhe në përqëndrime nanomolare. Meqë është e njohur se β-karotena nën stres oksidativ i nënshtrohet zbërthimit, ne kemi testuar edhe efektet e β-karotenës nën kushte të indukimit të stresit oksidativ në hepatocitet primare të *Rattus.* Kulturat primare të hepatociteve të *Rattus*, janë trajtuar me DMNQ (2,3-dimethoxy-1,4-naphthoquinone). Pastaj, kulturat janë analizuar për efektet cito- dhe gjenotoksike. Parametrat e vlerësuar kanë qenë: indeksi mitotik, përqindja e qelizave apoptotike dhe nekrotike, përqindja e qelizave me mikronukleuse (MN) si dhe numri i aberacioneve kromosomike (CA) dhe këmbimeve në mes kromatideve motra (SCE). Për më tepër, është analizuar edhe formimi i apo-karotenaleve. DMNQ e aplikuar në përqendrimin 40 μM ka indukuar rritje signifikante të MN, CA dhe SCE krahasuar me kontrollën e patrajtuar. Në prezencë të 1 dhe 5μM β-karotenë, është verejtur rritje e mëtutjeshme e MN, CA dhe SCE. Rritje statistikisht signifikante është vërejtur në 50μM β-karotenë. Bazuar në këto të dhëna, mund të konkludohet se β-karotena i nënshtrohet zbërthimit nën kushte të stresit oksidativ dhe shpreh efekte gjenotoksike të cilat, më së shumti ka të ngjarë që mund t'i atribuohen formimit të produkteve të zbërthimit të saj.

KDU 547

METAL - METAL INTERACTIONS IN BIOLOGICAL SYSTEM: A COMPETITIVE APPROACH. *REVIEW*

Lulzim Zeneli[a*]
Majlinda Daci-Ajvazi[b]

Dedicated to Professor Nexhat Daci on the occasion of his 75th birthday

Abstract

The increased availability of metals in biological environments, due to human intervention in the last century, raised concerns on the effects that metals might have on living organisms. Consequently, the toxicology of metals and bioinorganic chemistry has emerged as very active in this field of metals research. Different chemical forms can influence metal toxicokinetics and toxicodynamics and should be considered to improve human health risk assessment. Factors that influence metal speciation include: carrier-mediated processes for specific metal species; valence state; particle size; the nature of metal binding ligands; whether the metal is an organic versus inorganic species and biotransformation of metal species. The recent studies of the co-ordination chemistry of metal ions in biological systems (mostly X-ray crystallographic data) show the potential grouping metal ions according to their

[a] *University of Gjakova "Fehmi Agani" Gjakova, Kosova.*
[*] *Correspondent author:* lzeneli@gmail.com; lulzim.zeneli@uni-gjk.org.
[b] *Department of Chemistry, Univesity of Prishtina, Prishtina, Kosova.*

binding preferences (i.e. whether they seek out 0-, N- or S-containing ligands), on the other hand, the scientific results have shown us for the possibility of metal-metal interaction in biological systems despite their level of concentration. This review provides a compilation of research done on metal - metal interaction in biological system.

Key words: Interaction, metals, covalent index, ionic index, biomolecule.

Introduction

Studies of the behavior of metal ions in biological systems make possible the increase of our understanding of the relationship between the chemistry of metals and life process itself. Homeostasis of metal ions, is maintained through tightly regulated mechanisms of uptake, therefore their storage and secretion are critical for life and are maintained within strict limits [1]. Malfunction of metal-ion homeostasis can lead to the metal binding to protein sites which are different from those designed for that purpose or replacement of other metals from their natural binding sites [2]. Many researchers have considered that the breakdown process of metal-ion homeostasis has been involved in a plethora of diseases or public health problems [3-5]. Metal ions play an important role in biological systems either as metal-biomolecules or sometimes they exist as such. Each metal ion has its own chemistry. Metal ions are generally positively charged and act as electrophiles, seeking the possibility of sharing electron pairs with other atoms so that a bond or charge-charge interaction can be formed [6,7]. However, metal ions, often have positive charges greater than one, and have a larger ionic volume so that they can accommodate many ligands around them at the same time. Humans may be exposed to different elements such as cadmium and arsenic which have no recognized biological function and are even known to be toxic at low concentrations. In contaminated areas,

exposure to these elements arises from a variety of natural sources, including air, drinking water and food. Since redox active metals undergo redox-cycling reactions, for the group of redox-inert elements, the primary route for their toxicity and carcinogenicity is depletion of glutathione, bonding to sulphydryl groups of proteins and their metal – metal interactions [8, 9, 10].

This paper is an overview of some aspects of metal interactions in biological systems: basic concepts, the theoretical basis of covalent index ($X_m^2 r$) and ionic index (Z^2/r) and metal - metal interactions.

Basic concepts

In chemical toxicology, the term heavy metal is usually used to designate metals which are responsible for adverse biological reaction. For example, metals, lead (density 11.34 g/cm^3) and mercury (density 13.55) are called heavy metals in the sense that their densities are high and they have toxic effects in living organisms. But this classification is not always sharp. According to Ahrland et all [11], from the examined trends in the magnitude of equilibrium constants that show the stability of metal-ion/ligand complexes, metals could be classified into three categories. Metal and metalloid ions also are also assembled into three groups, thus reproducing the traditional groupings of metal ions: Class A (‘hard’ acids, oxygen donor-atom seekers), Class B (‘soft’ acids, nitrogen/sulfur donor-atom seekers), and intermediate class that contains metal ions which display ambivalent affinity for donor-atoms [12-14].

This classification of metals ions into distinct groups was based on empirical thermodynamic data, namely trends in the magnitude of equilibrium constants that shows the stability of metal-ion/ligand complexes ones they are created, see the following expressions:

$M + L = ML$

$K_{ML} = [ML] / [M] [L]$

M - represents the metal ion, L - the ligand, ML - the metal-ligand complex and K_{ML} - the stability constant while the bracket represents the concentration of each species in mol/dm^3.

Class A metals ions, based on the magnitudes of the complex equilibrium constants with halogen ions, have the following ligand or donor atom preference sequence: $F^- > Cl^- > Br^- > l^-$. As it concerns metal ion complexes with halogen atoms as donors, they show these tendencies: O > S ~ Se; while for chemical elements of 15 group one has N > As. If one compares all these ligands the general tendency is: O > N > S. However, class B metal ions complexes exhibit the opposite preference sequences: i.e. $I^- > Br^- > Cl^- > F^-$ and Se ≈ S > O; As > N; S>N>O. The borderline metal ions form an intermediate group which is ambivalent because these ions exhibit affinity for the above metal-binding donor atoms and ligands. Figure 1 shows the classification of 26 metal ions into three groups on the basis of these abovementioned criteria. Several features should be noted in it. The separation between class A metal ions and borderline metal ions is very sharp, while the distinction between class B ions and borderline metal ions is less clear.

Type A metal ions

For type A metal ions, an electrostatic model explains to a large extent the stability of metal-ligand complexes. It predicts that the stability of these complexes is positively correlated with the charge squared to radius ratio, (Z^2/r) for both the metal ion and the ligand species.

Therefore, small metal ions two positively charged of alkaline earth group form stronger complexes as shown by the relative stability constant values according to the following sequence:

$Mg^{2+} > Ca^{2+} > Sr^{2+} > Ba^{2+}$

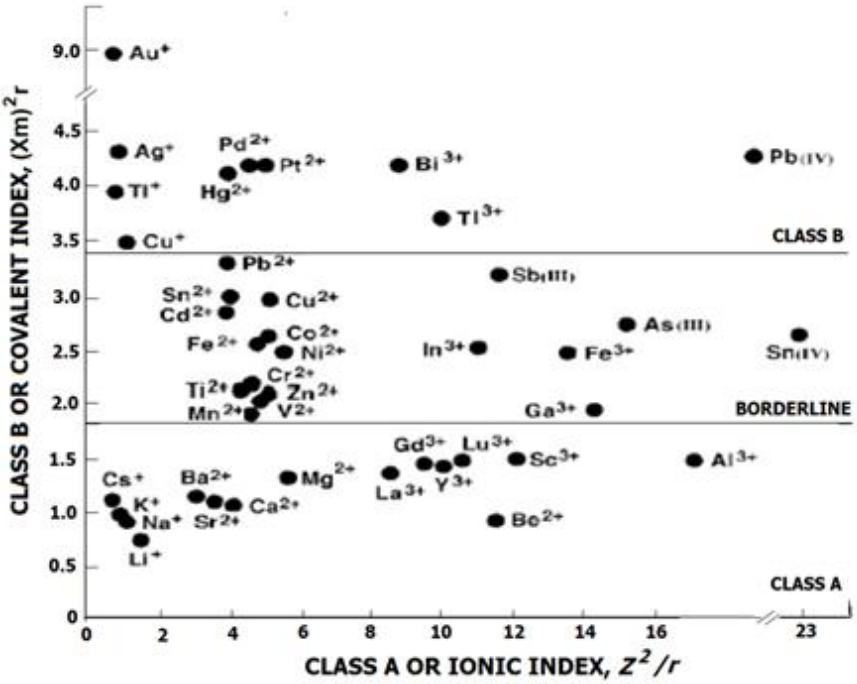

Fig. 1. Classification of metal ions according to their preference for donor atom binding. The "ionic index," being a function of charge squared to atom or ion size ratio (Z^2/r), is a suitable measure of the ability of metal ions to participate in ionic interactions. The covalent index, which is a function of square of electronegativity and atom size (Xm^2r), reflects the tendency for covalent bonding. Reprinted (with modifications) from Nieboer *et al*., 1999.

The borderline metal ions

The intermediate group formed by the borderline metal ions is ambivalent due to the fact that these ions exhibit a cationic affinity for the above metal-binding donor atoms and ligands. Most of biological micronutrients, including Mn, Cu and Zn ions, are found in borderline group [15].

Type B metal ions

The type B metal ions include several metals which are known to be toxic to organisms. It is composed of metals ions with nd^{10} and nd^{10} $(n+1)\ s^2$ type electron configurations. Such cations have readily distorted electronic distributions; in other words, they exhibit high polarizability. This class is closely equivalent to the soft metal ion category of the Pearson system based on hard-soft theory. In the group are also included Ag^+ [$Kr(4d^{10})$], Zn^{2+}[$Ar(3d^{10})$], and Pb^{2+} [$Xe(4f^{14}\ 5d^{10}\ 6s^2)$] ions [16].

The theoretical basis of covalent index ($\chi_m^2 r$) and ionic index (z^2/r)

Observations concerning metal-associated ligands are largely empirical, so the question is whether one can identify a model to predict metal ion reactivity and metal-ligand stability. Although models have been developed for toxicity-inducing metals in mammalian organisms, they have seldom considered metal speciation. A noteworthy model to predict metal ion reactivity and metal-ligand stability is the classification system proposed by Nieboer and colleagues. This system was developed from the fundamental properties of metal ions. It is based upon the electronegativity value, the tendency for the metal atom to become positively charged, and the metal coordination number, the number of sites at which complexed ligands are attached to a metal ion [17,18].

According to Pauling, a chemical bond between two atoms may have a certain amount of covalency or ionicity [19]. The covalency and ionicity of a bond are very useful qualitative concepts for chemists [20], Pauling was the first to give a quantitative measure of these concepts based on the electronegativity differences of the atoms involved in the bond.

The bond order which we call the bond index is defined in terms of two other indices: the covalent bond index and the ionic bond index.

Metal atoms according to their ability to form covalent bonds are represented by the covalent index $(\chi_m)^2 r$, where χ_m is the electronegativity and r is the ionic radius of the species with the most common coordination number. This index is interpreted as the difference between the valence orbital energy and the ionic energy, and thus reflects the relative ability to form covalent versus ionic bonds. That is a covalent index. A second index was devised as z^2/r to represent ionic interactions (ionic index), where z is the ion charge and r is defined as above. The graph of these two values for the ions of 36 metals and two metalloids is shown in Fig. 1. All groups of the periodic chart containing metals are represented, as are all periods of the chart with the exception of the actinides. For a fixed value of the ionic index in Fig. 1, toxicity generally rises with the magnitude's increase of the covalent index. For example, Hg(II) produces more toxicity than Ca(II). Conversely, for a fixed value of the covalent index, toxicity generally augments with the magnitude's increase of the ionic index. For instance, As(III) produces more toxicity than Cu(II). In addition, for a fixed value of the covalent index, stability with nearly all ligands correlates positively with the ionic index. Similarly, for a fixed value of the ionic index, stability generally increases with the rise of the covalent index value. For example, Pb(II) functionally displaces Ca(II) in neurons by impeding Ca(II) entry through membrane voltage-sensitive channels [20,21] and by exhibiting greater potency to activate Ca(II)-dependent enzymes and proteins (22-24]. Cd(II) has a similar action on voltage-sensitive Ca(II) channels. Thus, this model suggests that increased metal-ligand stability results in increased toxicity.

Metals in biological systems

With the regard to biology, inorganic elements comprise the bulk of the periodic table (Fig. 2), because a significant number of chemical elements are either essential for life with known functions, or present in

organisms. Metals of biological systems are usually identified as essential in all species. However, some elements are essential to only a few organisms. According to Maret, biological metals are categorize in the following way: (i) elements that are essential to all species; (ii) elements that are used in a significant number of species (V, Ni); and (iii) elements that are used only in a few organisms in special ecological niches (W, Cd, Lanthanides)[25]. For humans, we now know that 11 metals and 10 non-metals, i.e., 21 elements, are essential. Among these elements, chromium is also included although its status as an essential element is controversial. To improve human health risk assessment, chemical forms (i.e., species) can influence metal toxicokinetics and toxicodynamics and should be considered as such. The International Union for Pure and Applied Chemistry (IUPAC) in 1997 developed a definition recommending that speciation "Refers to the chemical form or compound in which an element occurs in both non-living and living systems. It may also refer to the quantitative distribution of an element." Chromium is an example of the importance of chemical speciation in biology: Chromium (III) complexes are the ones having beneficial functions and little toxicity, whereas Cr(VI), in chromate, is a human carcinogen. Although the importance of metal speciation in toxicokinetics and toxicodynamics is appreciated, metal speciation has not been determined in most studies [26]. Many metals have more than one biologically relevant valence state such as: Ag(0,I and II), Am(III, IV, V and VI), As(III and V), Co(II and III), Cr(III and VI), Cu (0, I and II), Fe(0, II and III), Hg(0, I and II), Mn(II, III and IV), Mo(II, III, IV and VI), Ni(II and IV), Pu(III, IV, V and VI), Sb(III and V), Se(II, IV and VI), Sn(II and IV), Te(0, II, IV and VI), Tl(I and III), U(III and VI), V(IV and V) and Zn(0 and II).

Valence state of the metal can affect the absorption, distribution, biotransformation, and elimination of a metal and therefore its toxicity [27]. Some metals have more than one biologically relevant isotope that can also affect in the absorption process including ^{226}Ra and ^{228}Ra; the anthropogenic ^{232}U and ^{233}U and the natural ^{234}U, ^{235}U and ^{238}U; ^{238}Pu and ^{239}Pu; and ^{228}Th, ^{230}Th and $_{232}$Th.

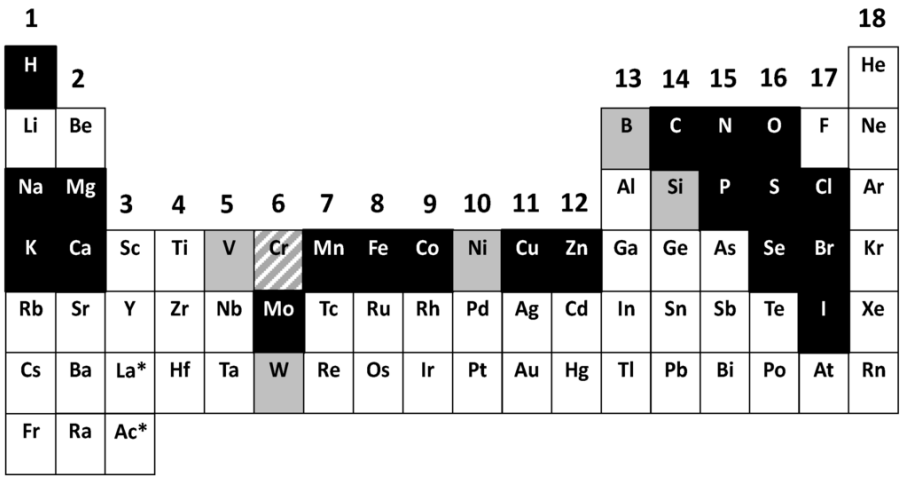

Fig. 2. The essential elements are shown in black with the exception of chromium (Cr), which is shown with an upward diagonal pattern (see text), and the essential elements that are more restricted for some forms of life are shown in grey. Reprinted from Maret, 2015.

Sometimes the chemical coordination and oxidation-reduction properties of essential metals, have given them an additional behavior so that they can escape control mechanisms such as homeostasis, transport, compartmentalization and binding to required cell constituents. These metals by competition inhibition bind with protein sites displace original metals from their natural binding sites causing malfunctioning of cells and ultimately toxicity [28]. Previous research has found that oxidative deterioration of biological macromolecules is primarily due to the binding of heavy metals to the DNA and nuclear proteins [29]. In the last decades, the natural environment concentrations of several chemical elements (toxic and essential) have been largely increased, mostly as a result of anthropogenic activities [30-32]. The results of some recent studies show that at high concentrations, all metals (essential and nonessential) are toxic [33]**,** but some metals such as arsenic, mercury, and uranium are very harmful even at low levels of concentration [34-

35]. The metabolic functions are disrupted by heavy metals in two ways: a) by accumulating and thereby disrupting function in vital organs and glands such as the heart, brain, kidneys, bone, liver, etc. b) by displacing the vital nutritional minerals from their original place, thereby, hindering their biological function. Analyses of trace elements concentrations in human biological material are performed using inductively coupled plasma mass spectrometry and atomic absorption spectrometry, but also electrochemical methods and X-ray fluorescence spectroscopy. All the predominant sample matrices include blood and bone, as well as urine, hair, nail, and saliva. In general metals play an important role in the development of biomarkers and make a significant contribution to development of the biomonitoring approach [36]. To characterize first biological effects, diverse parameters are treated as "biomarkers of effect", like d-aminolaevulinic acid dehydratase (ALAD) and erythrocyte porphyrins (EPs) in blood as well as d-aminolaevulinic acid (ALA) in urine and plasma and coproporphyrin in urine.

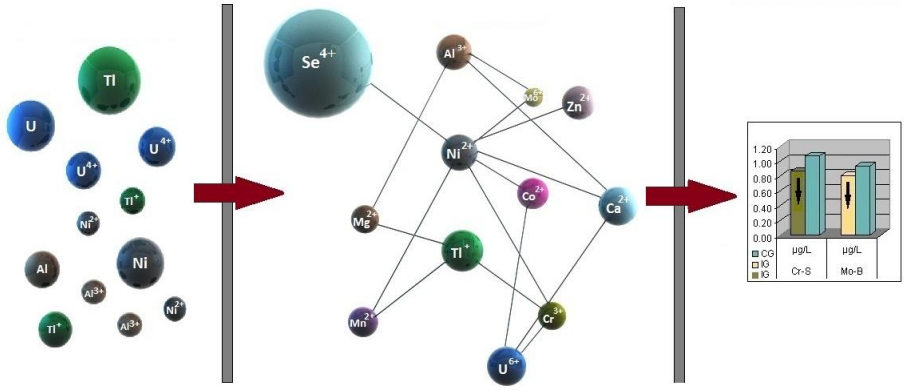

Scheme 1. Schematic diagram of the interaction between aluminum, nickel, thallium and uranium and essential elements (Ca, Mg, Zn, Se, Mn, Co, Cr and Mo), involved biomarkers of exposure – interaction–biomarkers of effects. Reprinted from Zeneli *et al*., 2015.

Metal – metal Interaction

Metal accumulation and the resultant interactions between trace elements have been investigated in vivo (in humans and farm animals in polluted areas) [36-40] and in vitro (experimental studies) [41-43]. Metal - metal interactions are of significant importance, especially from the health point of view, because, depending on their interaction (synergistic or antagonistic nature), concentration of elements may either increase or decrease.

The interaction can either be "one-way" by decreasing or increasing the level of only one of interacting elements, or of "two-ways" that is, the interacting elements can mutually affect each other's concentration by increasing or decreasing the level of either of the elements involved, the effect being non mutual [44]. Interactions between metals can vary depending on the metal bioavailability (or biologically available metals), consequently, from the metal ions biochemistry. Many metal ions control the essential biological processes of living cells and without their catalytic presence many biological reactions would not take place [45]. While Na^+, K^+, Mg^{2+} and Ca^{2+} ions are important neurotransmitters; zinc, iron, copper, and related d-block metals are emerging as significant players in both neurophysiology and neuropathology, particularly with regard to aging and neurodegenerative diseases [46], while Zn^{2+} ions through the zinc finger play an important role in the regulation of DNA transcription and replication [47]. On the other hand, the binding of metal ions to different sites on biomolecules can stabilize or destabilize the secondary structure, but it can also cause a change in conformation. A correlation between two trace elements in biological samples, in blood, or serum, indicates that interactions can be suspected. For example, the concentrations of copper (Cu) and zinc (Zn) are known to correlate and to interact in the body [48,49]; The concentrations of selenium (Se) and a number of toxic metals have also been shown to correlate [50, 51]; Aluminum (Al) correlates with magnesium

(Mg) and calcium (Ca); Nickel stay in correlations with a number of essential elements, such as calcium (Ca), zinc (Zn), selenium (Se), manganese (Mn), cobalt (Co), chromium (Cr) and molybdenum (Mo). Thallium (Tl) correlates with calcium (Ca), manganese (Mn) and chromium (Cr)[34]; Strontium (Sr) correlates with molybdenum (Mo); and uranium (U) with calcium (Ca) and chromium (Cr)[35].

Nonessential elements, due to the high value of covalent and ionic index compared with the essential elements, are powerful competitors to essential elements in biochemical processes [35,36]. Consequently, the increasing competition between nonessential/essential elements in biological systems produces more toxicity.

Nonessential metals exhibit their toxicity by inactivating biomolecules through either blocking essential functional groups, by displacement of essential metal ions from their native binding sites or through ligand interactions. Correlation can also show if a common source of exposure sufficiently contributes to the total biological levels.

Conclusion

The assumption that metal - metal interactions in biomolecule reflect the competition until now was supported by a limited thus insufficient number of studies. It is required more work with a wider range of metals including those with more divergent Z^2/r values. Regardless of the limitations, the theory of covalent index and its interpretation provides a firm bases for further understanding of metal-metal interactions.

References

1. Bertini, I. and Cavallaro, G. J Biol Inorg Chem., 2008, 13, 3-14.
2. Nelson, N. Biochim. Biophys. Acta, 1992, 1100, 109–124.
3. Valko, M., Morris, H., and Cronin, M. T. D. Curr. Med. Chem., 2005, 12, 1161–1208.
4. Mates, J. M.; Perez-Gomez, C.& De Castro, I. N. Antioxidant enzymes and human diseases. Clin. Biochem., 1999, 32, 595–603.
5. Halliwell, B. and Gutteridge, J.M.C. Free Radic Biol Med. 1995,18, 125–126.
6. Glusker, J.P.,Katz ,K. and Bock Ch. The Rigaku Journal, 1999, 16 (2), 1-8.
7. Bock, C. W., Katz, A. K. and Glusker, J. P. J. Am. Chem. Soc., 1995, 117, 3754–3765.
8. Speisky, H., Gomez, M., Carrasco-Pozo, C., Pastene, E., Lopez-Alatrcon, C. and Olea-Azar, C. Bioorg Med Chem,2008, 16, 6568-6574.
9. Sinicropi, M.S., Amantea, D. and Caruso, A. and Saturnino C. Arch.Toxicol., 2010, 84, 501-520.
10. Peralta-Videa, J.R., Lopez, M.L., Narayan, M. and Saupe, G.J. Int. J. Biochem. Cell. Biol., 2009, 41, 1665-1677.
11. Ahrland, S., Chatt, J. and Davies, N.R. Q. Rev. Chem. Soc., 1958, 12, 265-276.
12. Nieboer, E. and Richardson, D.H.S. Environ. Poll. Series B – Chem. Phys., 1980, 1:3–26.
13. Nieboer, E., Fletcher, G. G. and Thomassen, Y. J. Environ. Monit., 1999, 1:1–14.
14. Martell, A., Hancock R., Smith R. and Motekaitis, R. Coordination Chemistry Reviews, 1996, 149, 311-328.
15. Haas, K.L. and Franz, K.J. *Chemical Reviews, 2009,* 10, 4921-4960.
16. Pearson, R.G.J. Am. Chem. Soc. 1963,85:3533.
17. Perrin, D.D. and Dempsey, B. Buffers for pH and Metal Ion Control. Chapman and Hall; New York. 1979, p. 94.

18. Cowan, J.A.In: Biological Inorganic Chemistry: Structure and Reactivity, Bertini I, Gray HB, Stiefel EI, Valentine JS, editors, University Science Books, Sausalito, CA, 2007, p. 175.
19. Pauling, L. The nature of the chemical bond, 3rd edn., 1960, Cornell University Press, New York.
20. Gould, M.D., Taylor, Ch., Wolff, S.K., Theor. Chem. Account., 2008, 119, 275–290.
21. Suszkiw, J., Toth, G., Murawsky, M., and Cooper, G. P. Brain. Res.,1984, 323, 31–46.
22. Shao, Z. and Suszkiw, J. B. J. Neurochem.,1991, 56, 568–574.
23. Long, G. J., Rosen, J. F., and Schanne, F. A. J. Biol. Chem. 1994, 269, 834–837.
24. Kern, M., Wisniewski, M., Cabell, L., and Audesirk, G. NeuroToxicology, 2000, 21, 353–63.
25. Maret, W. Int. J. Mol. Sci.,2016, 7(1), 66-73.
26. Boisset, M. Comp. Rend. L'Acad. d'Agric. 2000, 86, 49–65.
27. Niesiobędzka, K., Krajewska E. Environmental Protection and Natural Resources, 2009, 40:261-269
28. Jaishankar, M., Mathew, B.B., Shah, M.S. and Gowda, K.R.S. J. Environ. Poll. Human Health, 2014, 2(1), 1– 6.
29. Flora, S.J.S., Mittal, M. and Mehta, A. Indian J. Med. Res., 2008, 128, 501–523.
30. Andersen, M.E. Toxicol. Lett., 1995, 79, 35-44.
31. Zeneli, L., Daci-Ajvazi, M., Daci, N. M., Hoxha, D. and Shala, A. Hum. Ecol. Risk. Assess., 2013, 19, 1618–1627.
32. Zeneli, L., Daci, N., Pacarizi, H. and Daci-Ajvazi, M. Indoor Built Environ.,2011, 20, 479–482.
33. Daci-Ajvazi, M., Zeneli, L., Daci, N., Krasniqi, A., Ymeri, N. Fresen. Environ. Bull., 2018, 27(1), 172-179.
34. Zeneli, L., Sekovanič, A., Ajvazi, M., Kurti, L. and Daci, N. Environ. Geochem. Health, 2016, 38(1), 65-72.
35. Zeneli, L., Sekovanič, A. and Daci, N. J. Environ. Sci. HealthA, 2015, 50(6), 540-546.
36. Zeneli, L. and Daci, N. Toxicol. Environ. Chem. 2014, 96(5), 808-813.

37. Koh, T.S. and Judson, G.J. Bull. Environ. Contam. Toxicol. 1986, 37, 87–95.
38. Langlands, J.P., Donald, G.E. and Bowles, J.E. Cadmium concentrations in liver, kidney and muscle in Australian sheep and cattle. Aust. J. Exp. Agr., 1988, 28, 291–297.
39. Telišman, S., Prpič-Majič, D., Kersanc, A. Relationships between blood lead and indicators of effect in cows environmentally exposed to lead. Toxicol. Lett., 1990, 52, 347–356.
40. Zeneli, L., Daci, N.M., Pacarizi, H. and Daci-Ajvazi, M. Am. J. Pharm. Toxicol., 2010, 5(1), 48–51.
41. Reddy, C.S., Mohammad, F.K., Ganjam, V.K., Martino, M.A. and Brown, E.M. Bull Environ. Contam. Toxicol, 1987, 39, 350 - 357.
42. Wentink ,G.H., Wensing, T., Baars, A.J., van Beek, H., Zeeuwen, A.A.P.A. and Schotman, A. J. H. Bull. Environ. Contam. Toxicol., 1988, 40, 131 – 138.
43. Smith, R.M., Griel, L.C., Muller, L.D., Leach, R.M. and Baker, D.E. J. Anim. Sci., 1991, 69, 4078–4087.
44. Kalavrouziotis, I.K., P.H. Koukoulakis, P., Robolas, A.H., Papadopoulos, V. and Pantazis, V. Water Air Soil Pollution, 2008, 190, 1-4, 309-321.
45. Anastassopoulou, J. J. Mol. Struct., 2003, 651–653, 19–26.
46. Jové, M., Portero-Otín, M., Naudí A., Ferrer, I. and Pamplona, R. *J. Neuropathol. Exp. Neurol.***,** 2014, 73(7), 640–657.
47. Rich, A.M., Bombarda, E., Schenk, A.D., Lee, P.E., Cox, E.H., Spuches, A.M., Hudson, L.D., Kieffer,B. and Wilcox, D.E. *J. Am. Chem.Soc.*, 2012,***134*** (25), 10405-10418
48. Reunanen, A., Knekt, P., Marniemi, J., Maki, J., Maatela, J. and Aromaa, Eur. J. Clin. Nutr.,1996, 50, 431-437.
49. Milanino, R., Marrella, M., Gasperini, R., Pasqualicchio, M., Velo, G. Inflamm. Res., 1993, *39*(3), 195-209.
50. Orct, T., Lazarus, M., Jurasović, J., Blanuša, M., Piasek, M., Kostial, K. J. Appl. Toxicol., 2009, 29, 585-589.
51. Lazarus, M., Orct, T., Jurasović, J., Blanuša, M. BioMetals, 2009, 22 (6), 973–983.

INTERAKSIONI METAL-METAL NË SISTEMIN BIOLOGJIK: QASJA KONKURRUESE

Lulzim Zeneli
Majlinda Daci-Ajvazi

Përmbledhje

Ky punim revial trajton qasjen konkurruese ndërmjet elementeve kimike (metaleve dhe metaloideve) në sistemin biologjik. Në dy dekadat e fundit është parë një përparim i dukshëm në vlerësimin e rolit të metaleve në gjurmë në nivel të biomolekulave dhe rezultatet e publikuara deri me tani, kanë qenë të një spektri të gjerë të hulumtimit nga fusha e biokimisë, bioinorganikës dhe toksikologjisë.

Në molekulat biologjike, jonet metalike janë prezente si komponente me rëndesi esenciale të cilat determinojnë edhe funksionalitetin e saj (psh. në enzima), por gjithashtu metalet si ksenobiotik (të tilla si: Pb, As, Cd, Hg, Ni, Al, U, Tl, etj) i hasim në sistemet biologjike si rezultat i ekspozimit kronik përmes ndotjes së mjedisit me to.

Qasja konkurruese e joneve metalike në interaksionin metal - metal bazohet në specifiken e kimisë së joneve, e cila adresohet në këtë punim përmes teorisë së indeksit kovalent (IK) dhe indeksit jonik (IJ). Elementet kimike jo esenciale (metalet dhe metaloidet) krahasuar me elementet esenciale dallojnë dukshëm për nga vlerat e indeksit kovalent dhe indeksit jonik dhe si të tilla këto elemente dominojnë në reaksionet kompetitive në nivel të biomolekulës.

Rezultatet e hulumtimit kanë treguar se në sistemin biologjik elementet joesenciale të tilla si As, Hg, U, dhe Tl, janë konkurrues të fuqishëm të elementeve esenciale edhe kur përqendrimi i tyre është brenda vlerave të lejuara (referente).

KDU 53

ANALYSIS OF GALILEAN INVARIANCE USING THE LAW OF COSINES

Shukri Klinaku*

Abstract

Using the invariance of the law of cosines, as a very easy case to understand invariance, we will explain the Galilean invariance – the invariance of Galilean transformation, the invariance of velocity addition formula and invariance of the law of force.

Keywords: Galilean relativity, the law of cosines, invariance

1. Introduction

Let us take a triangle ABC (Fig. 1*a*). According to the law of cosines (LC) we can write this equation for this triangle:

$$a^2 = b^2 + c^2 - 2bc \cdot cos\alpha. \quad (1)$$

* Department of Physics, University of Prishtina, 10000 Kosova.
Corresponding author address: klinaku@uni-pr.edu

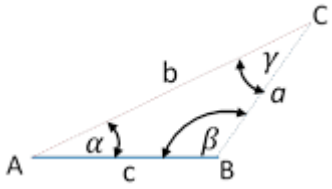

a)

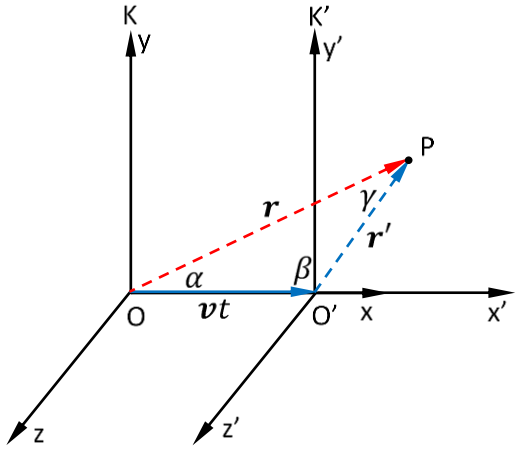

b)

Fig. 1. The triangle ABC (*a*); the relative motion of particle (body) P (*b*).

Equation (1) is a quadratic equation and if we solve it for b we obtain:

$$b = a\sqrt{1 - \frac{c^2}{a^2}sin^2\alpha} + c \cdot cos\alpha. \quad (2)$$

Now, let us assume two inertial systems of reference K and K'; system K' will move away from system K with velocity v, while particle (body) P moves with velocity u' relative to the origin of the inertial

system K' (Fig. 1*b*). We can see that triangle ABC in Fig. 1*a* is the same as triangle OO'P in Fig. 1*b*, so this enables us the comparison between geometrical situations and "dynamic" conceptions, therefore according to equations (1) and (2) for Fig. 1*b*, for a time t we can write:

$$r = r'\sqrt{1 - \frac{v^2t^2}{r'^2}sin^2\alpha} + vtcos\alpha. \quad (3)$$

Both frames of reference share the same time, because we are in the realm of Galilean relativity. As we can see, instead of edge c in Fig. 1*a* (equations 1 and 2), we have vt in Fig. 1*b* (equation 3); r is the magnitude of the position vector of particle (body) P relative to system K; r' is the magnitude of the position vector of particle (body) P relative to system K', and for the velocity of P in K' we have: $u' = r'/t$. Let us note the velocity of P relative to origin O with u, and this velocity will be $u = r/t$. Using these velocities for equation (3) we obtain:

$$r = r'\sqrt{1 - \frac{v^2}{u'^2}sin^2\alpha} + vtcos\alpha. \quad (4)$$

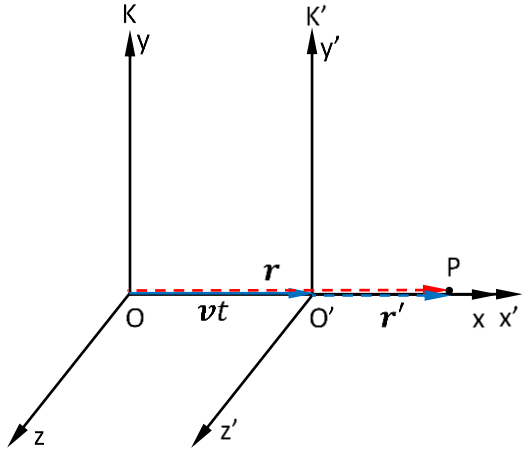

Fig. 2. The case of Galilean relative motion when $\alpha = 0°$.

We have called equation (4) the general Galilean transformation [1], because as we can see, for $\alpha = 0°$ between r and v, Fig. 1*b* is transformed to Fig. 2, and from equation (4) we obtain:

$$r = r' + vt \quad (5)$$

which presents the well-known Galilean transformation according to this figure. In these circumstances, equation (4) can be called the general Galilean transformation (GGT) for the resting observer at origin O. Indeed, for the situation in Fig. 1*b* we know the vector form of Galilean transformation:

$$\boldsymbol{r} = \boldsymbol{r}' + \boldsymbol{v}t \quad (6)$$

while equation (4) represents the same thing but expressed through the magnitudes of vectors. In other words, equation (6) is general Galilean transformation in the vector form, while equation (4) is general Galilean transformation expressed by the vector magnitudes. Ongoing the Galilean invariance for Galilean transformation, velocity addition formula and for force will always be presented by relying on the explanation of relative motion using the LC. We consider that the invariance of the force presented here is very important because from many authors and textbooks [2-6] we obtain the confusing idea that the value of force in relative motion is invariant regardless of the observer measuring it. The invariance of other quantities according to this method can be explained by students or may be the subject of another paper.

Table 1. The invariance of law of cosines relative to points of view.

Point of view	For any value of α	For $\alpha = 0° \Rightarrow \beta = 180°$ and $\gamma = 0°$
A	$a = \sqrt{b^2 + c^2 - 2cbcos\alpha}$	$a = b - c$
	$b = \pm a\sqrt{1 - \frac{c^2}{a^2}sin^2\alpha} + ccos\alpha$	$b = a + c$
	$c = \pm a\sqrt{1 - \frac{b^2}{a^2}sin^2\alpha} + bcos\alpha$	$c = b - a$
B	$b = \sqrt{a^2 + c^2 - 2accos\beta}$	$b = a + c$
	$c = \pm b\sqrt{1 - \frac{a^2}{b^2}sin^2\beta} + acos\beta$	$c = b - a$
	$a = \pm b\sqrt{1 - \frac{c^2}{b^2}sin^2\beta} + ccos\beta$	$a = b - c$
C	$c = \sqrt{a^2 + b^2 - 2abcos\gamma}$	$c = b - a$
	$a = \pm c\sqrt{1 - \frac{b^2}{c^2}sin^2\gamma} + bcos\gamma$	$a = b - c$
	$b = \pm c\sqrt{1 - \frac{a^2}{c^2}sin^2\gamma} + acos\gamma$	$b = c + a$

2. Galilean invariance

Galilean invariance is a synonym for the principle of relativity first described by Galileo in 1632 [7], according to which the laws of motion are the same in all inertial systems. In other words, the principle of relativity holds that the laws should be the same regardless of the observer measuring them. Now we return again to the LC and triangle of Fig. 1*a*. Did the edges of this triangle have the same magnitude? Of course not! But if we stay at summit A and we want to know the magnitudes of the edges, according to the LC we will find three equations which are the same as the equations found if we stand at summit B or C. In other words, the LC is invariant regardless of the point of view. All this is

presented in table 1. As we can see, in the second column are the magnitudes of edges for any angle α, while in the third column stay the magnitudes for a special case, and according to the rules of triangle geometry we have chosen one from both signs in front of the square root.

2.1. Invariance of the Galilean transformation

Now according to the analogy which we used to obtain equation (4) from equation (2), we can obtain the complete table (2) from table (1). Table (2) responds to Fig. 1*b*.

Table 2. The invariance of Galilean transformation relative to the observer's view.

Observer	For any value of α	For $\alpha = 0° => \beta = 180°$ and $\gamma = 0°$
O	$r' = \sqrt{r^2 + v^2t^2 - 2vtrcos\alpha}$	$r' = r - vt$
	$r = \pm r' \sqrt{1 - \frac{v^2}{u'^2} sin^2\alpha} + vtcos\alpha$	$r = r' + vt$
	$vt = \pm r' \sqrt{1 - \frac{u^2}{u'^2} sin^2\alpha} + utcos\alpha$	$vt = r - r'$
O'	$r = \sqrt{r'^2 + v^2t^2 - 2r'vtcos\beta}$	$r = r' + vt$
	$vt = \pm r \sqrt{1 - \frac{u'^2}{u^2} sin^2\beta} + u'tcos\beta$	$vt = r - r'$
	$r' = \pm r \sqrt{1 - \frac{v^2}{u^2} sin^2\beta} + vtcos\beta$	$r' = r - vt$
P	$vt = \sqrt{r'^2 + r^2 - 2rr'cos\gamma}$	$vt = r - r'$
	$r' = \pm vt \sqrt{1 - \frac{u^2}{v^2} sin^2\gamma} + utcos\gamma$	$r' = r - vt$
	$r = \pm vt \sqrt{1 - \frac{u'^2}{v^2} sin^2\gamma} + u'tcos\gamma$	$r = vt + r'$

As we can see from each system of reference, we can find the magnitude of each edge using the same laws. Usually in textbooks we see the invariance only for observers at O and O', while here we have presented complete invariance, thus including the hypothetical observer at P.

2.2. Invariance of the velocity addition formula

If we divide equation (4) by time t, we obtain the relative velocity, calling it the velocity addition formula (VAF). For this law, we also have the table of invariance (table 3).

Here we deal with VAF, and the principle of relativity claims that among velocities in relative motion there is no privileged velocity; that implies that each velocity can be a part of a relative velocity and can also be the relative velocity between two other velocities (Fig. 3). In other words, the invariance of VAF, implies that each of velocities preserve its magnitude and there is an invariant law (that is VAF) which represents the sum of the whichever two of the three velocities present in the relative motion.

Table 3. The invariance of velocity addition formula relative to the observer's view.

Observer	For any value of α	For $\alpha = 0° \Rightarrow \beta = 180°$ and $\gamma = 0°$
O	$u' = \sqrt{u^2 + v^2 - 2vucos\alpha}$	$u' = u - v$
	$u = \pm\sqrt{u' - v^2 sin^2\alpha} + vcos\alpha$	$u = u' + v$
	$v = \pm\sqrt{u' - u^2 sin^2\alpha} + ucos\alpha$	$v = u - u'$
O'	$u = \sqrt{u'^2 + v^2 - 2u'vcos\beta}$	$u = u' + v$
	$v = \pm\sqrt{u^2 - u'^2 sin^2\beta} + u'cos\beta$	$v = u - u'$
	$u' = \pm\sqrt{u^2 - v^2 sin^2\beta} + vcos\beta$	$u' = u - v$
P	$v = \sqrt{u'^2 + u^2 - 2u'ucos\gamma}$	$v = u - u'$
	$u' = \pm\sqrt{v^2 - u^2 sin^2\gamma} + ucos\gamma$	$u' = u - v$
	$u = \pm\sqrt{v^2 - u'^2 sin^2\gamma} + u'cos\gamma$	$u = v + u'$

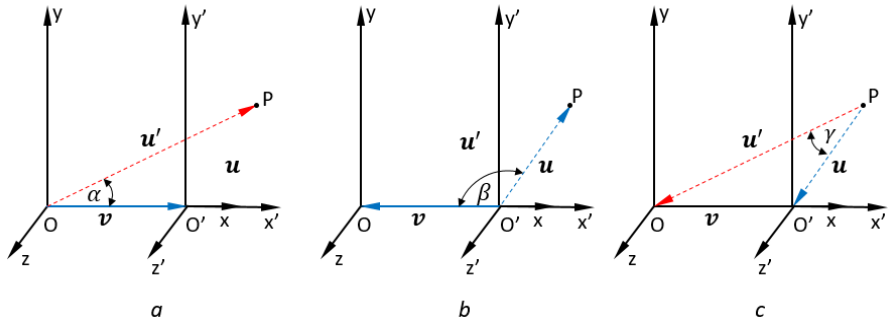

Fig. 3. The observer's at O point of view (*a*); the observer's at O' point of view (*b*); the observer's at P point of view (*c*).

2.3. Invariance of the force

Since the mass in Galilean relativity doesn't depend on velocity, we will present only the invariance of the law of acceleration in relative motion (table 4). As we can see in the second column of table 4, the law of accelerations is the same regardless of the observer measuring them, but this doesn't imply that the values of all three accelerations present in relative motion are the same in each frame of reference. Indeed, the relative velocity (VAF) doesn't depend only on the magnitudes of ingredient velocities, but also on their directions. In other words, the law of force in relative motion is invariant regardless frame of reference, but in special case (when the ingredients of relative velocity have the same direction), also the magnitudes of all three forces in relative motion are the same regardless of the observer measuring them (third column, table 4). If we compare the third columns of tables 2, 3 and 4, we can see that only to acceleration we have the same magnitudes, but we don't conclude about invariance relying on this, but relaying on invariance of general law of physical quantity in relative motion, i. e. relying on second columns of tables 2, 3 and 4.

Table 4. The invariance of the law of acceleration relative to the observer's view.

Observer	For any value of α	For $\alpha = 0° \Rightarrow \beta = 180°$ and $\gamma = 0°$
O	$a' = \frac{d\left(\sqrt{u^2 + v^2 - 2vucos\alpha}\right)}{dt}$	$a' = a$
	$a = \frac{d\left(\sqrt{u' - v^2 sin^2\alpha} + vcos\alpha\right)}{dt}$	$a = a'$
	$a_v = \frac{d\left(\sqrt{u' - u^2 sin^2\alpha} + ucos\alpha\right)}{dt}$	$a' = a$
O'	$a = \frac{d\left(\sqrt{u'^2 + v^2 - 2u'vcos\beta}\right)}{dt}$	$a = a'$
	$a_v = \frac{d\left(\sqrt{u^2 - u'^2 sin^2\beta} + u'cos\beta\right)}{dt}$	$a' = a$
	$a' = \frac{d\left(\sqrt{u^2 - v^2 sin^2\beta} + vcos\beta\right)}{dt}$	$a' = a$
P	$a_v = \frac{d\left(\sqrt{u'^2 + u^2 - 2u'ucos\gamma}\right)}{dt}$	$a' = a$
	$a' = \frac{d\left(\sqrt{v^2 - u^2 sin^2\gamma} + ucos\gamma\right)}{dt}$	$a' = a$
	$a = \frac{d\left(\sqrt{v^2 - u'^2 sin^2\gamma} + u'cos\gamma\right)}{dt}$	$a = a'$

3. Conclusions

We have used the law of cosines to describe the Galilean relative motion, and we saw that this method is very efficient. Then, knowing the invariance of the law of cosines, and using the analogy, we have explained the invariance of laws of Galilean relative motion. And finally, we conclude that the law of force in relative motion is invariant regardless frame of reference, but only in special case (when the ingredients of relative velocity have the same direction), also the magnitudes of all three forces in relative motion are the same regardless of the observer measuring them.

References

[1] Klinaku, S. The general Galilean transformation. *Physics Essays*, 2017, 30, 3, 243 – 245.

[2] Halliday, D.; Resnick, R.; and Walker, J. Fundamentals of Physics, John Wiley & Sons, Inc, 7th ed., 2004. p. 75.

[3] French, A. P. Special Relativity, W W Norton & Company INC, New York, 1968. p. 68-69.

[4] Matveev, A. N. Mechanics and Theory of Relativity, Mir Publishers, Moscow. p. 82.

[5] Mohallem, J. R. Galilean invariance in Lagrangian mechanics. *Am. J. of Phys.* 2015, 83(10), 857-860.

[6] Preti, G.; de Felice, F. and Masiero, L. On the Galilean non-invariance of classical electromagnetism, *Eur. J. Phys.* 30, 2009, 381–391.

[7] Galilei, G. Dialogue Concerning the Two Chief World Systems, 1632, translated by Drake, S. University of California Press, 1953.

ANALIZA E INVARIANCËS GALILEANE DUKE PËRDORUR LIGJIN E KOSINUSEVE

Shukri Klinaku

Përmbledhje

Duke përdorur invariancën e ligjit të kosinuseve, si një rast shumë i lehtë për të kuptuar invariancën, do të shpjegojmë invariancën Galileane – konkretisht invariancën e transformimit të Galileit, invariancën e formulës për mbledhjen e shpejtësive dhe invariancën e ligjit të forcës. Fillimisht është përdorur ligji i kosinuseve për të gjetur transformimin e përgjithshëm të Galileit:

$$r = r'\sqrt{1 - \frac{v^2}{u'^2}sin^2\alpha} + vtcos\alpha$$

e pastaj, është përdorur invarianca e këtij ligji, për të paraqitur ngjashëm edhe invarianca Galileane. Kjo mënyrë e paraqitjes së invariancës Galielane eviton gabimin e shpeshtë kur flitet për këtë problem, sepse ngatërrohet invarianca e ligjit me invariancën e vlerës së një madhësie fizike. Ky ngatërrim më shpesh haset kur flitet për invariancën e ligjit të forcës te lëvizja relative. Në këtë punim tregohet qartë se intensiteti i një force nuk është i njëjtë në të gjitha sistemet e referimit, por është ligji i kësaj force i njëjtë në të gjitha sistemet e referimit.

KDU 621

A SURVEY ON CHANNEL MODELLING AND AVAILABILITY MEASUREMENTS FOR TV FREQUENCY BANDS

Hëna Maloku[a]
Zana L. Fazliu[a]
Mimoza Ibrani[a]
Myzafere Limani[a,b]

Abstract

The VHF and UHF frequency bands, traditionally allocated to TV broadcasters, have garnered significant attention from researchers, due to their superior propagation conditions and coverage. Furthermore, with transition from analogue broadcasting to digital television, a significant amount of spectrum has become newly available for potential opportunistic use by cognitive radio. These portions of the spectrum, unused by their licensed owners, are known as TV White Spaces. However, it is known that determination of TV white space availability can vary from country to country. Therefore, spectrum measurements are necessary in order to obtain a better overview of the actual availability

[a] FIEK, Universiteti i Prishtinës, Rr. "Nëna Terezë" nr. 5. 10000 Prishtinë, Kosovë. myzafere.limani@uni-pr.edu)

[b] Akademia e Shkencave dhe e Arteve e Kosovës, Rr. "Agim Ramadani" nr 305, 10000 Prishtinë, Kosovë.
myzaferelimani@ashak.org.

of TV frequency bands and identify potential white spaces. Once spectrum measurements are available, they can be processed in order to obtain a realistic channel model for the propagation, and furthermore detection mechanisms can be applied to determine which frequencies are occupied in which locations. In this paper we provide a comprehensive survey on spectrum measurements studies performed around the globe, and an overview of the TV white space availability, in the respective countries. Next we provide a brief overview on the path loss models most commonly used for modelling propagation in TV bands. Finally, we describe some of the detection techniques which can be used in absence of geo-location databases of TV broadcasters, to quantify occupation and usage of these frequencies.

Keywords: TV white space, cognitive radio, spectrum measurements, radio propagation model, spectrum availability detection, energy detection, detection threshold

Introduction

The exponential increase in broadband traffic has underscored the need for a more efficient and opportunistic use of the available spectrum. Researchers have highlighted the underutilization of licensed portions of the spectrum as a potential opportunity in addressing the spectrum congestion problem. The electromagnetic radio spectrum is a natural resource and as such is managed by government agencies and policymakers. Traditionally, frequency spectrum is divided into chunks and allocated for different types of services such as radio and television broadcasting, cellular telephony and military and maritime applications. The chunks are then further divided into sub-bands and assigned (licensed) to specific parties for use, such as television and radio broadcasters and mobile telephone providers. The allocation is done both in

the context of a time period, where the license is valid for a limited time frame, and in the context of location, where the license is valid for a specific area. While, this kind of spectrum assignment is convenient both for regulators and licensees, as it ensures interference-free use of the assigned frequency band, it has raised concerns over its inefficiency. In fact, plenty of research has shown that the spectrum as is managed today, is vastly under-utilized; while there are some frequency bands that are heavily used at all times, there are licensed bands that are un-occupied most of the time, even in highly populated urban areas [1].

The use of already licensed portions of the spectrum would be enabled by cognitive radios, which behave as secondary users and use the spectrum whenever the primary users, i.e., the license owners, are not using it. A cognitive radio (CR) is a radio that can change its transmission parameters based on interaction with the environment in which it operates [2]. The use of such radios has been approved both by USA and UK regulatory bodies, in 2009 and 2012 respectively [3]. The move was motivated by the digital transition in TV broadcasting, which made large swathes of TV spectrum accessible for opportunistic use. This group of vacant channels is known as TV white space (TVWS). However, the availability of TVWS spectrum varies from country to country and depends largely on the channels chosen for TV broadcasting. This is why the TVWS availability assessment is crucial for each location/country.

Frequency bands corresponding to TVWS spectrum are: VHF 30-300 MHz and UHF 300-1000 MHz except for the channels reserved for emergency transmissions. In Europe a challenging aspect of TVWS use is that TV spectrum is not only occupied by fixed TV broadcasting signals but also by licensed Programme Making Special Event (PMSE) devices, e.g., wireless microphones used in small events, concerts or security agencies. PMSE can operate in licensed or unlicensed basis. The detection of such equipment is the subject of research project [4]. Furthermore, their protection should be guaranteed based on legislative regulations [5].

It is largely expected that these bands will be used to augment spectrum resources for already existing technologies, such as WiFi, WiMax, etc., when needed, and it's unlikely that TVWS based broadband access will completely substitute them [6]. The two main reasons for using TVWS are: the superior propagation characteristics for wireless communication resulting in larger coverage area and also the minimal infrastructure requirements which makes them ideal for rural and undeveloped areas. This is especially convenient for developing countries such as those in Western Balkans. According to ITU reports, broadband penetration rates are increasing rapidly in these countries [7, 8]. In Albania alone, in the last five years, the number of active mobile broadband subscribers has gone from 8.8 to 52.6 per 100 inhabitants [7, 8]. Furthermore, access through wireless broadband networks through TVWS could be preferred since providing fiber optic connection is not cost efficient for service providers [9]. Nevertheless, the successful implementation of this technology depends on the ability to effectively manage and avoid the possible interference caused to the primary users. This is made possible with the CR continuously sensing the channel to detect the presence of the primary user. In case of primary user detection, secondary user has to immediately vacate the channel in order to avoid causing interference to primary user. To ensure that primary users are protected at all times, the UK regulator, Ofcom and Federal Communication Commission (FCC) in the USA, have proposed three methods to be used by secondary users: i) beacons, ii) sensing and iii) geolocation with database.

For the first method, secondary users will only start transmitting if they have already received a beacon signal implying the vacant channel. This requires the infrastructure of beacons to be implemented and maintained which is considered the main drawback of this method [10]. The second method is based on sensing. The secondary users will sense the spectrum and try to detect the presence of primary users. This is based on the amount of energy received. Operations from secondary users are possible only when they do not detect any primary signals.

The main drawback of this method is the device complexity because cognitive radios besides detecting the signal, must know many other signal characteristics such as modulation and bandwidth [11].

The third technique uses geo-location and databases. The database contains information regarding the spectrum usage in the vicinity during the specific time period. Secondary users have to send a query and the database will respond with the list of available frequencies including all transmission parameters that need to be followed for secondary transmission to start. This implies that the database must be kept updated at all times and that secondary users must have geo-location capability. The challenge on using this method is for secondary users that are indoors where GPS connectivity may not be available due to the signal disruption from buildings, walls, etc., [12]. Alternative techniques for outdoor and indoor localization using cellular and wireless network signals are also possible [13]. Techniques that use sensing and geo-location databases have also been proposed and tested [14]. To test a number of aspects of white space technology, including the white space device and geo-location database interactions, the validity of the channel availability/powers calculations by the database and associated interference aspects on primary services, several trials have been conducted by Ofcom in UK [15]. The opportunities are more appealing for indoor TVWS network usage because of the isolation from the licensed primary transmissions. The best use cases include femtocells and wireless LAN's [16, 17].

The first step towards usage of cognitive wireless devices and networks over TVWS is the spectrum measurements in order to understand the spectrum usage and availability. Since the measurements depend heavily on the location due to different environments, conducting measurements in each country is crucial. In addition, using accurate radio propagation models is the key to determining the precise spectrum availability and its potential for opportunistic use. The propagation models vary widely from one area to another because of its dependency on the terrain characteristics.

In this work, we first present the state of the art on the spectrum availability assessment in different countries of the world. We present the results of TVWS spectrum occupancy and availability assessed through measurement campaigns. We then continue to provide an overview of analytical studies for channel modeling where we present some of the most recent works on determination of propagation model that suits specific countries. And finally, in the last section, drawing from a significant amount of literature, we describe various methods for sensing and assessing the availability of TV frequency bands, using fixed and adaptive detection thresholds.

Spectrum measurements

In order to determine the potential of TV band, the assessment of the actual white space availability has to be conducted first. The best way to do this is by spectrum measurements. The spectrum measurement is done by conducting measurements in an area of interest. Even though the measurements are time consuming and costly, the results are very reliable. There have been many measurements campaigns conducted all over the world regarding TVWS assessment. Most of the work is done in USA, followed by UK and other developed countries and fewer similar works were conducted in developing countries. In order to calculate the spectrum occupation ratio, most of the referenced studies, applied the energy detection as the spectrum sensing method of choice. Some of the measurement campaigns conducted in different countries are listed below:

USA: - The authors in [18] have performed a band by band measurement of the spectrum occupancy in the spectral region between 30 MHz from 3,000 MHz in Chicago. They report that the average spectrum occupancy in the VHF band is less than 50% and around 60% for the UHF band. Similar study is performed in Chicago [19] some years later

for the same frequency band. They report the spectrum occupancy less than 40% for VHF band and less than 60% occupancy for UHF band.

UK: - The authors in [3] have done measurements on availability of TVWS channels for UHF band in 18 major population centers in England, Wales and Scotland. The results are different for different locations. For any given location, however, a minimum of 12 channels (96 MHz) are accessible to low-power cognitive devices, while the averaged per location capacity is just over 150 MHz. In the case of city of London where the density of the population is highest, a total of 96 MHz spectrum is in principle available, only 16 MHz can be utilized for contiguous frequency access.

Europe: - Several measurement campaigns were performed in Spain [20, 21], Romania [22], Turkey [23], Greece, [24], Macedonia [25], Hungary [26] and Bosnia [27].

In Spain, the average spectrum occupancy observed in [20] is significantly low, specifically 22.57% for the whole frequency range between 75 MHz and 3 GHz. The other study conducted in Spain [21], for the same frequency band reports that the occupancy levels are 42% for outdoor location and 33.7% for indoor location. In Romania [22], the authors conducted the spectrum measurements for the frequency band 25–3400 MHz. Reported occupancy levels for TVWS band (25–960 MHz) were: 37.23 % in case of the urban environment while for the rural area was as low as 19.19 %. Spectrum occupancy for UHF band was assessed in Samsun city center in Turkey [23]. From the study it results that available TV white space is 37.5% even in the dense area of Samsun city center. Another similar study was done in Greece where the authors estimated the actual white space capacity in the Peloponnese region [24]. They conclude that an average of 125 MHz of TVWS spectrum is available in every location where on average, the maximum contiguous TVWS spectrum block per location is 27MHz. A measurement campaign in the Macedonian capital Skopje [25] revealed that after the transition to digital broadcasting, a white space of 144 MHz between the frequencies 574 and 718 MHz was present, while the digital divi-

dend 800 MHz band from 790 to 862 MHz was unoccupied. In Budapest, Hungary, likewise, results from spectrum measurements [26], show that the occupancy ratios there can vary from 8% to 44%. A limited spectrum measurement study performed in Bosnia [27], shows that there is around 24 – 40 MHz of potentially unused spectrum in some areas of the country, however this conclusion was derived from observing just eight TV channels.

A limited assessment on TV band availability in Kosova can be found in [28]; however, the work is not comprehensive as measurements were performed in few locations, and for short periods of time. The occupancy ratio resulting from this study shows that occupancy ratios in Prishtina, Kosova, are below 12.5%.

Asia: - The objective of the authors in [29] was to find the spectrum usage in frequencies from 80 MHz to 5.85 GHz in Singapore. For the TVWS band, they show that the occupancy in the bands 174 to 230 MHz and 490 to 614 MHz is 49.05% and 52.35%, respectively. The same analysis of the measurements and the identification of spectrum holes are conducted in the capital city Kuala Lumpur [30]. The results show that the rate of utilized spectrum is 27.89%. The spectrum usage characteristics are evaluated for particular sites located in the most populated region of Japan [31]. The results show that for VHF band the occupancy ratio is 17.46% while for UHF band the occupancy ratio is 13.9%. Authors in [32] report that the occupancy of TV bands being 92.1% in just one urban location and occupancy rate in the range of 41.9 – 44.5 % for other suburban locations in China. More similar studies have been conducted in India [33, 34]. The average spectrum occupancy evaluated for VHF band (174-230 MHz) is 3.55% and 7.22% for UHF band (470-806 MHz) and UHF band the occupancy ratio is 0.4 % respectively.

Africa - This research is focused on evaluating the amount of television white space (TVWS) in the UHF band in Nigeria [35]. Results show that the average number of UHF channels per state in Nigeria is 2 which imply that there is about 368 MHz of available spectrum which secondary users can access.

Table 1: Spectrum occupancy ratio from measurements campaigns worldwide

Measurement country	Frequency range	Spectrum occupancy %
USA –Chicago [18]	(30-3000) MHz	VHF <50% UHF =60%
USA –Chicago [19]	(30-3000) MHz	VHF <40% UHF <60%
UK –England, Wales and Scotland	(470-860) MHz	Average 38%, London average 24.4%
Spain	75MHz- 3GHz	22.57% for the hole band
Spain	(75- 1000) GHz	42% for outdoor and 33.7% for indoor
Romania	25-960 MHz	37.23%
Turkey	(470-790) MHz	37.5%
Greece	(470-860) MHz	31.8%
Macedonia	(460 – 860) MHz	~46%
Hungary	(590 – 800) MHz	8 – 44%
Singapore	(174-614) MHz	VHF 49.05% UHF 52.35%
Malaysia	(470 – 798) MHz	27.89%
Malaysia	(470 – 798) MHz	20-40%
Japan	(170-810) MHz	VHF 17.46% UHF 13.9%
China	20 MHz - 3 GHz	(41.9-44.5%)
India	(174-806) MHz	VHF 3.55% UHF 7.22%
India	(700-806) MHz	0.4%
South Africa	(470-960) MHz	0.75%

It is important to mention that in many countries were the measurements have been conducted, have already switched to digital TV transmission. They have also built up their spectrum databases which are implemented in online platforms for TVWS spectrum availability, such as: http://whitespaces.microsoftspectrum.com/ or https://www.-google.com/get/spectrumdatabase/

Channel modeling - Analytical studies

Many works have tested the implementation of different propagation models to achieve the performance results that are similar with path loss results from measurements. The related work shows that different countries have considered different propagation models' taking into account that propagation of the wireless signal depends heavily on the terrain. In [36] the authors use 6 different types of propagation models: Longley-Rice model, Hata model, Egli model, Ericsson 9999 model, CCIR model and Free Space Path Loss (FSPL). The authors conclude that compared to the measured data in South Africa, the model that with the closest performance is Ericsson 9999 model. Another study from the same country that uses the same types of propagation models is [37]. The authors conclude that the FSPL is the closest model to the measurements. They point out that this is attributed to the fact that there was line of sight between transmitter and measurement point. For the other points the model that was more accurate was the Longley-Rice model. In [38] the authors considered FSPL model, Okumura-Hata model, Walfisch-Ikegami model and ECC-33 model to compare with the path loss value form measured data in India. They found that ECC-33 and Okumura- Hata were the best-fit models for the area. In [39] the authors decided on Log-normal Shadowing, Lee, Stanford University Interim (SUI), COST231, Hata, Egli and the ECC-33 models. They conclude that the SUI and the Log-normal Shadowing models gave better values of path loss compared to measured data in Malaysia. In [40]

the authors conducted a study using 9 path loss models and compare their performance with measured data in Nigeria. The models used are: Hata, COST 231, Walfisch-Ikegami, Egli, ITU-R P.529-3, ITU-R P.1546-4, CCIR, Davidson and FSPL. They conclude that in transmitter proximity, the CCIR model fits best the measured data. In larger distances the Hata, Davidson and COST 231 models give better results. In [41] authors compare the measured data in 5 biggest cities of Brazil with the data from using different propagation models. The propagation models they use are: ITU-R P .526, DeygoutAssis Knife Edge, ITU-R P .1546, and CRC-Predict. They conclude that ITU-R P.1546 model fits better in cities with low variance in altitude.

Table 2: Propagation models used for experiments worldwide

Country	Propagation models used for experiments	Best-fit propagation model
South Africa	• Longley-Rice model, • Hata model, • Egli model, • Ericsson 9999 model, • CCIR model and • Free Space Path Loss (FSPL)	Ericsson 9999 model
South Africa	• Longley-Rice model, • Hata model, • Egli model, • Ericsson 9999 model, • CCIR model and • Free Space Path Loss (FSPL)	Free Space Path Loss (FSPL) for LOS Longley-Rice model, for NLOS
India	• Free Space Path Loss model,	ECC-33 and Okumura- Hata models

	• Okumura-Hata model, • Walfisch-Ikegami model and • ECC-33	
Malaysia	• Log-normal Shadowing, • Lee, • Stanford University Interim (SUI), • COST231, • Hata, • Egli and • the Electronic Communication Committee (ECC)-33 models	SUI and the Log-normal Shadowing models
Nigeria	• Hata, • COST 231, • Walfisch-Ikegami, • Egli, • ITU-R P.529-3, • ITU-R P.1546-4, • CCIR, • Davidson and • FSPL	Hata, Davidson and COST 231 models
Brazil	• ITU-R P .526, • Deygout Assist Knife Edge, • ITU-R P .1546, and • CRC-Predict	ITU-R P.1546 model

Spectrum availability detection

CR networks are based on the key assumption that the CR users are regarded as visitors in the spectrum they occupy. Therefore, efficient spectrum management and non-interference with primary users are the two main principles on which these networks are built. CR hardware should be able to opportunistically identify portions of the spectrum with reduced licensed user activity and use them for communication. However, these licensed channels should be immediately vacated if the legitimate or primary users are detected.

Spectrum availability detection or spectrum sensing is the process during which secondary networks identify available TV channels that can be used without causing harmful interference to primary users. Sensing can be performed in three domains: time, frequency and space. Sensing can be also used also to identify the types of signals that are occupying the spectrum by determining their: carrier frequency, modulation type, bandwidth etc. Spectrum sensing can be performed using several techniques: energy detection, matched filtering, cyclostationary feature-based sensing, radio-identification based sensing and waveform-based sensing. The design of accurate detection mechanisms, have been studied carefully in the literature. A comprehensive survey on characterizing and modelling the availability of white spaces is provided in [42]. Below we list some of the most popular detection techniques applied in the context of CR spectrum sensing.

Energy Detection

One of the most common approaches to detect the presence of a signal in a channel is to apply what is often called the energy detection technique [42, 43]. This technique evaluates the energy of the sensed samples and compares it to a fixed pre-defined threshold. Its drawback is that it is very vulnerable to noise, which can lead to high rates of *false*

alarms, when the pre-defined threshold is set too low, or high number of *misdetections* when the pre-defined threshold is set too high.

When using the energy detector to sense the channel, the classical detection problem can be expressed as [43]:

$$\delta = \begin{cases} 1 & \text{if } E_n > \gamma \\ 0 & \text{if } E_n \leq \gamma \end{cases}$$

where E_n is the energy of the collected samples, and γ is the predefined threshold. The task of the detector is to reach a binary decision, δ, regarding the presence of a primary signal. The performance of the detector is quantified using two related metrics: the probability of false alarm, i.e., the probability of mistakenly detecting a signal when only noise is present, expressed as $\Pr_{FA} = Prob\{\delta = 1|0\}$, and the probability of misdetection, i.e., the probability of failing to detect the signal when the signal is present, expressed as $\Pr_{MD} = Prob\{\delta = 0|1\}$. These two metrics are closely related, and the design of the detector usually involves some sort of trade-off between the two metrics.

Matched filter

When the information of the primary user signal is known to the secondary user, the optimal detector in the presence of stationary Gaussian noise is the matched filter. The matched filter, as we know, maximizes the signal-to-noise-ratio in the presence of additive stochastic noise.

A matched filter is obtained by correlating a known signal, or template, with an unknown signal to detect the presence of the template in the unknown signal [44]. This is equivalent to convolving the unknown signal with a time-reversed version of the template. In the cog-

nitive radio scenario, however, the use of the matched filter can be severely limited since the information of the primary user signal is hardly available at the secondary user. In addition, it also requires additional electronic hardware components to generate the template signal, and some level of synchronization between the primary transmitter and the secondary user. If this information is not accurate, then the matched filter performs poorly.

Cyclostationary feature detection

Feature detection can be applied when the secondary users have partial knowledge of the primary signal. Specifically, they might have information regarding some of the features of the primary signal, which they can use to facilitate the process of detection. One well-known feature detector is the cyclostationary feature detector which relies on the fact that most modulated signal display some form of in-built periodicity [45]. More specifically, cyclostationarity is the property of stochastic signals whose mean and autocorrelation exhibit periodicity. The detection is performed by calculating the spectral correlation function (SCF) of the sensed signal, and searching for unique cyclic frequencies which correspond to the peaks of the SCF [45]. The detector is able to successfully distinguish a signal different from noise, by relying on the well-known fact that the SCF of white Gaussian noise exhibits a single peak located at the zero cyclic frequency, while other type of modulated signals will have peaks at other non-zero unique cyclic frequencies.

The main advantage of the feature detection scheme is its robustness against the uncertainty in noise power. While, a cyclostationary feature detector can perform better than an energy detector in differentiating different signal types, it is computationally complex and requires significantly longer observation time.

Detection Threshold Design

As shown in the previous section various sensing methods have been proposed in the literature [44, 45, 46], with different tradeoffs between required sensing time, complexity and detection capabilities. However, the energy detector has proven to be the most popular due to its simplicity, and the fact that it requires no prior knowledge regarding the characteristics of the signal or the noise. In most scenarios in CR, such knowledge is rarely accessible, which makes the energy detector the most attractive technique for spectrum availability assessment, especially where only the power measurements of the spectrum under evaluation are available.

Commonly the energy detector is implemented using a single predefined threshold. As already noted, the threshold plays an important role in assessing the availability of the spectrum; if set too low, the detector will be biased towards detecting the presence of a signal, even when there is only noise, increasing the probability of false alarm. A high rate of false alarms can lead to significant underestimation of the availability of the spectrum, rendering the process useless. On the other hand, a high threshold, can underestimate the presence of the primary signal, i.e. TV signal, therefore increasing the risk of causing harmful interference to the primary user, violating thus one of the core principles of CR.

The goal is therefore to design a threshold such that it strikes a balance between the opportunistic potential of licensed bands and protection of the primary users, i.e. licensees.

Therefore, we turn our attention to investigating how to improve the performance of the energy detector by assigning some form of intelligence to the predetermined threshold used during the detection. Namely, the threshold can be tailored to the environment, and it can even become adaptive by learning and adapting to changes in environment. This would make the energy detector less vulnerable to noise.

The design of the detection threshold has been widely researched in literature. The estimation of the detection threshold without prior knowledge about signal and noise characteristics is addressed in [47]. The use of iterative algorithms based on impulse suppression principles for spectrum sensing purposes is proposed in [48, 49]. The authors in [50, 51, 52] propose instead the application of adaptive double thresholds to enhance the performance of sensing process.

Noise floor estimation

The most straightforward way to approach the threshold setting problem is to estimate the noise floor, or the mean value of the noise power. This can be significant task on its own, as it is shown that the noise level can change both as a function of time [43], and frequency [47]. The approach proposed in [47], also referred to as PFA method, is quite attractive for CR scenarios, as it does not require any a priori knowledge about the characteristics of noise. Assuming a sufficiently static situation, this method relies on estimating the noise level from samples that are known to be noise-only. The threshold is directly linked to the targeted probability of false alarm, Pr_{FA}. Namely, once we set the desired Pr_{FA}, we find the threshold that our noise-only sample set exceeds with that probability. The values of Pr_{FA} can range from 10^{-4} to 0.1 [43,47].

It is important to note that the noise level may vary with frequency [47], therefore the threshold needs to be estimated for each frequency bin or, at least, for each frequency channel. While, this method is attractive due to its simplicity, it requires possession of known noise-only samples, which may not always be available.

FCME threshold

The forward consecutive mean excision (FCME) algorithm originally proposed to suppress outlier samples in time domain [48], has also been applied in literature to detect narrowband information signals spectrum sensing purposes [49]. Its appeal lies in its computational simplicity and effectiveness. Before the algorithm is started, the samples are sorted in ascending order, and a number of the lowest values (e.g. the 10% lowest values [50]) are included in the original clean set, denoted as Q. An initial threshold parameter, T, closely related to Pr_{FA}, assuming the noise exhibits, at least approximately, a Gaussian distribution, is set using the expressions provided in [47]:

$$T = -\ln(\mathrm{Pr}_{FA})$$

The procedure is further described in Figure 1.

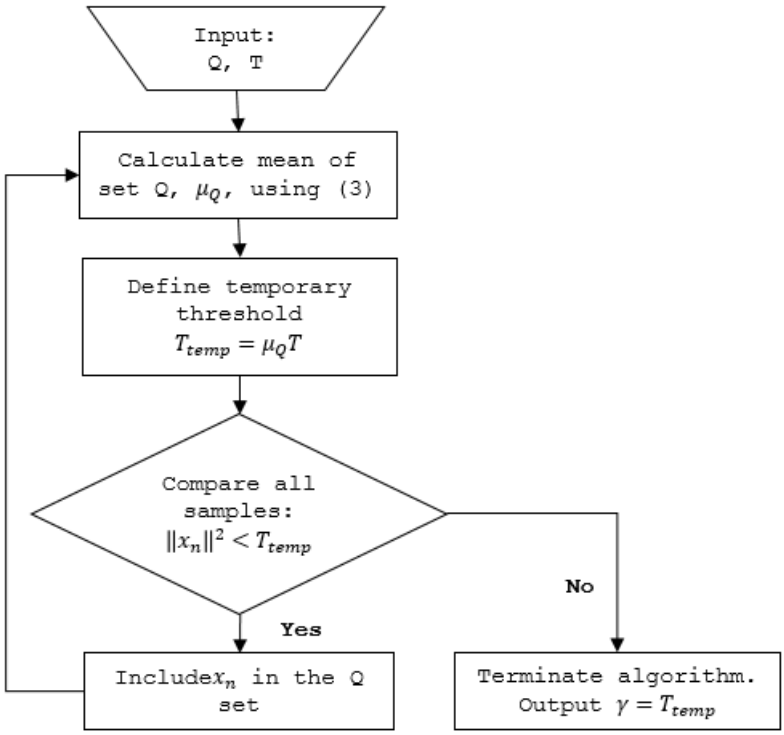

Fig. 1. The FCME algorithm

Once the two parameters are defined, the algorithm iteratively calculates the mean of the clean set:

$$\mu_Q = \frac{1}{|Q|}\sum_{x_n \epsilon Q}\|x_n\|^2$$

where $|Q|$ is the cardinality of Q, and x_n are the collected samples. In each iteration the rest of the samples are compared to temporary threshold T_{temp}, and included in the clean set Q if they are below the threshold. The algorithm stops once there are no more samples to be included in the clean set. The final threshold is set to the temporary threshold of the last iteration, $\gamma = T_{temp}$.

Adaptive double thresholds

In addition to properly setting the detection threshold, several papers have also proposed using double thresholds to improve the detection process [50-52]. The idea is to apply a lower and an upper threshold, namely γ_l and γ_u , both of which can be derived independently using the PFA or FCME techniques. The detector works as follows: if the measured samples are above the upper threshold, then a signal is detected; if the samples are below the lower threshold, then no signal is detected. If the samples are between the two, then further processing is required. The detection problem is then converted to:

$$\delta = \begin{cases} 1 & \text{if } E_n > \gamma_u \\ \text{apply clustering} & \text{if } \gamma_l < E_n \leq \gamma_u \\ 0 & \text{if } E_n \leq \gamma_l \end{cases}$$

An additional step is therefore required to reach a definite decision when measured samples are in the ambiguous region. The authors

in [43, 50], and apply a simple clustering technique to make a final decision. Initially all decisions in the ambiguous region are assigned "1s". Then the decisions are clustered so that any gap within a cluster smaller than 3, is disregarded. Namely, say the decisions for each frequency bin in a frequency channel are as follows: "1110111001". Because none of the gaps between the "1s", are bigger than two, the sequence is transformed to "1111111111". Finally, a cluster of "1s" is considered as "1", only if at least one of the samples in the cluster exceeds the upper threshold. If not, the samples are considered noise.

Conclusion

In conclusion, it is evident that TV bands show great promise for opportunistic use in the future. The occupancy ratio in most countries where measurements were conducted, are shown to be well below 60%, even in highly populated urban areas. In the other hand, different propagation models were implemented for channel modelling in many countries of the world. Analytical studies when comparing the measured data and the data obtained with simulations by using these propagation models show that the determination on propagation model depends heavily on country terrain profile. Nevertheless, the accuracy of the spectrum availability depends also on the predefined detection threshold. After explaining different detection mechanisms, we can conclude that the most used detection technique is energy detection with fixed threshold. However, the performance of the energy detection can be further improved by applying adaptive threshold which can adjust to the surrounding environment. Finally, we can note that availability of TVWS varies greatly from country to country, for several reasons: the allocation of TV frequencies to broadcasters is performed independently by each country and therefore can be significantly different, and the propagation conditions of the signal depend strongly on the terrain profile and the scattering environment.

Therefore, in order to accurately model TVWS availability, spectrum measurements and their subsequent processing is an inevitable step. In the future, we plan to conduct extensive spectrum measurement campaign, across the territory of Kosova, to depict a truthful picture of the level of usage of TV bands, and its potential for CR use.

Acknowledgement

This work is supported by the Academy of Arts and Sciences of Kosova through the project “Research on the usability and reusability potential of frequencies in the UHF, VHF and millimeter bands for wireless communication networks in Kosova”.

References

[1] B. Fette, Cognitive Radio Technology, Elsevier, 2008.

[2] Federal Communications Commission, " Notice of proposed rule-making and order: Facilitating opportunities for flexible, efficient, and reliable spectrum use employing cognitive radio technologies", ET Docket No. 03-108, Feb.2005.

[3] Maziar Nekovee, "Cognitive Radio Access to TV White Spaces: Spectrum Opportunities, Commercial Applications and Remaining Technology Challenges", IEEE DySPAN 2010 proceedings.

[4] http://www.cmsf.eu/projects/crew-tv.

[5] http://www.ecfr.gov/cgi-bin/text-idx"SID=5d71f66a87d99187939-94d55b 444edf9&node=se47.1.15 1712&rgn=div8.

[6] G.Villardi, C.Sum, C.Sun, Y.Alemseged, Z.Lan and H.Harada, "Efficiency of dynamic frequency selection-based coexistence mechanisms for TV white space enabled cognitive wireless access points”, IEEE Wireless Communications, December 2012.

[7] ITU Report. “The state of broadband 2012: achieving digital inclusion for all”, September 2012. (http://www.broadbandcommission.org/Documents/bb-annualreport2012.pdf)

[8] ITU Report. “The state of broadband: broadband catalyzing sustainable development”, September 2017. (https://www.itu.int/dms_pub/itu-s/opb/pol/S-POL-BROADBAND.18-2017-PDF-E.pdf)

[9] M.Deshmukh, K.Patil, F.Frederiksen, K.Skouby and R.Prasad, "Wireless broadband network on TVWS for rural areas: An Indian perspective", 16th International Symposium on Wireless Personal Multimedia Communications (WPMC), 2013.

[1] Maziar Nekovee, "A survey of Cognitive radio access to TV white spaces", International Journal of Digital Multimedia Broadcasting, 2010.

[11] T. Yucek and H. Arslan, "A survey of spectrum sensing algorithms for cognitive radio applications", IEEE Communications Surveys and Tutorials, 2009.

[12] Stephen J.Shellhammer, Ahmed K.Sadek and Wenyi Zhang, "Technical Challenges for Cognitive Radio in the TV White Space Spectrum", In-formation Theory and Applications Workshop, 2009.

[13] Hui Liu; Darabi, H.; Banerjee, P.; Jing Liu, "Survey of Wireless In-door Positioning Techniques and Systems". IEEE Transactions on Systems, Man, and Cybernetics, Part C: Applications and Reviews

[14] J. C. Ribeiro et.al.,"Testbed for combination of local sensing with geolocation database in real environments", IEEE Wireless Communications, August 2012

[15] O. Holland et.al. "A series of trials in the UK as part of the OFCOM TV white spaces pilot", 1st International Workshop on Cognitive Cellular Systems (CCS), September 2014.

[16] IEEE 802.22 WG, "IEEE Standard for Wireless Regional Area Networks Part 22: Cognitive Wireless RAN Medium Access Control (MAC) and Physical Layer (PHY) Specifications: Policies and Procedures for Operation in the TV Bands".

[17] Dimitris Makris, Georgios Gardikis and Anastasios Kourtis, "Quantifying TV White Space Capacity; A Geolocation-based Approach", IEEE Communications Magazine, September 2012.

[18] M.A. McHenry, P.A. Tenhula, D. McCloskey, D.A. Roberson, and C.S. Hood. Chicago spectrum occupancy measurements & analysis and a long-term studies proposal. In Proceedings of the first international workshop on Technology and policy for accessing spectrum (TAPAS), 2006.

[19] Tanim M Taher, Roger B Bacchus, Kenneth J Zdunek, and Dennis A Roberson. Long-term spectral occupancy findings in Chicago. In Proceedings of IEEE International Symposium on Dynamic Spectrum Access Networks (DySPAN), pages 100–107, May 2011.

[20] M.Lopez-Benitez, A. Umbert and F.Casadevall, "Evaluation of spectrum occupancy in Spain for cognitive radio applications", In Proceedings of IEEE 69th vehicular technology conference (VTC 2009 Spring), Spain, Barcelona, April 2009.

[21] J. Perez-Romero, Dominique Noguet, M. Lopez-Benitez, and Fernando Casadevall. Towards More Efficient Spectrum Usage: Spectrum Sensing and Cognitive Radio Techniques. Radio Science Bulletin, 7, 2011.

[22] Alexandru Martian, Razvan Craciunescu, Alexandru Vulpe, George Suciu1 and Octavian Fratu, "Access to RF White Spaces in Romania: Present and Future", Wireless Pers Commun (2016) 87:693–712 DOI 10.1007/s11277-015-2638-1.

[23] Cetin Kurnaz, Begum Korunur Engiz and Zafer Emre Albayrak, "Determination of TV White Space Spectrum Availability in Samsun Turkey", 24th Telecommunications Forum (TELFOR) 2016.

[24] Dimitris Makris, Georgios Gardikis and Anastasios Kourtis, “Quantifying TV White Space Capacity; A Geolocation-based Approach”, IEEE Communications Magazine, September 2012.

[25] P. I. Lazaridis, S. Kasampalis, Z. D. Zaharis, J. Cosmas, A. Bizopoulos, P. Latkoski, L. Gavrilovska, O. Fratu, and R. Prasad “UHF TV band spectrum and field-strength measurements before and after analogue switch-off”, Wireless VITAE Aalborg, Denmark, 2014.

[26] L. Csurgai-Horváth, I. Rieger, and J. Kertész, “A Survey of the DVB-T Spectrum: Opportunities for Cognitive Mobile Users”, Mobile Information Systems, 2016.

[27] M. Hadžialič, J. Mušovič, M. Hamza, M. Milišič, K. Huseinovič, J. Dizdarevič and M. Dulič, “TV White Space: Solution for bridging the gap between user's demand and the network capacities”, 22nd Telecommunications forum TELFOR Belgrade, 2014.

[28] H. Maloku, Z. L. Fazliu, M. Ibrani, A. Mekuli, E. Sela and M. Rajarajan, "Measurement of Frequency Occupancy Levels in TV Bands in Urban Environment in Kosova," 2018 18th Mediterranean Microwave Symposium (MMS), Istanbul, Turkey, 2018, pp. 268-271.

[29] Md Habibul Islam, Choo Leng Koh, Ser Wah Oh, Xianming Qing, Yoke Yong Lai, Cavin Wang, Ying-Chang Liang, Bee Eng Toh, Francois Chin, Geok Leng Tan, and William Toh, “Spectrum Survey in Singapore: Occupancy Measurements and Analyses” 2008 3rd International Conference on Cognitive Radio Oriented Wireless Networks and Communications (CrownCom 2008)

[30] Alaaldin H. Jaber, Norazizah Mohd Aripin and, Noora Salaim, “Evaluation of Spectrum Occupancy in Kuala Lumpur of UHF TV Band for Cognitive Radio Applications”, 2013 IEEE Student Conference on Research and Development (SCOReD), 16 -17 December 2013, Putrajaya, Malaysia

[31] Soraya Contreras, Gabriel Villardi, Ryuhei Funada and Hiroshi Harada, "An Investigation into the Spectrum Occupancy in Japan in the Context of TV White Space Systems", 2011 6th International ICST Conference on Cognitive Radio Oriented Wireless Networks and Communications (CROWNCOM)

[32] Sixing Yin, Dawei Chen, Qian Zhang, Mingyan Liu and Shufang Li, "Mining Spectrum Usage Data: A Large-Scale Spectrum Measurement Study", IEEE TRANSACTIONS ON MOBILE COMPUTING, VOL. 11, NO. 6, JUNE 2012

[33] Kishor Patill, Knud Erik Skouby and Ramjee Prasad, "Spectrum Measurement and Analysis of TV Band in Support of Cognitive Radio Operation in India", Wireless VITAE 2013

[34] Kishor Patil, Knud Skouby, Ashok Chandra and Ramjee Prasad, "Spectrum Occupancy Statistics in the Context of Cognitive Radio", The 14th International Symposium on Wireless Personal Multimedia Communications (WPMC), 2011.

[35] Yinusa. A. Adediran, Olabanji Kolade, Nasir Faruk, N.T. Surajudeen-Bakinde; Adeseko A. Ayeni and Olayiwola. W. Bello, "TV White Space in Nigeria in UHF Band: Geo-spatial Approach" IEEE 6th International Conference on Adaptive Science & Technology (ICAST), 2014.

[36] Hope Mauwa, Antoine B. Bagula, Marco Zennaro and Guy Lusilao-Zodi, "On the Impact of Propagation Models on TV White Space Measurements in Africa", International Conference on Emerging Trends in Networks and Computer Communications (ETNCC), 2015.

[37] H. Mauwa, A. Bagula, M. Zennaro, E. Pietrosemoli, A. Lysko and T.X. Brown, "Systematic analysis of geo-Location and spectrum sensing as access methods to tv white space" ITU Kaleidoscope: ICTs for a Sustainable World (ITU WT), 2016.

[38] P. Prajesh, and R.K. Singh, "Investigation of outdoor path loss models for wireless communication in Bhuj." 171-178.

[39] J. Chebil, A.K. Lawas, and M. D. Islam, "Comparison between measured and predicted path loss for mobile communication in Malaysia." World Applied Sciences Journal 21, 123-128, 2013.

[40] N. Faruk, A. Ayeni, and Y.A. Adediran, "On the study of empirical path loss models for accurate prediction of TV signal for secondary users." Progress In Electromagnetics Research B 49, 155-176. 2013.

[41] F.S. Silva, L.J. Matos, F.A.C. Peres, and G.L. Siqueira, "Coverage prediction models fitted to the signal measurements of digital TV in Brazilian cities." In Microwave & Optoelectronics Conference (IMOC), 2013 SBMO/IEEE MTT-S International, pp. 1-5. IEEE, 2013.

[42] J. J. Lehtomaki, R. Vuohtoniemi, K. Umebayashi, “On the Measurement of Duty Cycle and Channel Occupancy Rate”, IEEE Journal on Selected Areas in Communications, May 2013.

[43] H. Urkowitz, “Energy detection of unknown deterministic signals,” Proc. IEEE, vol. 55, no. 4, pp. 523–531, 1967.

[44] Zhang X., Gao F., Chai R., Jiang T., "Matched Filter Based Spectrum Sensing When Primary User Has Multiple Power Levels", IEEE China Communications, February 2015.

[45] L. Doyle, Essentials of Cognitive Radio, Cambridge University Press, 2009.

[46] A. Sahai, N. Hoven, and R. Tandra, “Some fundamental limits on cognitive radio,” in Proc. Forty-second Allerton Conference on Communications, Control, and Computing (Allerton Conference 2004), Sep. 2004, pp. 1–10.

[47] M. Lopez-Benitez and F. Casadevall, “Methodological aspects of spectrum occupancy evaluation in the context of cognitive radio,” European Transactions on Telecommunications, vol. 21, no. 8, pp. 680–693, Dec. 2010.

[48] H. Saarnisaari, P. Henttu, and M. Juntti, “Iterative multidimensional impulse detectors for communications based on the classical

diagnostic methods," IEEE Trans. Commun., vol. 53, no. 3, March 2005, pp. 395–398.

[49] J. Vartiainen and R. Vuohtoniemi, "False Alarm Rate Analysis of the FCME Algorithm in Cognitive Radio Applications", AICT 2015, The Eleventh Advanced International Conference on Telecommunications, June 2015.

[50] J. Vartiainen, H. Sarvanko, J. Lehtom¨aki, M. Juntti, and M. Latva-aho, "Spectrum sensing with LAD based methods," in Proc. IEEE PIMRC, Athens, Greece, Aug. 2007.

[51] A. Rauniyar, S. Y. Shin, "Adaptive Double-Threshold Based Energy and Matched Filter Detector in Cognitive Radio Networks", Scientific Cooperations International Workshops on Electrical and Computer Engineering Subfields, 22-23 August 2014.

[52] J. Vartiainen, J. J. Lehtomaki and H. Saarnisaari, "Double-Threshold Based Narrowband Signal Extraction", IEEE 61st Vehicular Technology Conference, 2005.

NJË STUDIM MBI MODELIMIN E KANALEVE DHE MATJEN E DISPONUESHMËRISË SË FREKUENCAVE NGA BREZI TELEVIZIV

Hëna Maloku
Zana L. Fazliu
Mimoza Ibrani
Myzafere Limani

Përmbledhje

Brezet VHF dhe UHF të frekuencave, tradicionalisht të alokuara për transmetues televiziv, kanë fituar shumë vëmendje nga hulumtuesit shkencor, kryesisht për shkak të vetive të mira të përhapjes dhe mbulueshmërisë që posedojnë. Për më shumë, me kalimin nga transmetimi analog në atë digjital, një sasi e konsiderueshme e këtij spektri është liruar, për përdorim eventual të mundshëm nga radiot kognitive si pajisje dytësore. Këto pjesë të brezit, të papërdorura nga pronarët e licencuar, njihen si hapësira të bardha TV (TVWS – *TV White Spaces*). Mirëpo, dihet se disponueshmëria e këtyre hapësirave të bardha, dallon nga shteti në shtet. Për këtë arsye, matjet e spektrit janë të domosdoshme për të ndërtuar një pasqyrë të qartë të disponueshmërisë aktuale të frekuencave televizive dhe për të identifkuar hapësirat e bardha potenciale. Në këtë punim, ofrohet një pasqyrë gjithpërfshirëse e studimeve të ngjashme mbi matjen e spektrit televiziv, të realizuara në mbarë botën, si dhe disponueshmërinë e hapësirave të bardha në shtetet respektive. Gjithashtu, është përpiluar një listë e modeleve të humbjeve të sinjalit, të cilat janë shfrytëzuar nga studimet e realizuara në vendet tjera, për të modeluar përhapjen e valëve në frekeuncat televizive. Përfundimisht, janë përshkruar gjithashtu edhe disa nga teknikat zbuluese (detektuese) që mund të përdoren në mungesë të databazave të sakta të transmetuesve, për të përcaktuar shfrytzueshmërinë dhe disponueshmërinë e këtyre frekuencave.

Nga ky studim, është e qartë se brezet televizive janë shumë premtuese për përdorim në të ardhmen. Disponueshmëria e këtyre brezeve, në shumicën e vendeve ku janë realizuar matjet, është mbi 40%, edhe në zonat urbane me numër të madh të banorëve. Gjithashtu vërehet se në vende të ndryshme të botës, për të modeluar kanalin në këto breze, janë përdorur disa modele të ndryshme. Studimet analitike të realizuara gjatë krahasimit të vlerave të matura dhe të fituara nga simulimet e modeleve të përhapjes, tregojnë se përcaktimi i modelit varet në masë të madhe nga profili i terrenit në shtetin përkatës. Saktësia e shqyrtimit të disponueshmërisë se spektrit varet gjithashtu edhe nga mekanizmi i përdorur i detektimit. Ndonëse janë përshkruar disa mekanizma të ndryshëm, nga shqyrtimi i literaturës relevante mund të konludojmë se teknika më e përdorur është detektimi i energjisë me prag të fiksuar dhe të paracaktuar. Mirëpo, performanca detektorit të energjisë mund të përmirësohet dukshëm nëse, në vend të pragut fiks, të aplikohet pragu adaptiv i cili në mënyrë fleksibile përshtatet me ambientin rrethues.

Si përfundim, është e qartë se disponueshmëria e hapësirave të bardha në brezet televizive dallon shumë nga shteti në shtet për disa arsye: alokimi i frekuencave tek transmetuesit e ndryshëm realizohet në mënyrë të pavarur nga secili shtet, si dhe kushtet e përhapjes së sinjalit varen shumë nga profili i terrenit dhe ambienti rrethues. Prandaj, për të modeluar saktësisht disponueshmërinë e hapësirave të bardha, është e domosdoshme të realizohen matje të thukta të spektrit, dhe të përpunohen të dhënat e fituara gjatë matjeve. Në të ardhmen, planifikohet të realizohen disa kampanja gjithëpërfshirëse të matjeve, përgjatë gjithë territorit të Kosovës, për të ndërtuar një pasqyrë reale të nivelit të shfytzueshmërisë së brezeve televizive, dhe potencialin e këtij brezi për përdorim nga radiot kognitive.

GUIDE FOR AUTHORS:

Paper submitted in electronic version by mail will be considered for publication in Research.

Research welcomes original research papers which may contain original articles. reviews and short Communications.

Journal covers Natural and Applied Sciences specified in series A, B etc. Articles are to be presented in English with summary in Albanian.

Paper considered for publication in **Research** must not have been previously published elsewhere. Each submitted manuscript will be reviewed, the final decision concerning its acceptance resting with the editors. The manuscript should conform to the formal standards of the Journal available on our web site
http://www.ashak.org/repository/docs/GENERAL_INFORMATION_FOR_THE_JOURNAL_770777.pdf
ashak@ashak.org.

A single Word and PDF file containing text, tables, figures, references, etc., should be provided.

UDHËZIME PËR AUTORËT

Punimi i dorëzuar në formë elektronike me e-mail do të merret në shqyrtim për publikim në revistën Research-Kërkime.

Revista Research-Kërkime mirëpret punimet origjinale, revyale dhe kumtesat e shkurtra.

Revista përfshinë Shkencat e Natyrës dhe të Zbatuara të specifikuara në seri A, B. Artikujt duhet të shkruhen në gjuhën angleze me rezyme në gjuhën shqipe.

Punimi i dorëzuar për botim në Research nuk duhet të jetë në shqyrtim ose i publikuar në ndonjë revistë tjetër. Dorëshkrimi i dorëzuar do të recensohet dhe vendimi përfundimtar i pranimit të tij iu mbetet kryeredaktorit të revistës. Dorëshkrimi duhet të jetë konform standardeve formale të revistës që është në disponim në ueb faqen tonë

http://www.ashak.org/repository/docs/INFORMATE_E_PERGJITHSHME_PER_REVISTEN_188742.pdf

Autorët duhet të përgatisin një kopje të punimit që përmban tekstin, tabelat, figurat, referencat etj. në versionin Word dhe në PDF

RESEARCH 24 KËRKIME

2019

Botues:
AKADEMIA E SHKENCAVE DHE E ARTEVE E KOSOVËS

Redaktor teknik:
ASHAK

Realizimi kompjuterik:
ASHAK

Madhësia: 12 tabakë shtypi
Tirazhi: 200 copë
Formati: 16x24 cm

Shtypi:
Focus Print
Shkup

Subscription orders should be addressed to - Porositja mund të bëhet në këtë adresë:
Kosova Academy of Sciences and Arts
Akademia e Shkencave dhe e Arteve e Kosovës
Rr. “Agim Ramadani” Nr. 305, 10000 Prishtinë, Republika e Kosovës
Tel.+383(0) 38249 303; e-mail: ashak@ashak.org